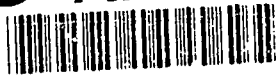


AD-A236 350



RL-TR-91-45  
Final Technical Report  
May 1991



2

# 5/15 GHZ SCATTERING STUDY

Thayer School of Engineering

Robert K. Crane

DTIC  
ELECTE  
MAY 31 1991  
S B D

*APPROVED FOR PUBLIC RELEASE; DISTRIBUTION UNLIMITED.*

91-00684



Rome Laboratory  
Air Force Systems Command  
Griffiss Air Force Base, NY 13441-5700

01 5 99 000

This report has been reviewed by the Rome Laboratory Public Affairs Division (PA) and is releasable to the National Technical Information Service (NTIS). At NTIS it will be releasable to the general public, including foreign nations.

RL-TR-91-45 has been reviewed and is approved for publication.

APPROVED: *Uve H. W. Lammers*

UVE H.W. LAMMERS  
Project Engineer

APPROVED: *John K. Schindler*

JOHN K. SCHINDLER  
Director of Electromagnetics

FOR THE COMMANDER:

*James W. Hyde III*

JAMES W. HYDE III  
Directorate of Plans & Programs

If your address has changed or if you wish to be removed from the Rome Laboratory mailing list, or if the addressee is no longer employed by your organization, please notify Rome Laboratory (EECP) Hanscom AFB MA 01731-5000. This will assist us in maintaining a current mailing list.

Do not return copies of this report unless contractual obligations or notices on a specific document require that it be returned.

# REPORT DOCUMENTATION PAGE

Form Approved  
OMB No. 0704-0188

Public reporting burden for this collection of information is estimated to average 1 hour per response, including the time for reviewing instructions, searching existing data sources, gathering and maintaining the data needed, and completing and reviewing the collection of information. Send comments regarding this burden estimate or any other aspect of this collection of information, including suggestions for reducing this burden, to Washington Headquarters Service, Directorate for Information Operations and Reports, 1215 Jefferson Davis Highway, Suite 1204, Arlington, VA 22202-4302, and to the Office of Management and Budget, Paperwork Reduction Project (0704-0188), Washington, DC 20503.

1. AGENCY USE ONLY (Leave Blank)		2. REPORT DATE May 1991	3. REPORT TYPE AND DATES COVERED Final Jun 88 - Aug 89	
4. TITLE AND SUBTITLE 5/15 GHZ SCATTERING STUDY			5. FUNDING NUMBERS C - F30602-88-D-0027 Task E-8-7109 PE - 28010F, 63789F PR - 478T TA - 00 WU - P1	
6. AUTHOR(S) Robert K. Crane			8. PERFORMING ORGANIZATION REPORT NUMBER N/A	
7. PERFORMING ORGANIZATION NAME(S) AND ADDRESS(ES) Thayer School of Engineering Dartmouth College Hanover NH 03755			10. SPONSORING/MONITORING AGENCY REPORT NUMBER RL-TR-91-45	
9. SPONSORING/MONITORING AGENCY NAME(S) AND ADDRESS(ES) Rome Laboratory (EECP) Hanscom AFB MA 01731-5000			11. SUPPLEMENTARY NOTES Rome Laboratory Project Engineer: Uve H.W. Lammers/EECP/(617) 377-3193 Prime Contractor: Syracuse University	
12a. DISTRIBUTION/AVAILABILITY STATEMENT Approved for public release; distribution unlimited.			12b. DISTRIBUTION CODE	
13. ABSTRACT (Maximum 200 words) Received signal level and multipath delay spread measurements were made at 5 and 16 GHz on a 161 km tropospheric scatter path over moderately rough terrain from Prospect Hill in Waltham, MA to Mt Tug in Lebanon, NH. The measurement campaign spanned the summer months of May through Aug 89. The signal level data were processed to obtain hourly median values for the estimation of the cumulative distribution function (cdf) of received signal level for use in troposcatter communication system design. Multipath delay spread observations were made at the higher frequency. These data were also processed to obtain the sample cdf of the hourly median values of the two square multipath delay spread estimates.  The data were sorted by the dominant propagation mechanism for each hour of observation. The propagation categories were clear weather conditions (forward scatter by clear air turbulence in thin horizontal layers), rain scatter, and duct propagation in elevated layers. The sample cdfs were well approximated by lognormal distributions for received signal level and by normal distributions for multipath delay spread. At 16 GHz (Ku band), the highest level field strengths were recorded during periods with rain while, at C band (5 GHz), the highest level fields were recorded during elevated ducting conditions.  (See reverse)				
14. SUBJECT TERMS Troposcatter, Ku band, C band; Transmission loss; Multipath delay spread			15. NUMBER OF PAGES 80	
			16. PRICE CODE	
17. SECURITY CLASSIFICATION OF REPORT UNCLASSIFIED	18. SECURITY CLASSIFICATION OF THIS PAGE UNCLASSIFIED	19. SECURITY CLASSIFICATION OF ABSTRACT UNCLASSIFIED	20. LIMITATION OF ABSTRACT UL	

Block 13 (Cont'd)

NOTE: Rome Laboratory/RL (formerly Rome Air Development Center/RADC

Abstract

Received signal level and multipath delay spread measurements were made at 5 and 16 GHz on a 161 km tropospheric scatter path over moderately rough terrain from Prospect Hill in Waltham Massachusetts to Mt Tug in Lebanon, New Hampshire. The measurement campaign spanned the summer months of May through August, 1989. The signal level data were processed to obtain hourly median values for the estimation of the cumulative distribution function (cdf) of received signal level for use in troposcatter communication system design. Multipath delay spread observations were made at the higher frequency. These data were also processed to obtain the sample cdf of the hourly median values of the two sigma multipath delay spread estimates.

The data were sorted by the dominant propagation mechanism for each hour of observation. The propagation categories were clear weather conditions (forward scatter by clear air turbulence in thin horizontal layers), rain scatter, and duct propagation in elevated layers. The sample cdfs were well approximated by lognormal distributions for received signal level and by normal distributions for multipath delay spread. At 16 GHz (Ku band), the highest level field strengths were recorded during periods with rain while, at C band (5 GHz), the highest level fields were recorded during elevated ducting conditions.



<b>Accession For</b>	
NTIS GRA&I	<input checked="" type="checkbox"/>
DTIC TAB	<input type="checkbox"/>
Unannounced	<input type="checkbox"/>
Justification	
By _____	
Distribution/	
<b>Availability Codes</b>	
Dist	Avail and/or Special
1-1	

## Table of Contents

Abstract	i
Table of Contents	ii
List of Tables	ii
List of Illustrations	iii
Acknowledgements	vi
1. Introduction	1
1.1 Program objectives	1
1.2 Summary of results	1
2. The experimental observations	3
2.1 Equipment configuration	3
2.2 Daily observations with the small aperture Ku band transmit antenna	4
2.3 Observations with the large aperture Ku band transmit antenna	7
2.4 Observations in rain	8
2.5 Observations with an elevated duct	8
3. Data summaries	10
3.1 Hourly data	10
3.2 Diurnal variations	11
3.3 Statistical distributions of hourly median values for clear weather conditions	12
3.4 Statistical distributions of hourly median values for rainy conditions	14
3.5 Statistical distributions of hourly median values for ducting conditions	15
4. Analysis	16
References	17

## List of Tables

1. Quarter day summaries.	18
---------------------------	----

List of Illustrations	Page
1. Troposcatter path profile for a $4/3$ effective Earth radius. The scattering volumes are displayed as filled areas. The scattering volume for the 3' antenna at 16 GHz encloses the scattering volume for the 29' antenna at 5 GHz.	20
2. Day plots for the small aperture Ku band transmit antenna under clear weather conditions on July 12, 1989: sample cumulative distribution functions for received power, received power time series, power spectra for received power fluctuations and coherency between the fluctuations at Ku and C band.	21
3. Day plots for the small aperture Ku band transmit antenna under clear weather conditions on July 12, 1989: time series of received power deviations from turbulent forward scatter model predictions, time series of the differences between received power deviations from turbulent forward scatter model predictions at Ku and C band, time series and sample cumulative distribution function for Ku band two sigma multipath delay spread.	22
4. Day plots for the small aperture Ku band transmit antenna under clear weather conditions on July 12, 1989: time series of mean Doppler frequency shift and Doppler frequency spread, time series and sample cumulative distribution function for carrier channel and delay channel measurements of Ku band received power levels..	23
5. Day plots for the large aperture Ku band transmit antenna under clear weather conditions on July 12, 1989: sample cumulative distribution functions for received power, received power time series, power spectra for received power fluctuations and coherency between the fluctuations at Ku and C band.	24
6. Day plots for the large aperture Ku band transmit antenna under clear weather conditions on July 12, 1989: time series of received power deviations from turbulent forward scatter model predictions, time series of the differences between received power deviations from turbulent forward scatter model predictions at Ku and C band, time series and sample cumulative distribution function for Ku band two sigma multipath delay spread.	25
7. Day plots for the large aperture Ku band transmit antenna under clear weather conditions on July 12, 1989: time series of mean Doppler frequency shift and Doppler frequency spread, time series and sample cumulative distribution function for carrier channel and delay channel measurements of Ku band received power levels.	26
8. Scatter distribution comparing simultaneous observations of the maximum hourly carrier channel and delay channel observations of Ku band received power levels.	27
9. Day plots for the small aperture Ku band transmit antenna under rainy conditions on July 5, 1989: sample cumulative distribution functions for received power, received power time series, power spectra for received power fluctuations and coherency between the fluctuations at Ku and C band.	28
10. Day plots for the small aperture Ku band transmit antenna under rainy conditions on July 5, 1989: time series of received power deviations from turbulent forward scatter model predictions, time series of the differences between received power deviations from turbulent forward scatter model predictions at Ku and C band, time series and sample cumulative distribution function for Ku band two sigma multipath delay spread.	29
11. Day plots for the small aperture Ku band transmit antenna under rainy conditions on July 5, 1989: time series of mean Doppler frequency shift and Doppler frequency spread, time	30

series and sample cumulative distribution function for carrier channel and delay channel measurements of Ku band received power levels.

- |     |   |    |
|-----|---|----|
| 12. | Day plots for the small aperture Ku band transmit antenna under elevated ducting conditions on August 1, 1989: sample cumulative distribution functions for received power, received power time series, power spectra for received power fluctuations and coherency between the fluctuations at Ku and C band.  | 31 |
| 13. | Day plots for the small aperture Ku band transmit antenna under elevated ducting conditions on August 1, 1989: time series of received power deviations from turbulent forward scatter model predictions, time series of the differences between received power deviations from turbulent forward scatter model predictions at Ku and C band, time series and sample cumulative distribution function for Ku band two sigma multipath delay spread. | 32 |
| 14. | Day plots for the small aperture Ku band transmit antenna under elevated ducting conditions on August 1, 1989: time series of mean Doppler frequency shift and Doppler frequency spread, time series and sample cumulative distribution function for carrier channel and delay channel measurements of Ku band received power levels.   | 33 |
| 15. | C band carrier received power levels for the month of June, 1989.   | 34 |
| 16. | Ku band carrier received power levels for the month of June, 1989.  | 35 |
| 17. | Ku band delay channel received power levels for the month of June, 1989.  | 36 |
| 18. | Ku band average Doppler frequency shifts for the month of June, 1989.   | 37 |
| 19. | C band average Doppler frequency shifts for the month of June, 1989.  | 38 |
| 20. | Ku band Doppler frequency spreads for the month of June, 1989.  | 39 |
| 21. | C band Doppler frequency spreads for the month of June, 1989.   | 40 |
| 22. | Ku band two sigma multipath delay spreads for the month of June, 1989.  | 41 |
| 23. | Average diurnal variation in C band received carrier power, summer, 1989  | 42 |
| 24. | Average diurnal variation in Ku band received carrier power, summer, 1989   | 43 |
| 25. | Average diurnal variation in C band Doppler frequency shift, summer, 1989   | 44 |
| 26. | Average diurnal variation in Ku band Doppler frequency shift, summer, 1989  | 45 |
| 27. | Average diurnal variation in Ku band Doppler spread, summer, 1989   | 46 |
| 28. | Average diurnal variation in Ku band two sigma multipath delay spread, summer, 1989   | 47 |
| 29. | Sample cumulative distributions for carrier received power levels, nighttime, summer, 1989, clear weather conditions.   | 48 |
| 30. | Sample cumulative distributions for carrier received power levels, morning, summer, 1989, clear weather conditions.   | 49 |

31	Sample cumulative distributions for carrier received power levels, afternoon, summer, 1989, clear weather conditions.	50
32	Sample cumulative distributions for carrier received power levels, evening, summer, 1989, clear weather conditions.	51
33	Sample cumulative distributions for carrier received power levels, large aperture antenna at Ku band, afternoon, summer, 1989, clear weather conditions.	52
34	Sample cumulative distributions for Ku band Doppler spread values, summer, 1989, clear weather conditions.	53
35	Sample cumulative distributions for Ku band two sigma multipath delay spread values, summer, 1989, clear weather conditions.	54
36	Sample cumulative distributions for carrier received power levels, nighttime, summer, 1989, rainy conditions.	55
37	Sample cumulative distributions for carrier received power levels, morning, summer, 1989, rainy conditions.	56
38	Sample cumulative distributions for carrier received power levels, afternoon, summer, 1989, rainy conditions.	57
39	Sample cumulative distributions for carrier received power levels, evening, summer, 1989, rainy conditions.	58
40	Sample cumulative distributions for Ku band Doppler spread values, summer, 1989, rainy conditions.	59
41	Sample cumulative distributions for Ku band two sigma multipath delay spread values, summer, 1989, rainy conditions.	60
42	Sample cumulative distributions for carrier received power levels, nighttime, summer, 1989, elevated ducting conditions.	61
43	Sample cumulative distributions for carrier received power levels, morning, summer, 1989, elevated ducting conditions.	62
44	Sample cumulative distributions for Ku band Doppler spread values, summer, 1989, elevated ducting conditions.	63
45	Sample cumulative distributions for Ku band two sigma multipath delay spread values, summer, 1989, elevated ducting conditions.	64
46	Sample cumulative distributions for carrier received power levels for different propagation mechanisms, summer, 1989.	65

## Acknowledgements

The experiment described in this report was sponsored by the Joint Tactical Communications (TRI-TAC) Program Office, Electronics Systems Division (ESD) and the Rome Air Development Center (RADC). The work at the Thayer School of Engineering, Dartmouth College was supported by ESD and RADC through the RADC Post-Doctoral Program. Uve H. W. Lammers and Richard A. Marr of the Electromagnetics Directorate, Rome Air Development Center, Hanscom Air Force Base, MA, were responsible for the operation of the transmitter site.

The receiver site on Mt. Tug is the cable head facility for Twin State Cable of West Lebanon, NH. The generosity of Twin State Cable in allowing us to use the facility is appreciated.

A number of graduate students at the Thayer School of Engineering have been involved in this project at one time or another. Special thanks go to Brad Anderson and Mark Hoppe for the effort they have expended in collecting and analyzing the data. Thanks also go Shailesh Chandra and Rajesh Prabhu for picking up the work and continuing the observation and analysis program after the graduations of Brad and Mark.

## 5 / 15 GHZ SCATTERING STUDY

### 1. Introduction

#### 1.1 Program objectives

The objective of this 5/15 GHz Scattering Study was to characterize the 16 GHz troposcatter channel for the design of digital tactical communication systems. Simultaneous measurements of received signal levels were made at two frequencies, 5 and 16 GHz, together with measurements of the Doppler frequency shift of the received carrier signals and the multipath delay spread of the higher frequency signal. The parameters needed to assess system performance, the received signal level, delay spread and Doppler spread (fade rate), were derived from the measurements. Tactical troposcatter communication systems presently operate at C band (5 GHz) and, therefore, the lower frequency observations were made to provide a known reference for comparison to the higher frequency (Ku band) measurements.

An earlier study had shown that adequate signal levels were present on the 161 km Prospect Hill to Mt Tug troposcatter path when a large aperture antenna was used at the transmitter site [Crane, 1988]. Questions were raised about the signal levels to be expected when small aperture antennas were employed at both the transmit and receive sites. This study also addressed the effect of antenna aperture size on received signal level statistics, delay spread statistics and Doppler spread statistics.

#### 1.2 Summary of results

The transmitter and receiver systems for the Prospect Hill to Mt Tug troposcatter path were configured for continuous, unattended operation with small aperture, matched beamwidth antennas at the receiver site for both frequencies and at both ends of the path for the higher frequency. The digital data recording system collected measurements of the carrier received power levels at 4.95 GHz (C band) and 15.73 GHz (Ku band), the average Doppler frequency shift and the standard deviation of the Doppler shift at both carrier frequencies and, at the higher frequency, the correlation detector received power levels at 15 consecutive lags (80 nanosecond time intervals) straddling the delay with the highest detected level. The receiver system was calibrated automatically twice a day. The observations were processed to provide hourly summaries that included the minimum, maximum and median values of two minute averages of each of the measured parameters. These summaries were then stored in a data bank for subsequent analyses.

Data were collected from 1 May through 21 August 1989. Operation was nearly continuous with the exception of a daily shutdown of one to two hours for maintenance and calibration and a series of afternoon measurements during July with the large aperture transmit antenna at Ku band. Problems with one of the two Ku band transmitters caused the loss of seven days of data in May eight days in June and thirteen days in July. The problem was fixed by the end of July but operations terminated August 21 when all three transmitters failed as the result of a lightning strike at the transmitter site. During the four month period up to the lightning strike, calibrated observations were obtained for 1232 hours or 45% of the time.

The observations revealed a strong diurnal variation in received signal level. The observed average hourly median transmission loss values were 163 dB at Ku band and 148 dB at C band for time periods with no indication of rain on the path and no enhanced signal levels due to propagation along elevated ducts. The corresponding Ku band signal level was within 12 dB of the predictions of several troposcatter models. The Signatron model [Parl, 1989; Matthews, 1989] predicted about 8 dB more signal than observed. The current CCIR model [CCIR, 1989] predicted 12 dB more signal than observed while their earlier model, the NBS

Tech Note 101 model [Rice et. al., 1965], predicted 3 dB less signal than observed. Our most recent model is within 3 dB of the average value for the summer months. At C band, the model prediction errors were smaller.

The average and spread (standard deviation) of the Doppler shifts of the carrier frequencies were monitored throughout the experiment. The average Doppler shift was used to identify intervals with rain scattered signals. The Doppler spread may be used to estimate the fade rate for the received signals. At Ku band, the observed Doppler spread averaged 8.6 Hz, a value close to the predicted value of 8.1 Hz if the prevailing wind is 12 m/s across the path at the height of the scattering volume. At C band, the observed Doppler spread was 2.2 Hz while, for the same average wind conditions as at Ku band, the Doppler spread should have been 1.0 Hz (corresponding to 90 fades per minute). The residual frequency variations in the transmit and receive equipment were too large to make successful Doppler spread measurements at C band and at all but the highest spread values at Ku band.

The average hourly median two sigma delay spread was 138 nsec. This value is identical to the predicted output from the RAKE correlation receiver system for a 12.5 Mbit/s bit rate at typical receiver signal-to-noise ratios if the scattering is dominated by a thin (100 m) scattering layer at a 1 km height. For the small aperture antennas and a smooth, slowly varying profile of scattering from clear air turbulence (uniformly filled scattering volume), the expected delay spread increases to 174 nsec. The observations were comparable to the 150 to 160 nsec median delay spread measurements made on a 138 km path with 8' antennas at C band using a 10 Mbit/s RAKE system [Sherwood and Suyemoto, 1976]. The theoretical calculations of delay spread indicate that the actual spread values should be less than 40% of the measured values (for a receiver with infinite bandwidth and no receiver noise).

Measurements were made using the large, 29' aperture antenna at Ku band at the transmitter site during twelve afternoons in July. The C band system was unchanged and was employed to provide the reference for the performance comparison between the large and small aperture antennas. The large antenna had an estimated gain of 58 dB at Ku band which is 16 dB higher than the estimated gain of the small, 3' antenna. Model calculations predict a hourly median transmission loss for the large aperture antenna that is only 2 dB lower than the predicted hourly median transmission loss for the smaller antenna for a uniformly filled scattering volume or 3.5 dB lower for a thin scattering layer. After normalization so the C band measurements had identical average hourly median transmission loss values for the summer afternoon time period (equal to 145 dB), the average measured hourly median transmission loss was less than 1 dB lower than expected for a uniformly filled scattering volume (at 156 dB) for the large antenna while the transmission loss was less than 1 dB higher than expected for the small antenna (at 159 dB). The observed differences between observation and prediction for either thin layers or a uniformly filled scattering volume were well within the measurement errors of the C and Ku band transmission systems.

For the larger aperture antenna, the predicted Doppler spread and delay spread values are smaller than for the small antenna. For the summer afternoon data sets, the observed Doppler spread at Ku band for the large antenna was half the value measured for the small antenna (3.8 vs 7.7 Hz). As predicted, the average hourly median multipath delay spread was also smaller for the large antenna (98 vs 128 nsec).

Work performed under this subcontract has also been reported in the master's theses: "Observations and analysis of tropospheric scatter propagation during rain at 16 GHz and 5 GHz" by Bradley T. Anderson [1989] and "The Study of the Ku-Band Tropospheric Scatter Channel During Clear-air Conditions via Data Collected On the Link Between Prospect Hill in Waltham, MA and Mt. Tug in Enfield, NH" by Mark A. Hoppe [1989].

## 2. The experimental observations

### 2.1 Equipment configuration

The earlier measurement campaign [Crane, 1988] employed the large, 29' aperture antenna at Prospect Hill in Waltham, Massachusetts for transmission at both frequencies. The receiver site on Mt Tug in Lebanon, New Hampshire had both standard gain horns and matched beamwidth parabolic reflector antennas that could be used for reception. The horns were employed for calibration and antenna pointing checks; the matched beamwidth antennas were utilized for data collection. As originally configured, the receiver system could use either the C or Ku band carrier frequencies for the phase reference for coherent detection. The signals were mixed down to baseband in the receivers, low pass filtered and sampled (both in-phase and quadrature components) for subsequent computer processing. The final low pass filters had a 120 Hz bandwidth.

The receiver system was modified to use the cesium beam frequency standards (one at the transmitter site and one at the receiver) as the phase reference for coherent measurements. The absolute Doppler frequency shifts could then be observed instead of the relative Doppler shift between the two carrier frequencies when one or the other carrier frequency was used to provide the phase reference. The data processing software was upgraded to provide Doppler shift and Doppler spread estimates based on the pulse-pair algorithm and the complex correlations between consecutive samples of the in-phase and quadrature signals.

The multipath delay profile measurements were made using correlation detection on a 1023 bit pseudo-noise sequence generated by a maximum-length shift register code (PRN code). Identical code sequences were produced at the transmitter and receiver. The transmitter sequence was phase modulated on the 15.73 GHz carrier at a 12.5 Mbit/s bit rate. The code sequence generated at the receiver was used to phase modulate one of the local oscillators. Correlation detection was accomplished by mixing the modulated local oscillator with the down converted received signal and averaging in the low pass filters (in-phase and quadrature). Under computer control, the receiver code could be shifted forward or backward in time relative to the transmitted sequence to change the time lag for correlation detection. The computer program automatically selected the lag giving the greatest output and, for data collection, shifted the sequence  $\pm 7$  lags to straddle the peak. For each lag, 200 samples of the the in-phase and quadrature channel output were simultaneously recorded at a 250 Hz rate for each channel.

The multipath delay spread algorithm was upgraded to obtain a continuous measurement of receiver noise level and to subtract the estimated noise power from the correlation detector outputs at the different lags. Two sigma delay spread estimates were calculated from the noise corrected power vs delay profile and averaged for two minutes prior to final recording. Received power estimates were calculated from the sum of the recorded powers for each correlation detector output (each lag) and from the carrier channel output. The correlation detector channel had an 18 dB higher signal-to-noise ratio than the carrier channel thus providing superior performance at low signal levels.

The received power should be spread over only a limited number of lags when turbulent layer scatter is the dominant propagation mechanism. When rain scattering occurred on the path, the delay spread was expected to increase dramatically. Initially, the position of the lag window used for the delay spread measurements was adjusted from one 30 second measurement cycle to the next. The anticipated slow drift of the cesium standards relative to each other could then be corrected and unattended delay spread measurement would be possible. Unfortunately, during rain the larger delay spreads caused the tracking system to "lose lock" and further delay measurement was generally not possible until lock was manually reacquired. The correlation detector power estimate was used to keep track of the operation of

the tracking system but could not be relied upon for routine power measurement. When it was found that the cesium beam standards did not drift fast enough relative to each other to require continuous tracking, the algorithm was changed to disable tracking after lock was initially acquired. The system worked reasonably well after that with lock being lost only occasionally. Delay spread measurements were then possible in rain.

A new Ku band traveling wave tube (TWT) transmitter was installed at Prospect Hill for use with the small, 3' aperture antenna. The older klystron transmitter that was used with the large, 29' antenna required continuous supervision while the new system could be run unattended. The C band TWT transmitter was also used with the large aperture antenna but it could also be run unattended. A possible drawback to the new Ku band system was its lower transmit power. Model calculations predicted that the use of 3.5 dB less transmit power and the expected 2 to 4 dB increase in transmission loss (decrease in signal level) caused by the change from the large to small aperture transmit antenna would not significantly affect the measurements. The expected median signal-to-noise ratio was still better than 20 dB with the new transmitter system and, for the correlation detection channel, the expected signal-to-noise ratio was better than 38 dB.

The Prospect Hill to Mt Tug troposcatter path profile is displayed in Figure 1. The figure presents a cross section view of the path in the great circle plane. The scattering volumes for the several antenna configurations are displayed as shaded areas. The scattering volumes are bounded by the 3 dB contours of the antenna patterns and the radio horizon rays from each antenna. The antennas were pointed at their local horizons along the great circle path. The receiver antenna beamwidths were matched but the transmitter antenna beamwidths varied with aperture size and frequency. The resulting common volumes (scattering volumes common to both antenna patterns) were long, horizontally oriented cylinders. At Ku band, the common volume was 69 km long when the small aperture transmit antenna was used but was only 18 km long for the large aperture antenna. At C band, the length of the common volume was 36 km. The lower edges of the common volumes were 820 m above mean sea level and 400 m above the terrain. The maximum vertical extents of the common volumes were 1060 m for the small antenna at Ku band, 240 m for the large antenna at the same frequency and 520 m at C band. The maximum cross-path horizontal extents were twice the vertical extents. Although the common volumes were long and thin, scattering was possible anywhere in the volume that was line-of-sight to the antennas at each end of the path. Rain scattering was important when the rain cells occurred over either antenna within the main lobe of one antenna and the far side lobes of the other as well as when the cell appeared within the common volume.

The terrain profile along the great circle path was relatively flat from the transmitter site to about 70 km from that site. The remainder of the path was hilly with a height variation of 400 m. A succession of wooded hills broke up the path. At least 4 diffracting obstacle ridges occurred on the path. The diffraction loss for this path significantly exceeded the maximum expected transmission loss for a turbulent volume scatter path. The path was asymmetrical with a higher horizon angle at the receiver than at the transmitter. The centers of the scattering volumes were therefore closer to the receiver site.

## 2.2 Daily observations with the small aperture Ku band transmit antenna

The observations were recorded continuously at the receiver site. For each parameter, 200 samples were gathered in a 0.8 second interval for processing to estimate the average value. The C band and Ku band carrier channels were sampled simultaneously but, for the different lags of the Ku band correlation detection channel, the samples were obtained sequentially. A full cycle for detecting the signal levels and setting the attenuators to place the signal in the center of the dynamic range for each receiver channel, for sampling all the channels, and for calculating the parameter estimates and recording their values took 30 seconds. The linear, coherent receivers had limited dynamic ranges and digitally controlled

attenuators were required to keep the widely varying signal within the dynamic range. The calculations included computations of the received power levels (non coherent processing) and of the mean and standard deviation of the Doppler frequency shifts (coherent processing).

Four consecutive observations were averaged for display and further analysis. Figures 2 through 4 present a full sequence of output for a single day of measurements with the small aperture antenna at Ku band and the normal system at C band. The upper right hand panel in Figure 2 presents the received signal levels from the carrier channels. Each recorded two minute average is displayed. The upper trace is for the C band signal level and the lower trace is for Ku band. The signal levels have been adjusted (calibrated) to represent the output from the receiver for a 30 watt (w) transmit power level. The actual Ku band carrier signal level at the input to the transmit antenna was 3.6 w; for C band the transmit power was 30 w. The receiver signal levels were referenced to the input port of the waveguide switch that selects the receive antenna or calibration noise diode for connection to the receiver. Transmission loss is defined to be the measured power level difference (loss) between the transmitter and receiver waveguide reference points. The receiver noise levels (after adjustment to compensate for differences in transmit power relative to the 30 w reference) are also displayed in the figure.

The upper left hand panel in the figure displays the sample cumulative distribution functions (cdfs) for the received signal levels at each frequency. The abscissa for the cdfs is the reduced variate for a normal probability distribution. If the cdf follows a straight line in this plot, it could be approximated by a lognormal distribution (the ordinate is in dB). Both cdfs appear to follow straight lines for the fraction of the day with data.

The lower panels present the signal level fluctuation power spectra and the coherency between the fluctuations at each carrier frequency. The power spectra were computed from the time series of two minute averages. The spectra are averages of consecutive 32 sample spectra (approximately one hour duration). The two minute averaging was done to reduce any variations due to Rayleigh fading on the troposcatter channel; spectral averaging was used to reduce the statistical uncertainties of the spectral estimates. The resulting spectra represent the slow variations in the parameters of the turbulent process that produced the fading. The semi-empirical statistical theory for turbulence in the clear atmosphere predicts that the spectra should obey a  $f^{-5/3}$  ( $f$  = fluctuation frequency) power-law relationship. This relationship is displayed as a dot-dashed line. The Ku band spectrum follows the expected relationship for fluctuation frequencies below 0.001 Hz. The C band spectrum shows relatively more higher frequency fluctuations than predicted. The coherency between the fluctuations at the two carrier frequencies is essentially zero. The differences in spectral shape and lack of coherency suggest that the turbulent layers or patches are either thin enough or of small enough horizontal extent to affect one but not both scattering paths (with different common volume sizes).

Figure 3 presents the relative behavior of the scattering channels (upper panels) and the two sigma multipath delay spread observations at Ku band. For the upper left hand panel, the received signal level deviations from the predictions of our model for forward scattering by clear air turbulence are displayed for both carrier frequencies. If the intensity of scattering from the turbulence was distributed in space in accordance with the model, the received signal traces would lie along the horizontal, 0 dB line (dot-dashed). If the turbulence had a uniform intensity throughout both common volumes, the traces for both carrier frequencies would lie on top of each other. The observations show differences in the positions of the curves of as much as 12 dB. These differences are plotted in the upper right hand panel. Usually, for scattering by turbulence the deviations between the model normalized curves are less than 6 dB.

The two sigma multipath delay spread closely followed a normal distribution (lower right hand panel) with a median spread value of 140 nsec. The predicted spread values vary between 140 nsec for a thin, 100 m layer and 175 nsec for turbulence filling the common volume (after correction for system bandwidth and receiver noise). For a point, intense

scatterer (infinite signal-to-noise ratio, zero delay spread) the expected two sigma delay spread values vary from 0 to 80 nsec depending on the delay of the scattered signal relative to the start time for a lag bin. Averaging over a uniform distribution of possible relative start times, a strong point scatterer would produce a 62 nsec two sigma multipath delay spread value. The cdf for delay spread shows that the scatterers produce more spread than a single point scatterer and generally less spread than expected for a uniformly filled scattering volume.

The left hand panels in Figure 4 summarize the Doppler frequency shift measurements for the day. The expected mean Doppler shift is zero. The turbulent scatterers move horizontally and, for a scattering path that is symmetric about the great circle path, the mean Doppler shift should be zero. A close examination of the local horizon at the receiver site shows that the pointing direction to produce the smallest scattering angle is 0.2 degrees to the east of the great circle direction. Because the scattered signal levels are a strong function of the scattering angle, the path is not symmetrical about the great circle plane and the mean Doppler shift should vary with the horizontal wind at the height of the lower edge of the scattering volume. For the prevailing air movement from the west, the result is a small negative average Doppler shift. Because the lower edge of the scattering volume is shaped by the local horizon and not the antenna beams, the magnitude of the observed Doppler shifts should vary in proportion to the carrier frequency. For time periods when the model normalized received signal levels coincide (0400 to 0800 h local time) the Doppler shifts were in the ratio of the carrier frequencies. At other times, the mean Doppler shifts were not simply related. Several occurrences of large, short period (single two minute sample) Doppler shifts are evident in the data. These are attributed to scattering by aircraft. The aircraft has to fly almost parallel to the scatter path for a sufficient time period to produce an output that survives the 120 Hz narrow band filtering and subsequent averaging over the 0.8 second sampling interval and the two minute (4 sample) averaging interval. The commuter flights from Boston, Massachusetts to Lebanon, New Hampshire have flight paths that can produce the observed scattering signatures.

The Doppler shift data were primarily used to identify periods with rain on the scatter path. For rain in the common volume, the expected Doppler shifts are greater than +9 Hz at Ku band and +3 Hz at C band. The expected rain scatter signatures would be clearly evident in the data in the figure.

The Doppler spread estimates are presented in the lower left hand panel of the figure. The observations at Ku band show some meteorological variation but the C band measurements do not. The Doppler spread is produced by the horizontal motions of the scatterers throughout the common volume. Model calculations show that the observed Ku band spread values are consistent with cross path winds of the order of 10 m/sec at a 1 km height. The C band observations are more than twice the value expected for such winds. The Doppler spread estimation algorithm is very sensitive to the receiver signal-to-noise ratio and estimates were not made for very low signal-to-noise values. The spread estimates may also be contaminated by low frequency phase modulation of the transmitted carrier or any of the receiver local oscillators. The C band transmitter had a 60 Hz modulation (later found to originate from a ground loop) that contributed to the large residual Doppler spread values. The Ku band TWT also had relatively strong 60, 90 and 120 Hz modulation lines but the phase shifts due to atmospheric motions were still dominant.

The right hand panels in Figure 4 display the performance of the correlation detection channel relative to the carrier channel. If all is working properly and the delay spread is small enough to keep the multipath delay profile within the lag window used for processing, the Ku carrier and Ku delay signal levels should be identical. The upper right hand panel displays both received signal level estimates and the estimated receiver noise level (normalized to the received signal for a modulated transmitted signal power of 30 w i.e. 9 dB below the actual received noise power and 18 dB below the value reported for the carrier signal level observations in Figures 2 and 3). The cdf shows the median delay channel power estimate is 2

dB higher than the median carrier power estimate for all periods when both channels were operating. The delay channel power levels varied about the carrier channel values by as much as 3 dB. The variations in the differences between the carrier and delay channel observations are attributed to statistical sampling errors. For an 0.8 second sample of a Rayleigh fading process with a fade rate of 1.5 times the Doppler spread, approximately 10 independent samples were used for the estimation of each received power level value (30 second samples). The expected deviations between the two minute averages of the power level estimates for each frequency should then exceed 3.8 dB for 10 percent of the samples. The varying differences between the two curves are therefore consistent with the expected statistical uncertainties in the power level estimates for each channel. For intervals with smaller Doppler spreads, the statistical uncertainties of the measurements will be larger. The difference in the median values is larger than expected by chance and indicates a calibration error in either of the receiver channels or between the total power measurements at the transmitter and the expected residual carrier leakage through the balanced modulator that is used for the carrier signal for detection.

### 2.3 Observations with the large aperture Ku band transmit antenna

Data from the time interval between 1000 to 1700 h is missing from Figures 2 through 4. During this interval, the large aperture antenna was employed for transmission at both frequencies. The observations with the large aperture antenna are presented in Figures 5 through 7. In these figures, the C band measurements are as reported above. The Ku band measurements were also processed as above but the calibration constants were for the small aperture antenna and TWT transmitter and not for the large aperture antenna and klystron transmitter. As a result, the reported Ku band observations are 8 dB higher than they should be. The difference in calibration is due to the differences in transmitter power, klystron bandwidth and the level of the residual carrier level leakage through the modulator.

The shapes of the cdfs and power spectra curves are nearly the same at the two frequencies and the coherency between the signal level fluctuations is high at the lower fluctuation frequencies. The C band data show a marked increase in signal level (~15 dB) during the 1000 to 1200 h interval. The Ku band carrier signal followed the C band carrier signal variations within the measurement (sampling) uncertainties for each channel.

The power levels from the correlation detector channel track the carrier power levels for Ku delay channel output values below -105 dBm (as reported with the calibration constants for the small aperture antenna transmitter). Above that level, the dynamic range of the receiver system was exceeded, the delay channel saturated, and the delay channel receiver noise level increased in response to receiver saturation (Figure 7). Normally, the receivers are operated with sufficient IF gain to keep the noise levels in the narrow band stages of the carrier channel high enough to mask the slowly varying dc biases produced in the final stage of mixing down to baseband. The high intermediate IF gains did not provide a sufficient dynamic range (40 dB above the expected levels in the carrier channel) to accommodate the higher level signals when the large aperture transmitter was in use. Figure 8 displays the maximum carrier channel signal level and delay channel signal level values for each hour with simultaneous data. The effect of receiver saturation is clearly evident (the data for the large aperture antenna transmissions is labeled July LA). By the end of July when the small aperture transmitter system was again on the air, the receiver gains and automatic gain control algorithm were adjusted to eliminate the saturation problem (but not the dc bias problem).

The two sigma multipath delay spreads were normally distributed and perhaps smaller than for the small aperture antenna. Figure 6 does not contain sufficient data to make a comparison. The effect of receiver saturation should be small because the noise subtraction step in the multipath delay spread estimation algorithm used the receiver noise estimates calculated for each measurement cycle. Saturation would reduce the received power values at the lag having the highest signal but, for the large aperture antenna, saturation would affect

only two lags at most with the result that the delay spreads estimates, which are already seriously over estimated, would have only slightly more error.

The mean Doppler shift measurements appear to be a continuation of the small aperture antenna observations but insufficient data are available in the figure for a comparison between the observations at different aperture sizes. The Doppler spread values are significantly smaller than for the small aperture transmit antenna. Model calculations suggest that the observed values are consistent with the same 12 m/s cross wind velocity invoked to explain the observations with the small aperture antenna. The observations show smaller hour-to-hour variations than expected or observed with the small aperture system. The problem may be that the small aperture results contain both meteorological and equipment produced spread components, the former time varying and the latter constant in time. With the expected smaller contributions to the meteorologically varying component, the large aperture antenna results may be dominated by equipment produced phase noise.

#### 2.4 Observations in rain

Figures 9 through 11 illustrate the effects of rain on the troposcatter signal for a day of observations using the small aperture antenna transmitter system. The set of three figures provide the same information as before. The carrier signals experienced more hour-to-hour variations than for the clear air day (Figures 2 through 7). The shorter time scale variations were reduced in magnitude and the coherency between the fluctuations was small. The daily medians of the C band and Ku band received signal levels were about 10 dB higher than for the clear air day. The cdf for the C band received signal levels was nearly lognormal but, for Ku band, the signal levels show a 10 dB or more decrease below the lognormal distribution for the smallest 5% of the observations (1.6 standard deviation and higher).

The mean Doppler shift record (upper left hand panel in Figure 11) show marked increases in the Doppler shift from 0500 h through the end of the day. This is the signature of rain on the path. Scattering by rain dominates over scattering by clear air turbulence at Ku band over a wide range of rain intensities while, at C band, it is dominant for only very high rain rates. The result is a rain signature at Ku band but no evidence of rain at the lower carrier frequency. The relative magnitudes of the Ku and C band signals show higher signals at Ku than at C band relative to the turbulent model predictions during most of the intervals with large Doppler shifts. An exception is evident between 2200 and 2300 h. During this short interval, the Ku band signal fell to more than 20 dB below the level expected from the C band measurements for scattering by turbulence. The problem is attenuation by rain on the path. The scattered signals are stronger than for clear air turbulence but attenuation by rain between the antennas and the scattering volume can reduce the signal levels by more than they are enhanced by rain scatter.

During the rain attenuation event, the carrier signal is reduced to near the noise level causing, in part, the increased Doppler spread observed during the event. The multipath delay spread increased to more than 400 nsec and exceeded the lag window used for Doppler spread analysis. Although some of the power was spread outside the analysis window, sufficient remained inside the window to show that the attenuation was not large enough to cause a loss of signal. During the periods with rain on the path the delay spread values were consistently larger than for times with clear air scatter.

#### 2.5 Observations with an elevated duct

The third propagation mechanism thought to be important on a troposcatter path across moderately rough terrain (height variations of the order of 400 m) is ducting or trapping in an elevated layer (or duct). The terrain is too rough to support surface ducts and, therefore, that

mechanism can be ignored. Also, the path has too many diffraction ridges for high level fields to occur due to diffraction during super refraction conditions.

The identifying features for coupling via atmospheric ducts are enhanced signal levels, especially at the lower frequency, combined with a significant reduction in the fade rate [Crane, 1981]. Because the ducting process is caused by refractive bending and trapping within an atmospheric waveguide, for a thick enough waveguide the phase variations observed on the path are not produced by a Doppler shift upon scattering but by the much slower variations in the integrated refractive index along the ray paths and in the physical lengths of the multiple ray paths between the temporally and spatially varying top and bottom of the guide. As a result, the average Doppler shifts should be reduced to near zero and show little variation during the intervals with slow changes in signal strength.

Figures 12 through 14 show intervals of elevated layer ducting between 0000 and 0800 h and again from 2200 h through the end of the day. The C band signal levels are more than 20 dB stronger than the Ku band levels and more than 10 dB larger than expected for scattering by clear air turbulence at either frequency. The fading rate is slow enough to be evident in the time series of two minute averages and the mean Doppler shift at C band is essentially zero. A short period of enhanced signal levels was observed at Ku band from 0100 to 0200 h. During this time interval, the Ku band Doppler shift was zero and the delay spread was twice reduced to a value approaching the spread value expected for a point scatterer or a strong path with no additional multipath components (such as for a line-of-sight path).

### 3 Data summaries

#### 3.1 Hourly data

The time series of two minute averages were partitioned into clock hour blocks (each starting on the hour). For each full clock hour of observations, the maximum, minimum, and median values were obtained and stored in a computer data base for further analysis. Each of the important variables: carrier received signal levels, Doppler shifts, and Doppler spreads were recorded as were the delay channel received signal level, two sigma multipath delay spread, and receiver noise level.

The dominant propagation mechanism for each hour was established automatically. Five propagation conditions were identified: clear air, rain, elevated ducting, rain attenuation and aircraft scatter. Most of the observations were designated as corresponding to clear air conditions. Hours were identified as dominated by rain scatter if both the maximum and median Ku band Doppler shifts were larger than preset thresholds (3 Hz for the median and 6 Hz for the maximum). If only the maximum Doppler shift exceeded the threshold and the median value was less than zero, the hour was identified as dominated by aircraft scatter. Hourly intervals with median and maximum C band signal levels significantly larger than the Ku band levels and with near zero Doppler shift at C band were identified as dominated by ducting in elevated layers (the thresholds were 17 dB for the median difference and more than 20 for the maximum values). The fifth category was rain attenuation. In this case the hourly median Ku band signal was more than 27 dB below the expected value for clear air turbulence as calculated from the C band measurements (more than 12 dB net reduction in signal level) and rain scattering was identified in that or an adjacent hour interval. A final manual check was made of the identified propagation mechanisms to insure that the rare occurrences of elevated duct propagation at Ku band would not cause the interval to be excluded from the ducting category.

The hourly value time series for the month of June are presented in Figures 15 through 22. The received carrier levels at C band are displayed in Figure 15. Three curves are plotted, the minimum and maximum hourly observations are the thin traces while the median value is given by the thicker trace between the thin traces. The curves are continuous where measurements were available for contiguous hours. The blanks indicate missing data. The missing observations are generally for periods when the Ku band transmitter failed. Afternoon observations on several of the days late in June were excluded because transmission was switched between the large and small antenna systems at half hour intervals. Receiver and transmitter system calibrations were then hard to maintain and the switched measurement campaign was abandoned for the series of afternoon observations with the large antenna that was conducted in July.

The propagation mechanism code is indicated by the positions of the diamond markers across the top of the figure: at -78 dBm for rain, -76 dBm for rain attenuation and -80 dBm for elevated ducting conditions. No markers are displayed for either clear air turbulence scatter conditions or for aircraft scatter. Elevated ducting conditions occurred during the nighttime, early morning hours on the 20th through the 23rd of June.

Figures 16 and 17 present the Ku carrier and delay channel received power levels respectively. The periods of enhanced signal levels with elevated ducting is evident in the carrier channel observations but not in the delay channel output where receiver saturation has taken its toll. The lowest Ku band signal levels observed during the summer were recorded during 15 - 16 June. Most of these observations were not associated with a rainy period. The signal levels were relatively low at both C band and Ku band although the Ku band signals are about 5 dB below the levels predicted from the C band measurements for scattering by clear air

turbulence uniformly filling the common volumes. The signal levels were high enough to be detected in the delay channel with about a 20 dB signal-to-noise ratio. The noise level is given by the thick curve along the bottom of Figure 17. The receiver noise level variations are not an indication of changes in receiver gain (and calibration) but are produced by the slowly varying dc biases generated in the final stage of mixing down to baseband.

Figures 18 and 19 display the median and extreme hourly values of the average Doppler shift for the Ku and C band carriers respectively. The periods with rain are clearly identified in the Ku band data. These data also show the slow meteorological changes in the horizontal wind in the scattering volume between rain events. The sharp, isolated positive and negative Doppler deviations are indicative of aircraft scatter. During the extended interval with low signal levels at Ku band, the average Ku band Doppler frequency dropped to -6 Hz. The transmitted carrier frequency is offset from the receiver local oscillator frequency by 6 Hz when mixed down to baseband. Correction for the frequency offset is made in the calculation of Doppler shift. The average frequency for noise is 0 Hz as is the frequency of the dc biases produced in the final mixing stage. After compensation, a zero frequency output from the receiver is reported as a -6 Hz Doppler shift. During the low signal level interval, the Doppler shift estimates were contaminated by the dc biases and receiver noise.

Figures 20 and 21 display the hourly Doppler spread values. At C band, the mean Doppler shifts showed significantly smaller deviations from zero than for Ku band. The shifts at the two frequencies were generally of the same sign indicating that both channels were responding to the motions of the scatterers. Both the C band and Ku band Doppler spread observations show isolated incidents of zero values. These arise in the spread estimation algorithm when a rapid change in carrier frequency occurs such as can be produced by scattering from aircraft.

Figure 22 presents the multipath delay spread observations for the month of June. In general, large values of spread are associated with occurrences of rain, small values with the elevated ducting occurrence and intermediate values for scattering by turbulence in the clear atmosphere. The magnitudes of the delay spread values during periods of clear air conditions indicate that the turbulence is confined to layers that are substantially thinner than the vertical extent of the common volume.

### 3.2 Diurnal variations

The observations for June showed day-to-day and within-a-day variations in signal strength. The hourly median data for the entire summer were separated by propagation mechanism, sorted by time of day, and averaged to display the diurnal variations and relative magnitudes of the different propagation mechanisms. Hours dominated by aircraft scatter were not included in the analysis because too few observations were available; the rain attenuation events were included with the rain events. Only 7 of the 1232 hours of observation were designated as dominated by rain attenuation (0.57% or 3.2% of the time with rain)

Figures 23 and 24 depict the diurnal variations of the received signal levels at the two carrier frequencies. The clear weather condition data show an average received signal level of about -105 dBm at C band (corresponding to a transmission loss of 150 dB) during the evening and early morning hours. At about 1000 h, the signal levels increase, reach a peak value of about -97 dBm (an increase of 8 dB) at about noon, then decline in magnitude for the rest of the day. This cycle also occurs at Ku band with a nighttime level of about -120 dBm (165 dB transmission loss) and the daytime peak at -113 dBm. Turbulence in the planetary boundary layer increases in intensity in response to warming by the sun. The thickness of the boundary layer grows during the morning hours and by 1000 h the top of the layer crosses the lower edge of the common volumes.

Rain can occur at anytime of the day or night. In contrast to the diurnal variations in the intensity of scattering by turbulence, the observed changes in the average signal levels during periods with rain show only a decrease in the late evening that may not be statistically significant.

Coupling via an elevated duct occurs only at night. The signal levels at C band are at their highest during the early morning hours. For the observations during the summer 1989 campaign, the signal levels were more than 10 dB higher than for scattering by clear air turbulence.

The average Doppler shift values show diurnal changes in response to the changes in the propagation mechanisms. In Figures 25 and 26, the average Doppler shifts are smaller during the daytime period when boundary layer turbulence occurs in the common volume and are higher when the scattering comes from the stable region above the boundary layer. Under ducting conditions, the the Doppler shifts are the smallest. During rain, the Doppler shifts are largest in response to scattering by the falling raindrops. Under clear weather conditions, the observed average Doppler shifts are proportional to carrier frequency. They are more than an order of magnitude larger than expected for scattering volumes that are symmetric about the great circle path. The problem is the asymmetry forced by the variations in the elevation angles to the radio horizon with azimuth from the great circle path at the receiver.

The Doppler spread values presented in Figure 27 were larger at night than during the day. The spread values were about the same for periods with elevated ducting and for clear weather conditions. This results from the relatively small increase in Ku band signal level in comparison to the change at C band when ducting occurs. At Ku band, rain scatter produced higher Doppler spread observations.

The average delay spread values also increased during periods of rain as shown in Figure 28.

### 3.3 Statistical distributions of hourly median values for clear weather conditions

The hourly observations were grouped by quarter day intervals for the preparation of sample cumulative distributions. The following time intervals were selected for analysis: nighttime, 2200 to 0400 h; morning, 0400 to 1000 h; afternoon, 1000 to 1600 h; evening, 1600 to 2200 h. Referring to Figure 23, the intervals were selected to group contiguous hours with similar signal levels. For clear weather conditions, the nighttime period corresponds to the lowest levels; the afternoon period corresponds to the highest levels. Table 1 presents the averages and standard deviations for each measurement by quarter day interval and by propagation mechanism.

The sample cumulative distribution functions (cdfs) for the observed median hourly received carrier power levels are presented by quarter day intervals for clear weather conditions in Figures 29 through 32. The thick curves are the sample cdfs. The scale for the reduced variate for a normal distribution is the number of standard deviations of that distribution. The dot-dashed lines are the median expected cdfs for lognormal distributions (the ordinate has a logarithmic scale) having an average value (lognormal  $m$  in Table 1) near the observed average value at C band and a model predicted value at Ku band based on the C band value. The model was for forward scattering by clear air turbulence. The standard deviations for the lognormal distributions (lognormal  $s$  in Table 1) were picked to match the slopes of the C band and Ku band distributions. The dashed curves above and below each lognormal model distribution bound the expected 5% to 95% range for sample cdfs obtained from the observed number of samples (assumed to be independent of each other) from the model probability distribution. If

the sample cdf was constructed from observations drawn from the model distribution, it would lie between the dashed curves with probability 0.9.

The lognormal model provides an excellent approximation to the C band signal level sample cdfs for all the quarter day intervals. The separation between the bounding curves depends upon the standard deviation of the assumed lognormal distribution and the number of independent samples used for the construction of the sample cdf: the fewer independent samples, the wider the bounds. The bounds were calculated on the basis of the number of hours of data listed in Table 1. The lognormal model was combined with the forward scatter model for clear air turbulence to predict the parameters of the lognormal distribution at Ku band. The forward scatter model provides two predictions depending upon the assumed structure of the turbulent region within the common volumes, 15.2 dB lower signal strengths at Ku band than at C band if the turbulence is entirely enclosed within a layer (or layers) that are thin in comparison with the vertical extents of both common volumes and 13.5 dB lower signal strengths at Ku band if the turbulence uniformly fills both common volumes. In practice, the ratio should lie between the two values. The value used for the calculation of the Ku band lognormal  $m$  value is listed in Table 1 as the lognormal  $m$  value in the column labeled "Ratio of Carrier Levels". The lognormal model for Ku band also provides an excellent fit to the sample cdfs.

The standard deviation values (lognormal  $s$ ) varied little with time of day, from 5.5 dB for the nighttime and morning periods, to 5.8 dB in the afternoon, and to 5.0 dB in the evening. At Ku band, a larger variation but of smaller values was required to provide a good match to the data, between 3.5 and 5.2 dB. The Ku band values were consistently smaller than the C band values. This result is in agreement with the predictions of the empirical model currently suggested for use by the CCIR [1989] for transhorizon propagation paths. The CCIR model attributes the reduction in variance to the increase in carrier frequency. That model cannot be correct because, for the large aperture antenna, the standard deviation value needed to match the lognormal model to the sample cdf the standard deviation increases with frequency not decreases. The physically based turbulent volume scattering model depends on frequency through an explicit model for the change in the bistatic scattering cross section per unit volume with frequency and an implicit model for the change in scattering volume with antenna size and scatter path geometry. The explicit model for frequency dependence affects only the median signal levels. The standard deviation values depend only on the relative sizes of the scattering volumes. Our observations show the larger the scattering volume, the smaller the variance. The expectation is that for scattering by turbulence, the variances would be identical if the scattering volumes were matched at the different frequencies.

The sample cdfs for observations with the large aperture antenna are presented in Figure 33. The thick, solid curves are the sample cdfs, the thin dot-dashed curves are the expected median distributions for the lognormal models with the parameters listed in table 1. The dashed curves are the expected 5%, 95% bounds for the sample cdfs. As above, the average value for the lognormal model at Ku band was calculated from the value at C band. Turbulent scatter model calculations predict a 11.5 dB difference between the C band and Ku band carrier power levels when the scattering volume for the large antenna is filled at Ku band. The thin, gray, solid curves are from the median lognormal model distributions for the small aperture antenna measurements reported in Figure 31. The C band system was unchanged for the two measurement sets and was recorded to provide a reference for the comparison between the large and small transmit antenna at Ku band. For the 12 days of observations with the large antenna, the C band signal levels were higher on average than for the rest of the 4 month data set. At the median level for the cdfs (0 reduced variate), the expected 5% to 95% ranges for the cdfs overlap showing statistical agreement between the afternoon observations on the different measurement days. The Ku band observations are consistently higher for the large antenna than for the small antenna and overlap occurs only at the low signal level tail of the distribution. The sample cdf at Ku band is in excellent agreement with the lognormal model predictions

showing that the apparent differences between the sample cdfs for the large and small antennas were expected. The standard deviation value needed to fit the tails of the distribution as well as the central region is larger for the large antenna at Ku band than for C band (and for the small antenna at Ku band).

The Doppler spread at Ku band provides information about the fade rate to be expected at the higher carrier frequency. Comparison is not possible to the spread values at C band because equipment noise was significantly larger than the variations due to propagation conditions on the path. Equipment induced frequency variations were also important at Ku band. The results are shown in Figure 34. In this case, only the high Doppler spread tail of the distribution shows any response to variations caused by conditions on the path. The observations could be used to set an upper limit to the spread values to be expected on the path. A better approach would be to estimate the cross path wind velocities in at the height of the common volumes and calculate the Doppler spread using the scattering model. In that way, more than the upper tail of the distribution would be used to estimate the parameters for the distribution.

The delay spread is another parameter that is needed for communication system design. The sample cumulative distributions for each quarter day interval are displayed in Figure 35. Because little variation was observed with time of day, the four sample cdfs were plotted on a single graph. The sample cdfs are well approximated by normal distributions. A model distribution for the number of samples in the afternoon time period was fit to the data. The morning and evening observations are consistent with the model distribution. The model for the nighttime data should have a higher average delay spread and a higher standard deviation value. For the afternoon time period, the average and standard deviation values should be lower. The ranges of the model parameters are small as illustrated in the column of Table 1 labeled "Ku band Delay Spread".

### 3.4 Statistical distributions of hourly median values for rainy conditions

Sample cdfs were constructed for rainy conditions on the path for each of the quarter day intervals. The received signal level distributions are displayed in Figures 36 through 39. The model distributions plotted in each figure are for clear weather conditions (Figures 29 through 32) but with the model bounds calculated for the number of hours of observations used for the construction of the sample cdfs. They are included for reference. In Figure 36, the C band measurements lie within the expected bounds of the lognormal model fit to the clear weather C band observations for the same time period. At Ku band the observations depart from the bounds about the model fit to the clear weather data. Rain scattering produces a significant increase in signal level relative to clear weather conditions for more than 60% of the time with rain. The signal levels are smaller than expected during clear weather conditions for less than 15% of the time with rain. The smaller signal levels are presumably due to rain attenuation on the path having more of an effect than the increase due to scattering.

For the morning hours, Figure 37, the signal levels are higher in rain than in the clear at both frequencies. At Ku band the enhancement in signal level is more pronounced than at C band. For the afternoon time period, the signal level cdfs differ little from the cdfs for clear weather conditions and, at night, rain scattering again produces higher signal levels than for clear weather conditions at Ku band while, at C band, the differences between rainy periods and clear weather conditions are not statistically significant.

Rain causes a slight increase in the Doppler spreads at Ku band as shown in Figure 40. In Figure 41, the sample cdfs for the two sigma multipath delay spread values are seen to be significantly higher than for clear weather conditions (the model curves).

### 3.5 Statistical distributions of hourly median values for ducting conditions

Figures 42 through 45 present the sample cdfs for times with occurrences of enhanced signal levels at C band due to trapping in elevated ducts. Figures 42 and 43 present the carrier power level cdfs for the nighttime and morning hours. Enhanced signal levels relative to the expected clear weather, turbulent layer scatter levels occur at both frequencies. The signal levels at C band are significantly higher as required by the conditions set to identify a time interval as associated with ducting conditions. The additional requirement of a small average Doppler shift (magnitude less than 0.5 Hz) limited the selection such that the signal level distributions for clear weather and ducting conditions overlapped in signal magnitude.

The Ku band delay and Doppler spread distributions do not deviate significantly from the clear weather sample cdfs. Deviations from the Doppler spread model distribution are evident for all the propagation models but this is caused by the equipment.

#### 4. Analysis

The propagation mechanism for each clock hour of data from the summer 1989 measurement campaign was identified on the basis of the signal level and average Doppler shift observations. With the separation into the three basic categories used for analysis, clear weather, rain and elevated ducting conditions, the sample cdfs for received signal level for each category could be modeled by lognormal probability distributions. The sample cdfs for multipath delay spread could be modeled by normal probability distributions. The lognormal behavior for the received power level distributions was evident in the quarter day data. The differences between the median value parameters (lognormal  $m$ ) from one quarter day interval to the next were of the same magnitude as the standard deviation values for a time interval. The single composite sample cdfs for all the observations for a single propagation mechanism were also lognormal. They are presented in Figure 46. This figure presents a summary of the signal level observations for the entire summer.

The hourly median clear weather received carrier power observations are consistent with the lognormal model for signal levels at both C band and Ku band. The median values for the summer months are -103.5 dBm (148.3 dB transmission loss) at 4.95 GHz and -118.4 dBm (163.1 dB transmission loss) at 15.73 GHz. The standard deviations are 6 dB at 4.95 GHz and 5 dB at 15.73 GHz. The sample cdfs lie entirely within the expected 5% and 95% bounds for lognormal cdfs with the median and standard deviation values listed above. They are consistent with the hypothesis that each hourly median value is an independent sample from a lognormal process.

For rain, the cdf of the hourly median received carrier power levels at Ku band is consistent with a lognormal model distribution with a median value and standard deviation larger than for clear weather conditions: -115.1 dBm (159.9 dB transmission loss) and 7.1 dB respectively. At C band, the rainy condition observations do not differ significantly from the clear weather conditions except for the highest 2% of the observed values.

During periods with coupling via elevated ducts, the median and standard deviation values for the hourly median received carrier power levels at C band are significantly higher than for clear weather conditions: -91.3 dBm (136.1 dB transmission loss) and 9.0 dB respectively. The median level and standard deviation values at Ku band are comparable to the Ku band values for rain. The sample cdf at C band is also consistent with the lognormal distribution hypothesis.

The ratios of the received carrier power levels at the two frequencies are consistent with the predictions of a thin layer, turbulent volume forward scatter model for both the large and small aperture transmit antennas at Ku band and the large aperture transmit antenna at C band. As predicted, the signal levels that result from the use of the small antenna at 16 GHz were not significantly lower than the signals obtained using the large aperture antenna. The same model, when used for scattering by rain, predicts similar results relative to the magnitudes of the scattered signals. Table 1 lists results for rain scatter for the two aperture sizes at Ku band. For the 8 hours of observations in rain with the large aperture antenna, the average of the hourly median signal levels at Ku band was 9.6 dB lower than for C band. For the 216 hours of observations in rain with the small aperture antenna, the Ku band signal was 12.7 dB lower than the C band signal. The 3.1 dB difference that resulted from a change in aperture is within the expected measurement error of the 2 dB value predicted for scatterers uniformly filling the common volumes.

## References

- Anderson, B. T. [1989]; Observations and Analysis of Tropospheric Scatter Propagation during Rain at 16 GHz and 5 GHz, M. E. Thesis, Thayer School of Engineering, Dartmouth College, Hanover NH.
- CCIR [1989]; Propagation Data and Predictions Methods Required for Trans-Horizon Radio-Relay Systems, Rept 238-5 (MOD F), Study Group 5 (Propagation in Non-Ionized Media), ITU, Geneva.
- Crane, R. K. [1981]; A review of transhorizon propagation phenomena, *Radio Sci.*, **16(5)**, 649-669.
- Crane, R. K. [1988]; Tropospheric Scatter Propagation at 5 and 15 GHz: Results for a 161 km Path, Final Report on Research Conducted Under Subcontract to Georgia Institute of Technology as a Part of the Post-Doctoral Program, Rome Air Development Center, Hanscom AFB, MA.
- Hoppe, M. A. [1989]; The Study of the Ku band Tropospheric Scatter Channel during Clear-Air Conditions via Data Collected on the Link between Prospect Hill in Waltham, MA and Mt. Tug in Enfield, NH., M. E. Thesis, Thayer School of Engineering, Dartmouth College, Hanover NH.
- Matthews, D. [1989]; Internal Memo, The MITRE Corp., Bedford MA.
- Parl, S. [1989]; Tactical Ku-band Troposcatter, Internal Memo, Signatron
- Rice, P. L., A. G. Longley, K. A. Norton and A. P. Barsis [1965]; Transmission Loss Predictions for Tropospheric Communication Circuits, Vol. I and II, NBS Tech. Note 101, U. S. Dept. of Commerce, Washington D. C.

Table 1 Quarter Day Summaries

	Ratio of Carrier Levels (dB)	Ku band Carrier Level (dBm)	C band Carrier Level (dBm)	Ku band Doppler Shift (Hz)	Ku band Doppler Spread (Hz)	C band Doppler Shift (Hz)	C band Doppler Spread (Hz)	Ku band Delay Spread (nsec)	Ku band Transmission Loss (dB)	C band Transmission Loss (dB)
Small Aperture Antenna										
<b>Clear Weather</b>										
Night										
Hours	238	238	238	233	238	238	238	186		
Average	14.9	-119.6	-104.7	-2.9	9.2	-0.7	2.2	144.7	164.4	149.5
Standard Deviation	4.5	4.2	5.7	2.5	2.6	1.1	0.3	38.3		
Lognormal m	14.8	-119.8	-105.0						164.6	149.8
Lognormal s		3.5	5.5							
Morning										
Hours	203	203	203	198	203	203	203	156		
Average	15.7	-120.5	-104.8	-2.2	9.2	-0.4	2.1	137.0	165.2	149.5
Standard Deviation	4.1	4.8	5.7	2.7	2.5	0.9	0.3	33.2		
Lognormal m	15.2	-120.2	-105.0						165.0	149.8
Lognormal s		4.5	5.5							
Afternoon										
Hours	169	169	169	169	169	169	169	136		
Average	14.7	-114.4	-99.8	-2.0	7.7	-0.2	2.1	127.6	159.2	144.6
Standard Deviation	3.8	5.5	6.0	2.5	2.1	1.0	0.3	30.8		
Lognormal m	15.2	-114.5	-99.3		8.5			138.0	159.3	144.1
Lognormal s	4.0	5.2	5.8		2.5			30.0		
Evening										
Hours	240	240	240	234	240	240	240	179		
Average	14.1	-118.1	-104.0	-2.1	8.1	-0.5	2.2	138.1	162.9	148.8
Standard Deviation	3.9	4.2	5.2	2.2	2.3	1.0	0.3	30.0		
Lognormal m	14.2	-118.0	-103.8						162.8	148.6
Lognormal s		4.0	5.0							
<b>Rain</b>										
Night										
Hours	56	56	56	56	56	56	56	38		
Average	12.8	-117.0	-104.3	5.4	10.1	0.5	2.4	183.6	161.8	149.0
Standard Deviation	6.7	7.5	4.2	6.6	2.9	1.5	0.3	45.3		
Morning										
Hours	39	39	39	39	39	39	39	34		
Average	9.6	-112.2	-102.6	9.2	9.2	1.0	2.3	173.0	156.9	147.4
Standard Deviation	5.3	7.1	6.3	5.9	1.8	2.8	0.4	41.5		
Afternoon										
Hours	58	58	58	58	58	58	58	45		
Average	14.1	-114.5	-100.3	7.6	10.9	1.5	2.4	196.0	159.2	145.1
Standard Deviation	6.3	7.0	7.5	8.2	2.6	2.7	0.3	45.0		
Evening										
Hours	63	63	63	63	63	63	63	50		
Average	13.3	-115.8	-102.6	7.9	9.8	1.1	2.3	188.2	160.6	147.3
Standard Deviation	5.8	6.2	4.7	5.0	2.6	2.3	0.4	37.6		

Table 1 Quarter Day Summaries

	Ratio of Ku band Carrier Levels (dB) - (dBm)	C band Carrier Level (dBm)	Ku band Carrier Level (dBm)	Ku band Doppler Shift (Hz)	Ku band Doppler Spread (Hz)	C band Doppler Shift (Hz)	C band Doppler Spread (Hz)	Ku band Delay Spread (nsec)	Ku band Transmission Loss (dB)	C band Transmission Loss (dB)
<b>Elevated Duct</b>										
Night										
Hours	32	32	32	32	32	32	32	27		
Average	23.9	-115.6	-91.6	-1.4	9.7	-0.2	2.3	126.4	160.4	136.4
Standard Deviation	4.6	7.9	10.4	1.0	3.4	0.2	0.1	41.5		
Morning										
Hours	23	23	23	23	23	23	23	19		
Average	23.9	-115.8	-91.9	-1.2	9.2	-0.2	2.1	143.4	160.6	136.6
Standard Deviation	2.6	5.7	6.4	1.5	3.3	0.1	0.0	32.2		
Afternoon										
Hours	2	2	2	2	2	2	2	2		
Average										
Standard Deviation										
Evening										
Hours	1	1	1	1	1	1	1	1		
Average										
Standard Deviation										
<b>Large Aperture Antenna</b>										
<b>Clear Weather</b>										
Afternoon										
Hours	50	50	50	50	50			46		
Average	11.4	-109.2	-97.8	-0.5	3.8			97.3	154.0	142.6
Standard Deviation	2.8	6.0	5.1	1.4	0.3			14.0		
lognormal m	11.5	-108.9	-97.4						153.7	142.2
lognormal s		6.0	5.0							
<b>Rain</b>										
Afternoon										
Hours	8	8	8	8	8			7		
Average	9.6	-106.3	-96.7	5.5	6.4			118.8	151.1	141.5
Standard Deviation	2.0	2.8	3.3	7.2	4.2			46.9		

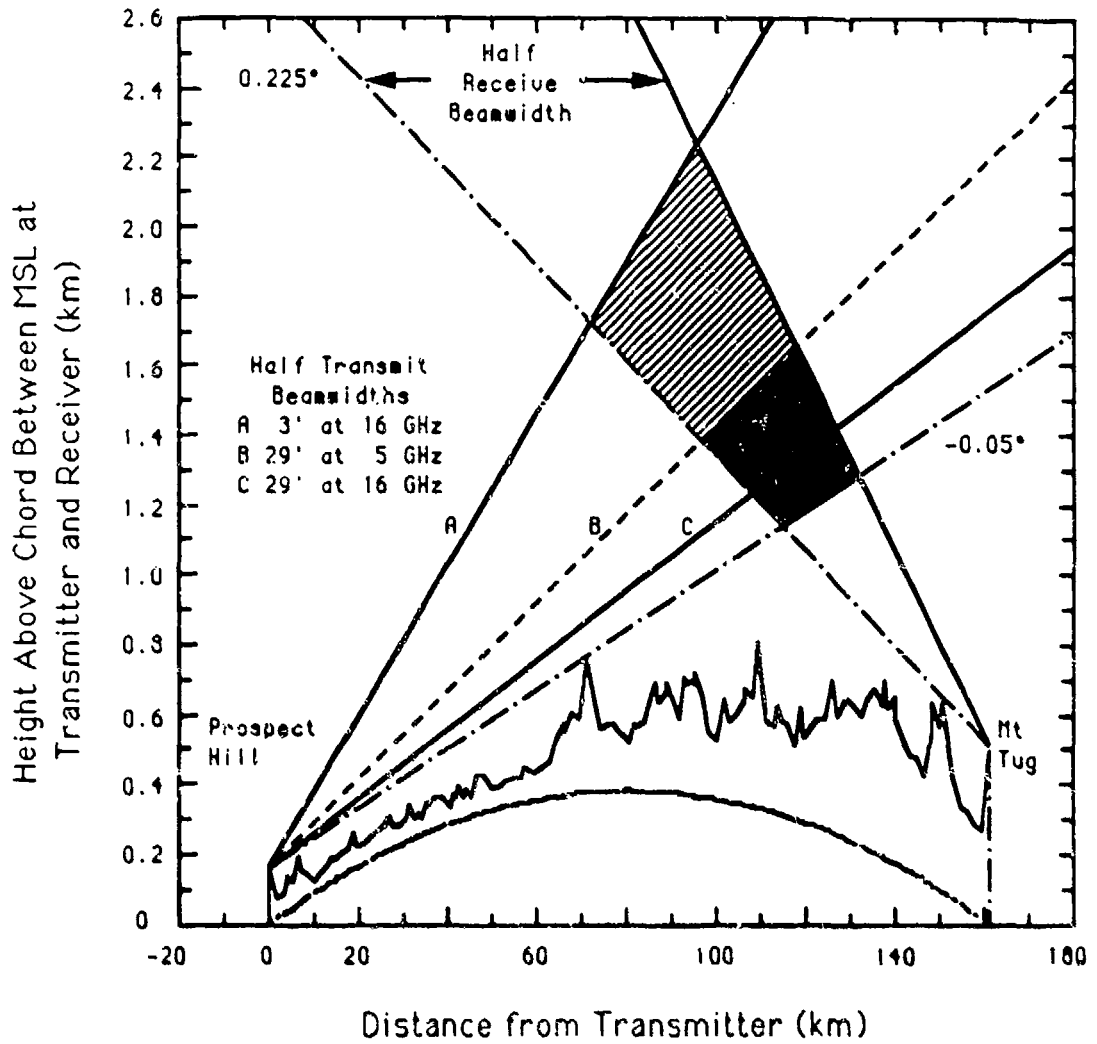


Figure 1: Troposcatter path profile for a  $4/3$  effective Earth radius. The scattering volumes are displayed as filled areas. The scattering volume for the 3' antenna at 16 GHz encloses the scattering volume for the 29' antenna at 5 GHz.

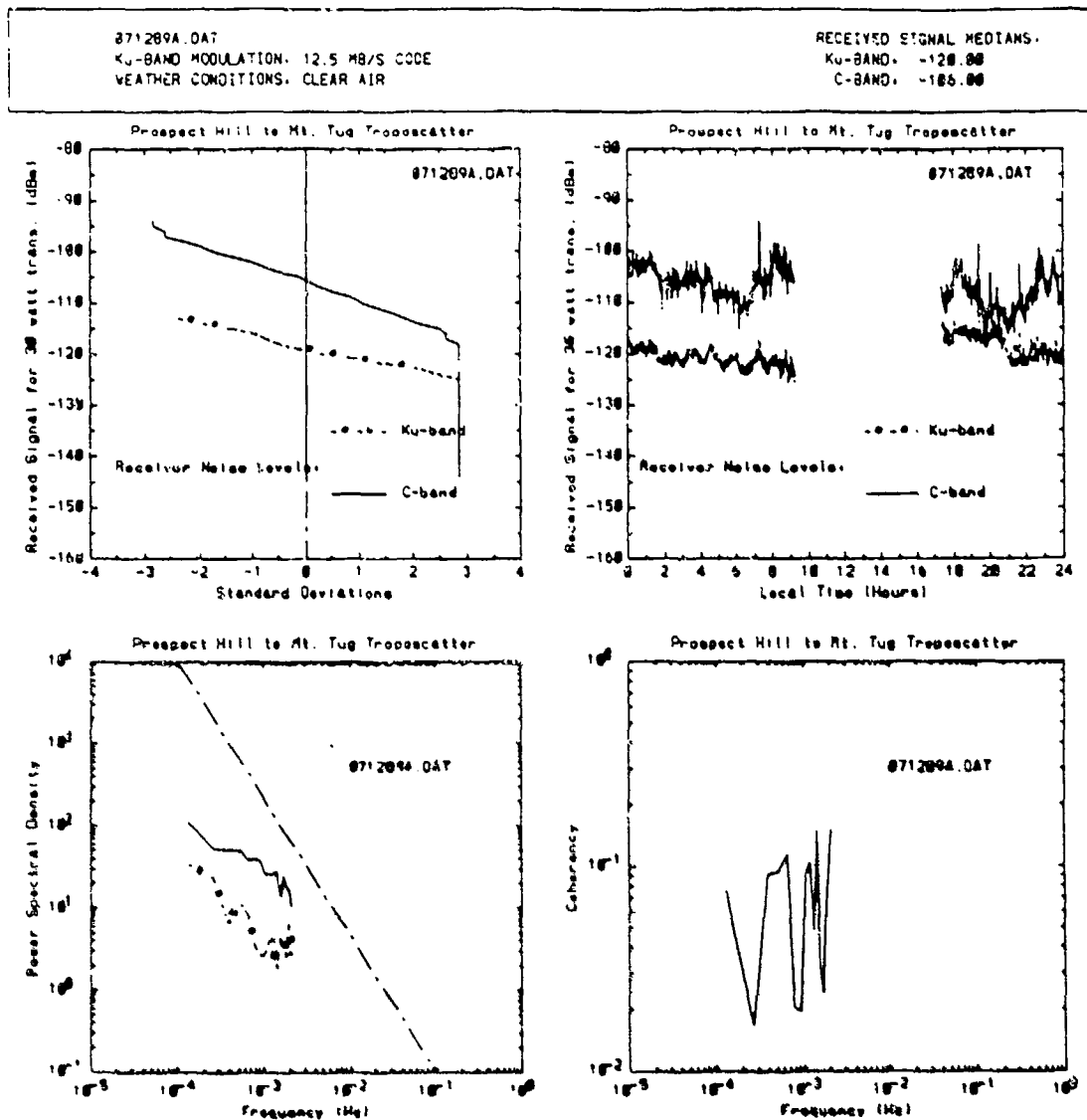


Figure 2: Day plots for the small aperture Ku band transmit antenna under clear weather conditions on July 12, 1989: sample cumulative distribution functions for received power, received power time series, power spectra for received power fluctuations and coherency between the fluctuations at Ku and C band.

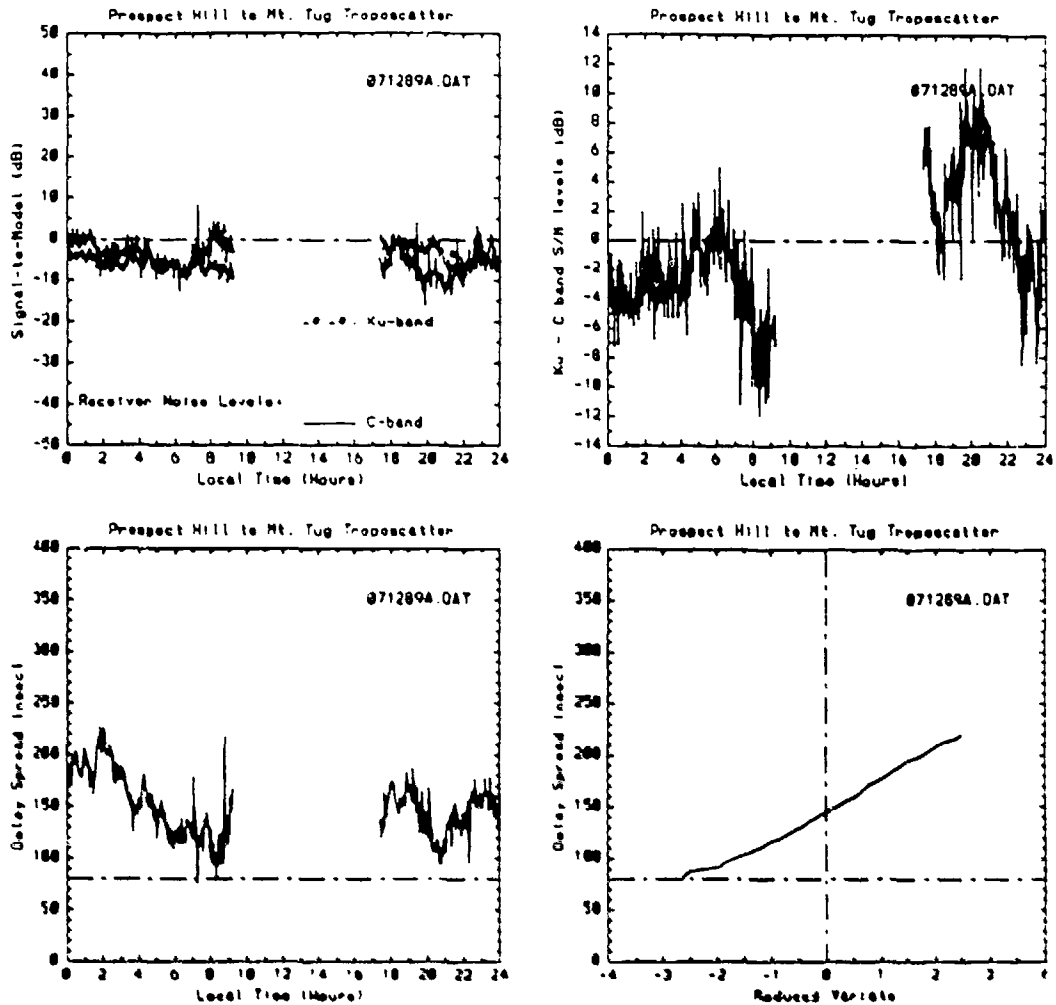


Figure 3: Day plots for the small aperture Ku band transmit antenna under clear weather conditions on July 12, 1989: time series of received power deviations from turbulent forward scatter model predictions, time series of the differences between received power deviations from turbulent forward scatter model predictions at Ku and C band, time series and sample cumulative distribution function for Ku band two sigma multipath delay spread.

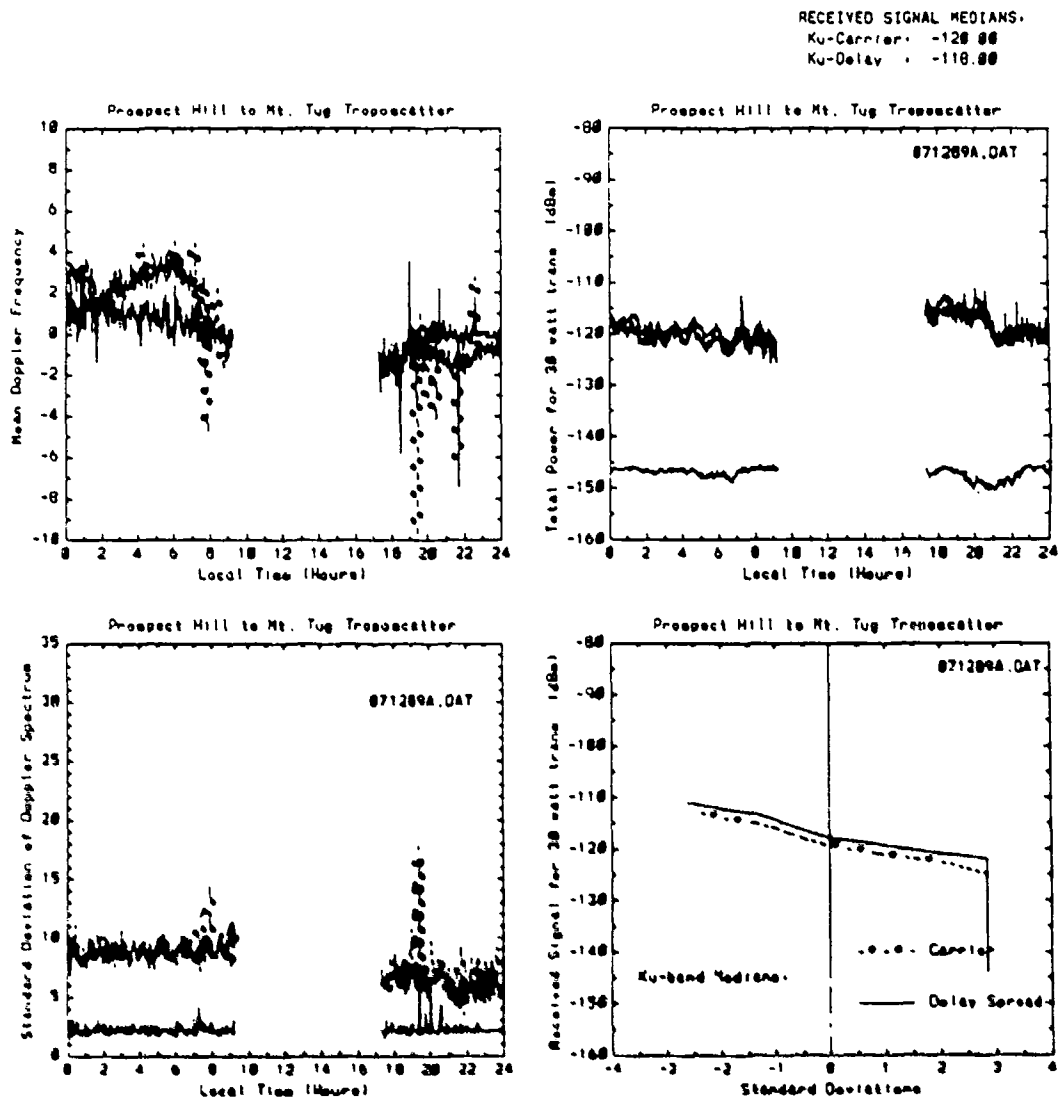


Figure 4: Day plots for the small aperture Ku band transmit antenna under clear weather conditions on July 12, 1989: time series of mean Doppler frequency shift and Doppler frequency spread, time series and sample cumulative distribution function for carrier channel and delay channel measurements of Ku band received power levels..

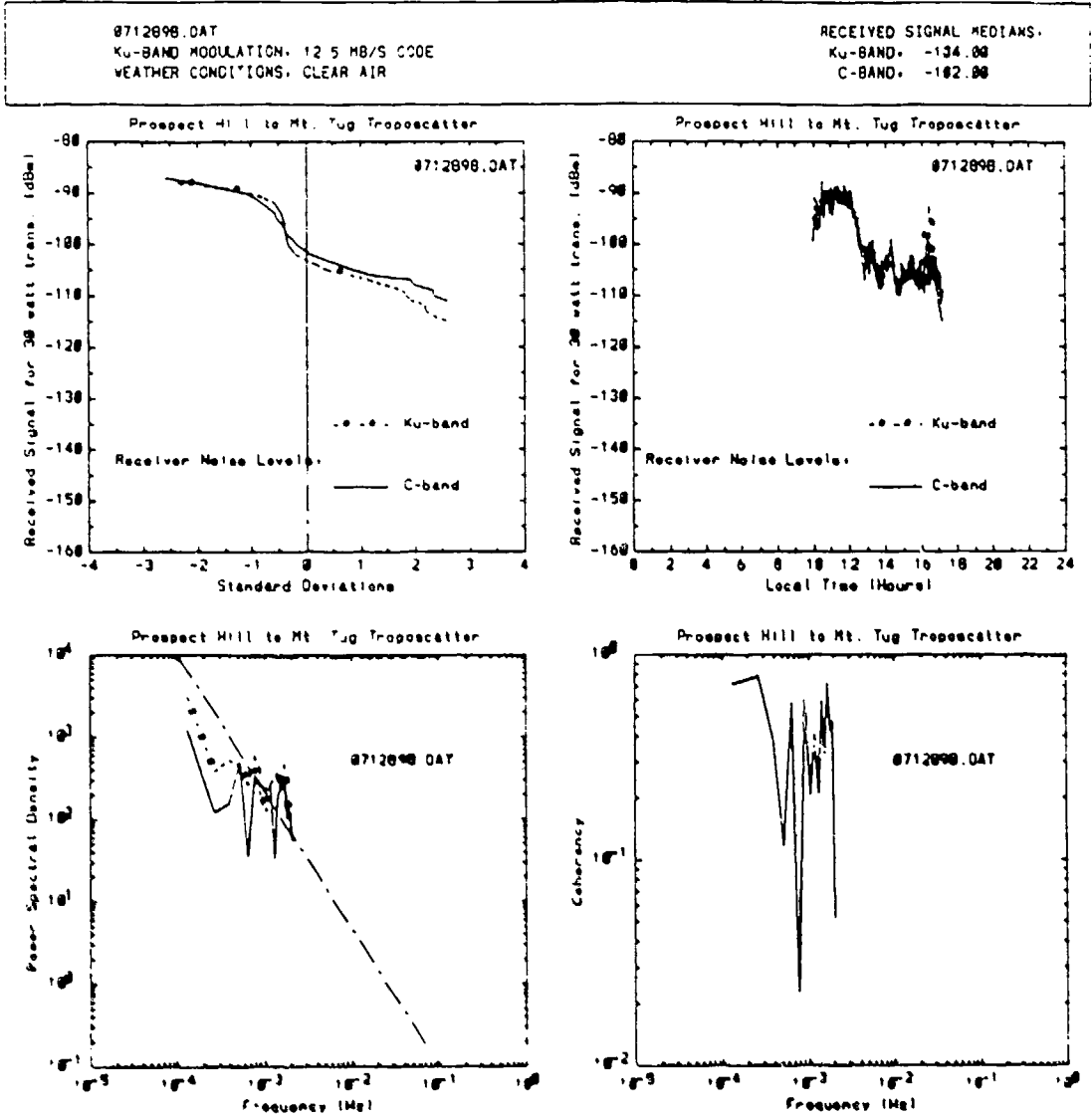


Figure 5: Day plots for the large aperture Ku band transmit antenna under clear weather conditions on July 12, 1989: sample cumulative distribution functions for received power, received power time series, power spectra for received power fluctuations and coherency between the fluctuations at Ku and C band.

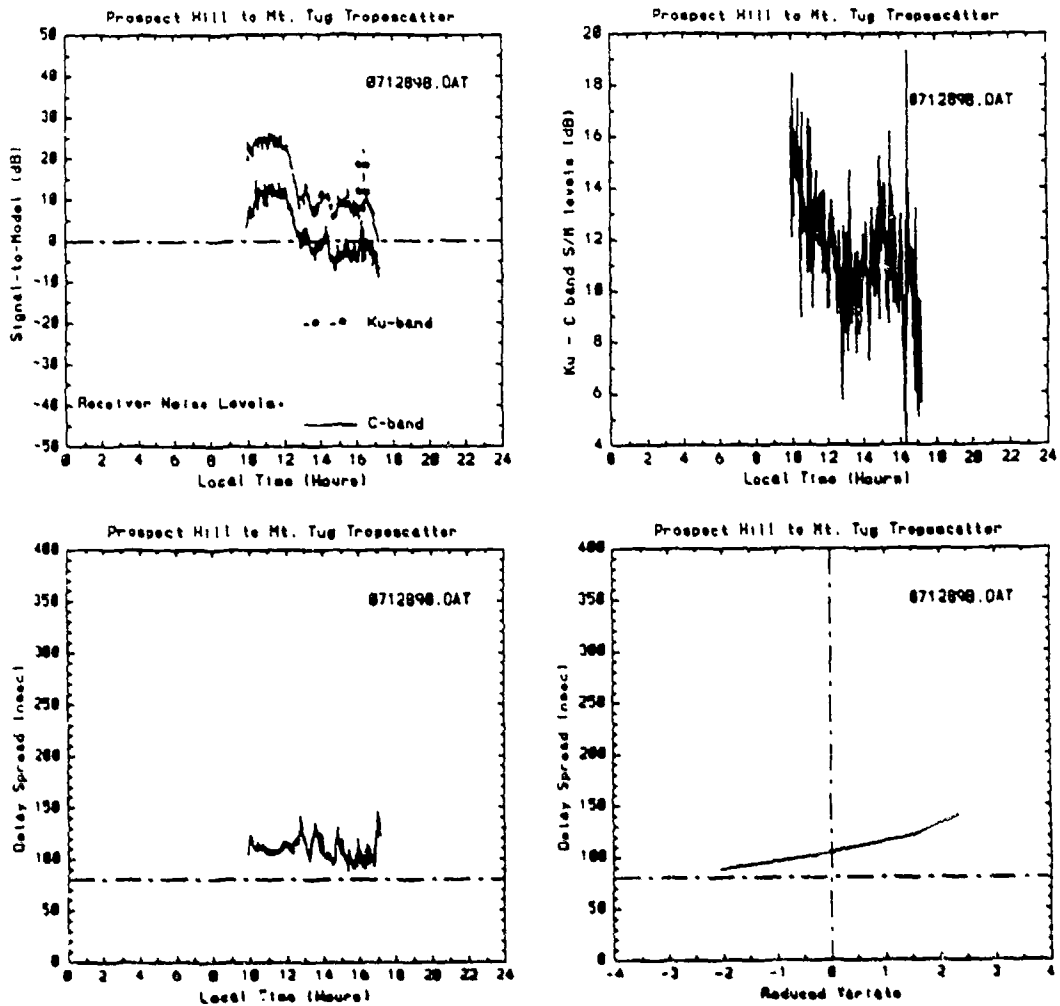


Figure 6: Day plots for the large aperture Ku band transmit antenna under clear weather conditions on July 12, 1989: time series of received power deviations from turbulent forward scatter model predictions, time series of the differences between received power deviations from turbulent forward scatter model predictions at Ku and C band, time series and sample cumulative distribution function for Ku band two sigma multipath delay spread.

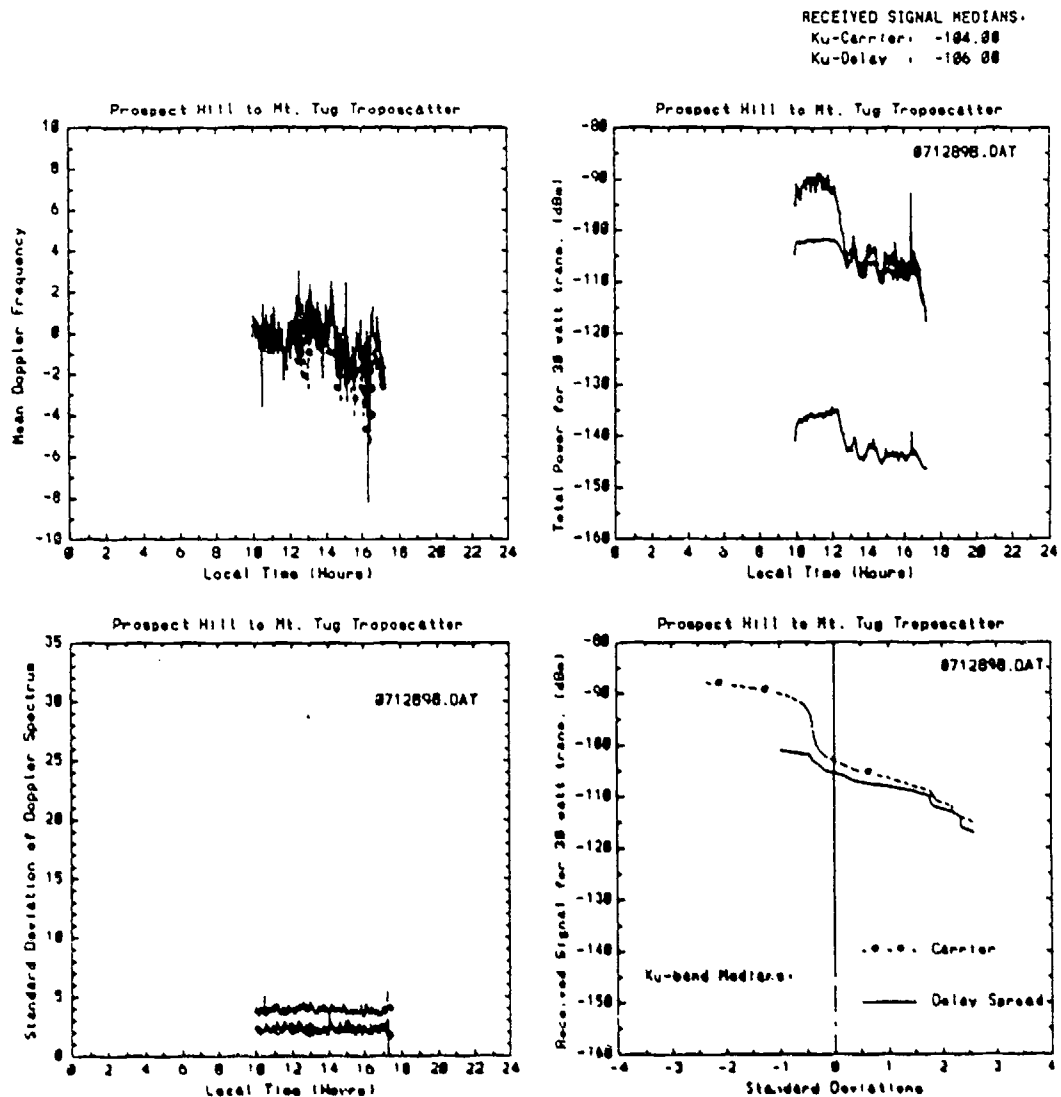


Figure 7: Day plots for the large aperture Ku band transmit antenna under clear weather conditions on July 12, 1989: time series of mean Doppler frequency shift and Doppler frequency spread, time series and sample cumulative distribution function for carrier channel and delay channel measurements of Ku band received power levels.

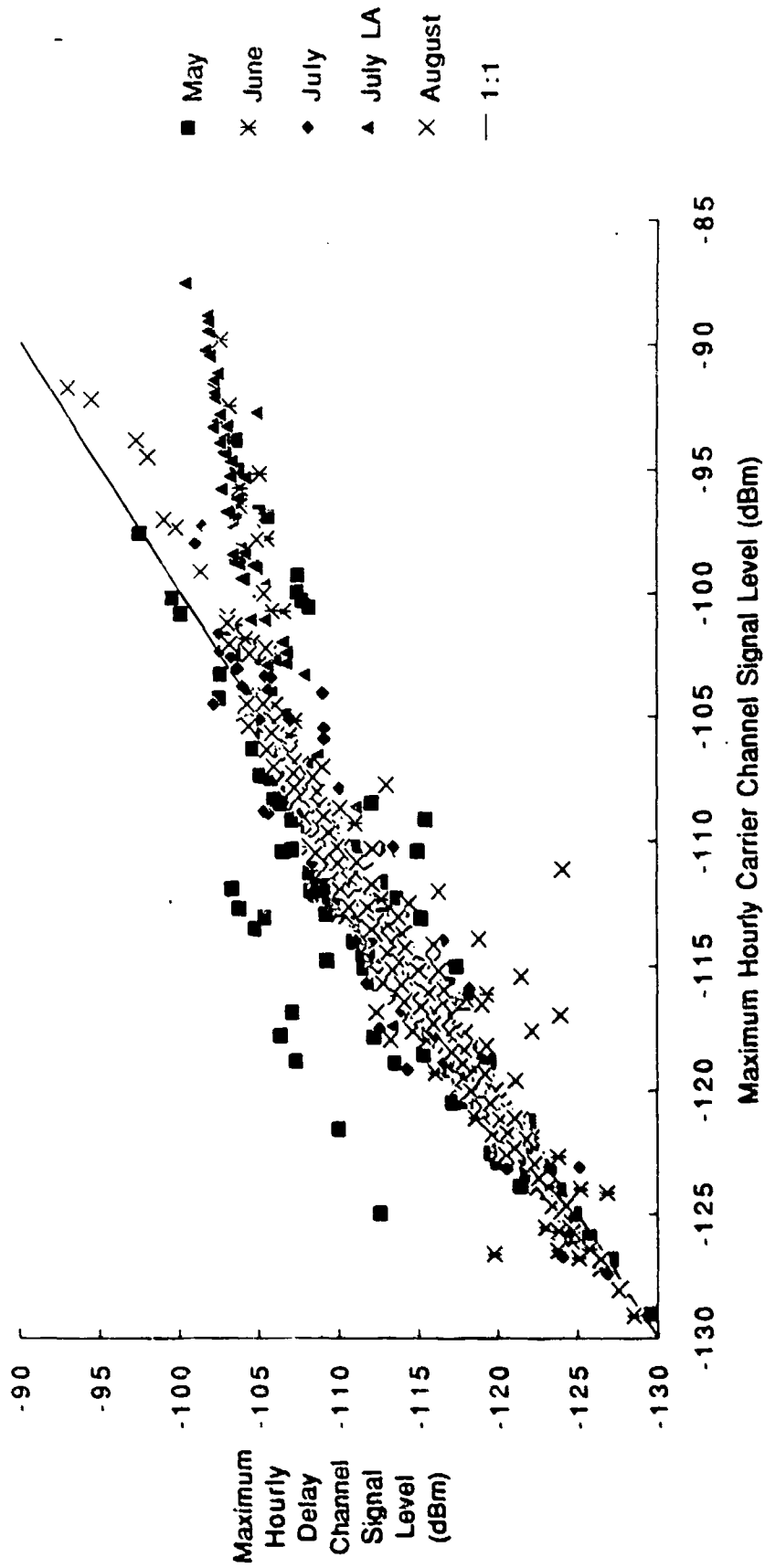


Figure 8: Scatter distribution comparing simultaneous observations of the maximum hourly carrier channel and delay channel observations of Ku band received power levels.

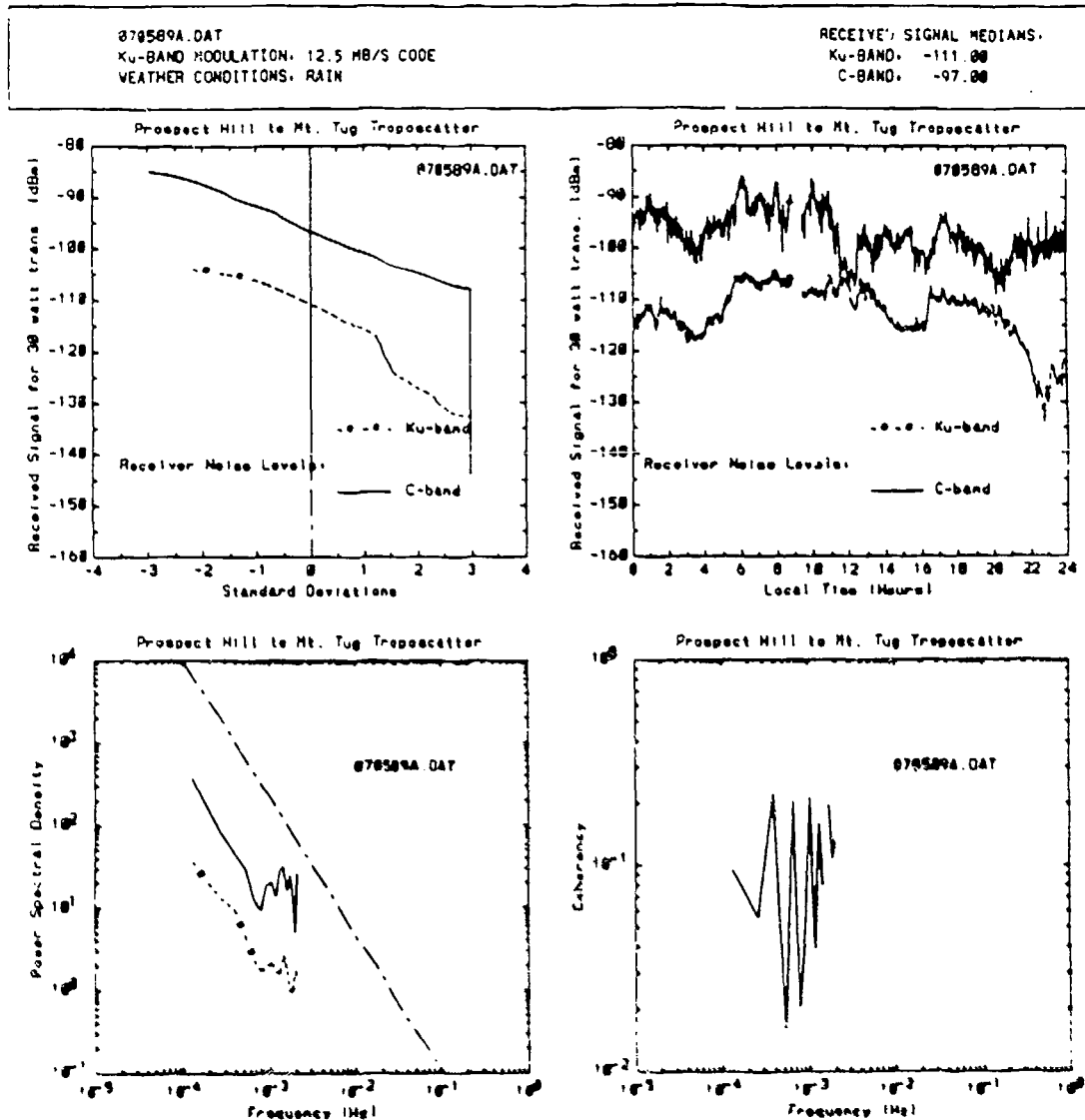


Figure 9: Day plots for the small aperture Ku band transmit antenna under rainy conditions on July 5, 1989: sample cumulative distribution functions for received power, received power time series, power spectra for received power fluctuations and coherency between the fluctuations at Ku and C band.

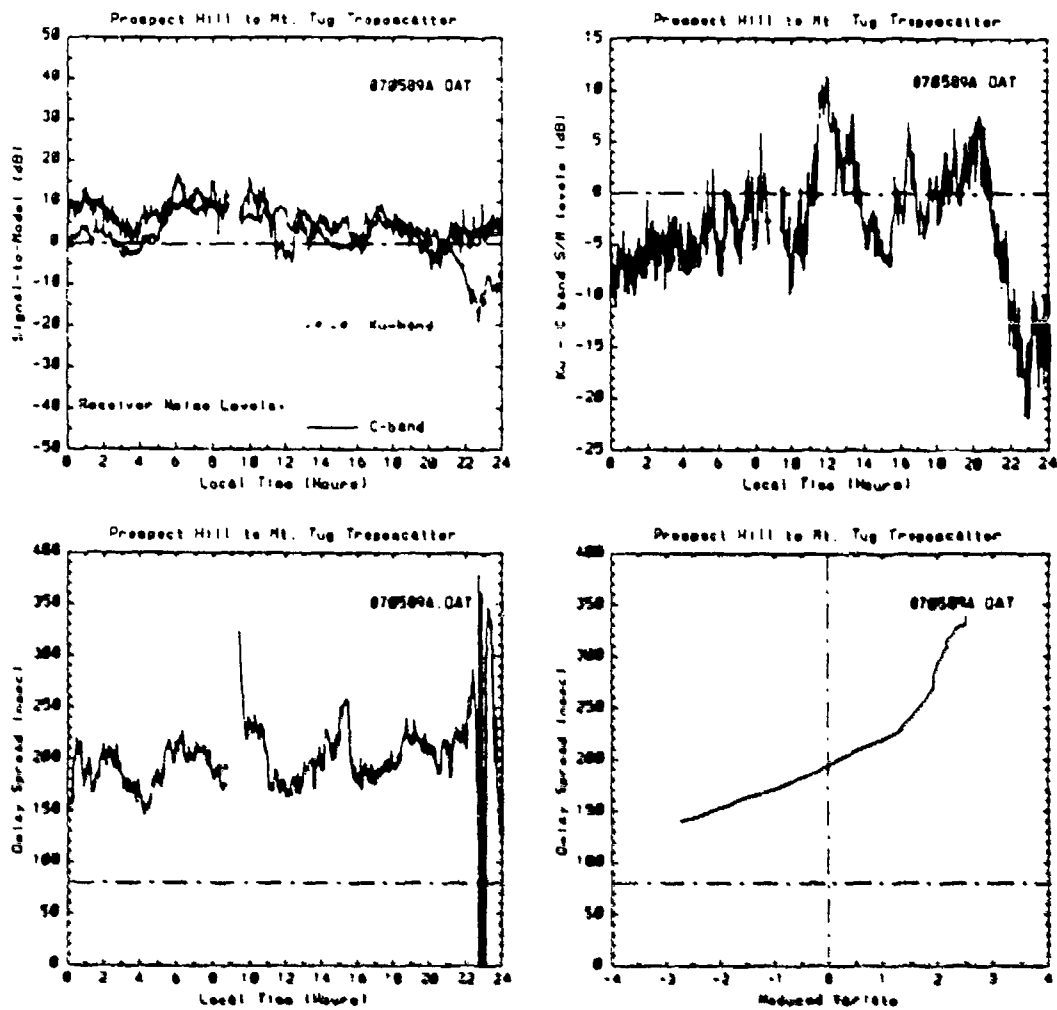


Figure 10: Day plots for the small aperture Ku band transmit antenna under rainy conditions on July 5, 1989: time series of received power deviations from turbulent forward scatter model predictions, time series of the differences between received power deviations from turbulent forward scatter model predictions at Ku and C band, time series and sample cumulative distribution function for Ku band two sigma multipath delay spread.

RECEIVED SIGNAL MEDIANS.  
 Ku-Carrier: -111.30  
 Ku-Delay: -113.30

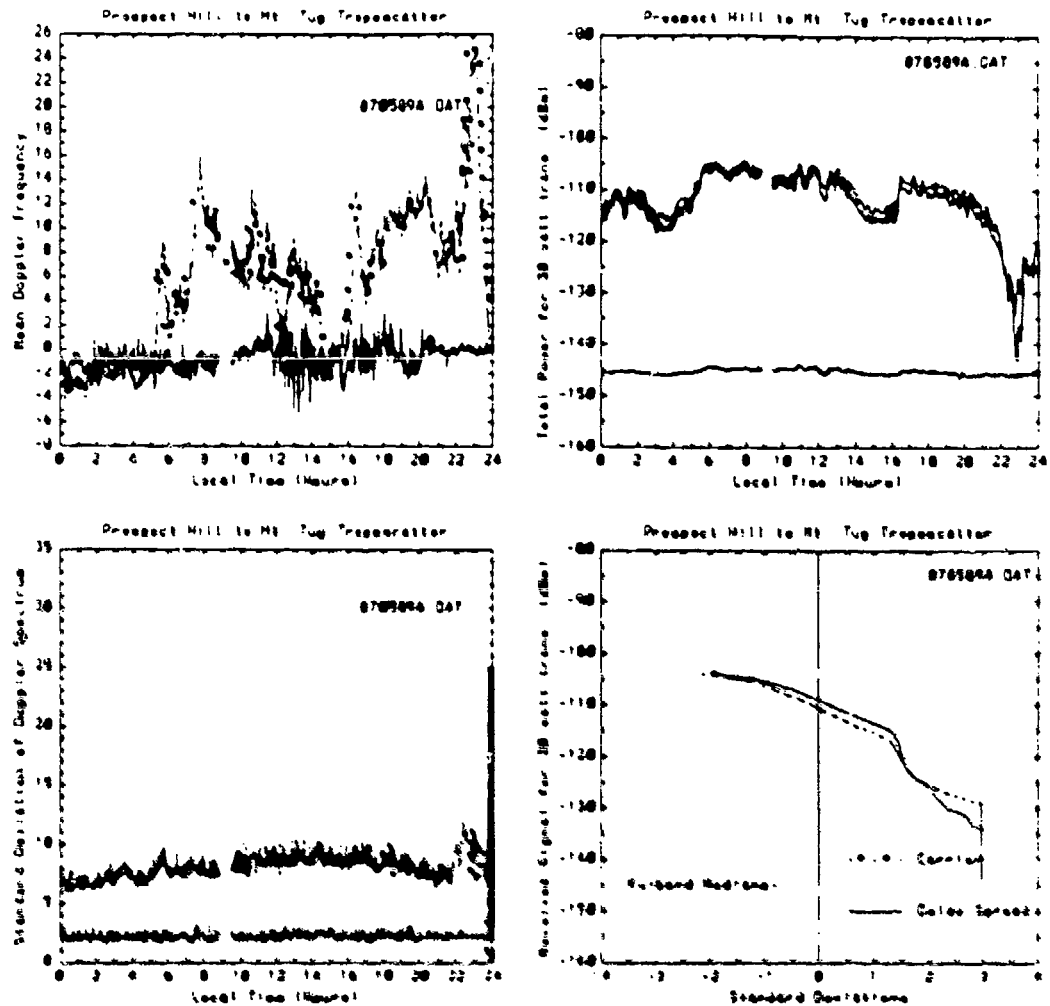


Figure 11: Day plots for the small aperture Ku band transmit antenna under rainy conditions on July 5, 1989: time series of mean Doppler frequency shift and Doppler frequency spread, time series and sample cumulative distribution function for carrier channel and delay channel measurements of Ku band received power levels.

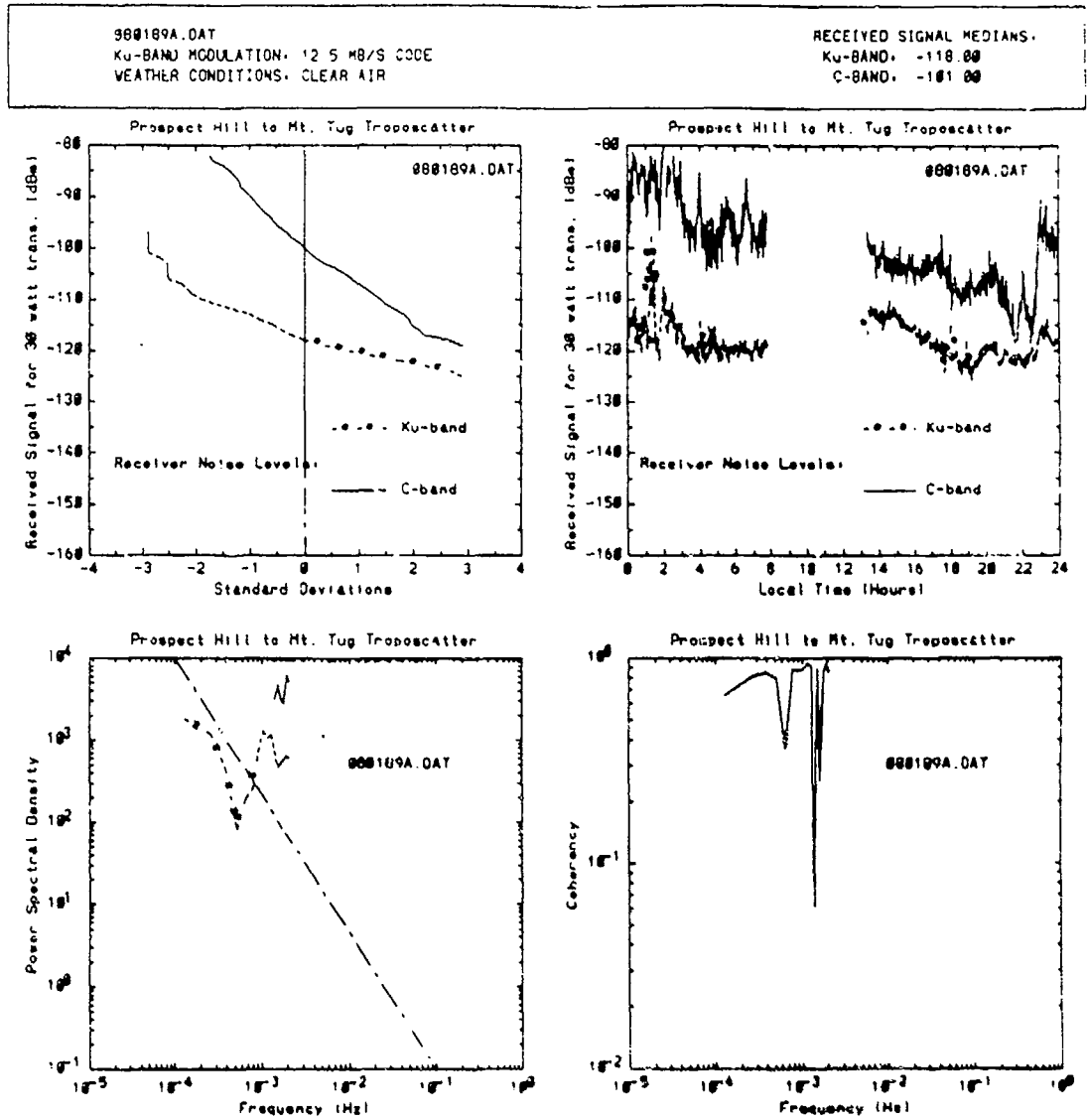


Figure 12: Day plots for the small aperture Ku band transmit antenna under elevated ducting conditions on August 1, 1989: sample cumulative distribution functions for received power, received power time series, power spectra for received power fluctuations and coherency between the fluctuations at Ku and C band.

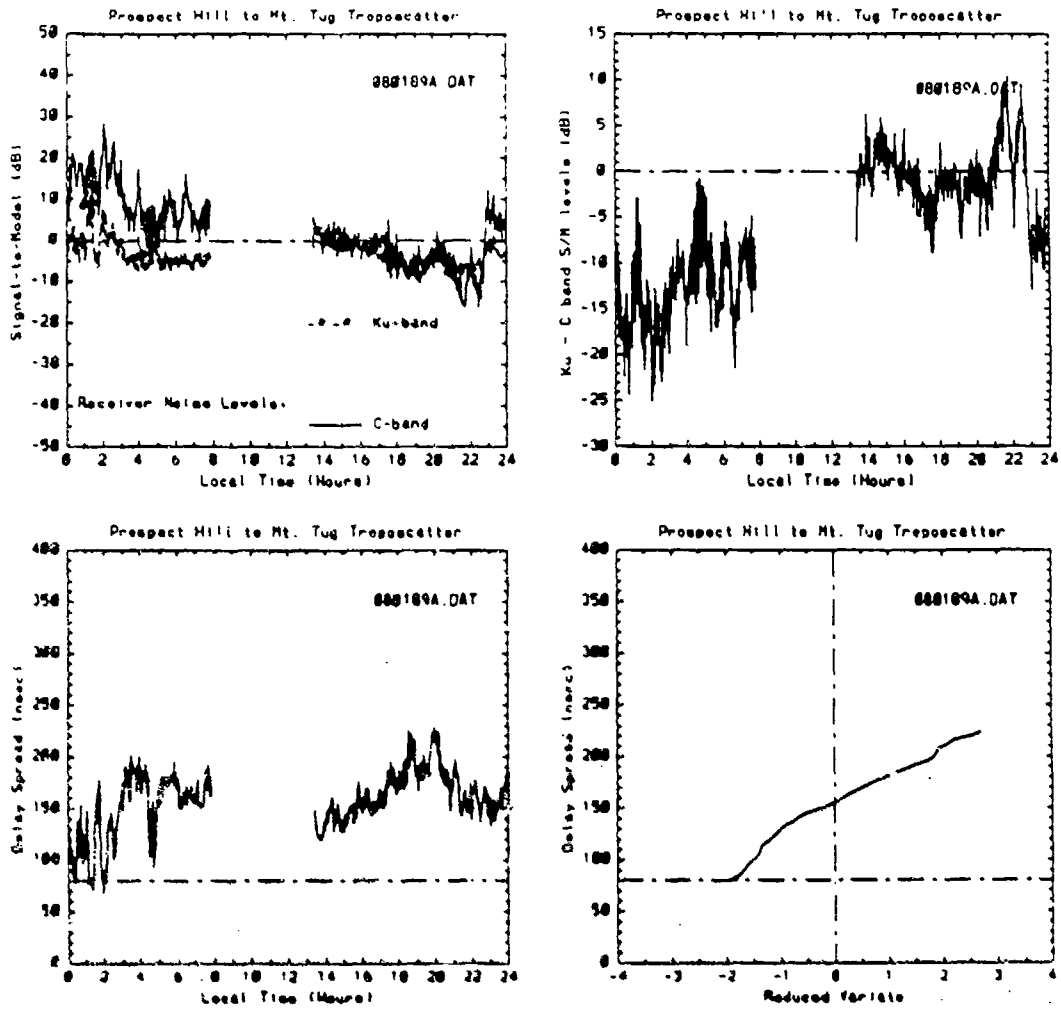


Figure 13: Day plots for the small aperture Ku band transmit antenna under elevated ducting conditions on August 1, 1989: time series of received power deviations from turbulent forward scatter model predictions, time series of the differences between received power deviations from turbulent forward scatter model predictions at Ku and C band, time series and sample cumulative distribution function for Ku band two sigma multipath delay spread.

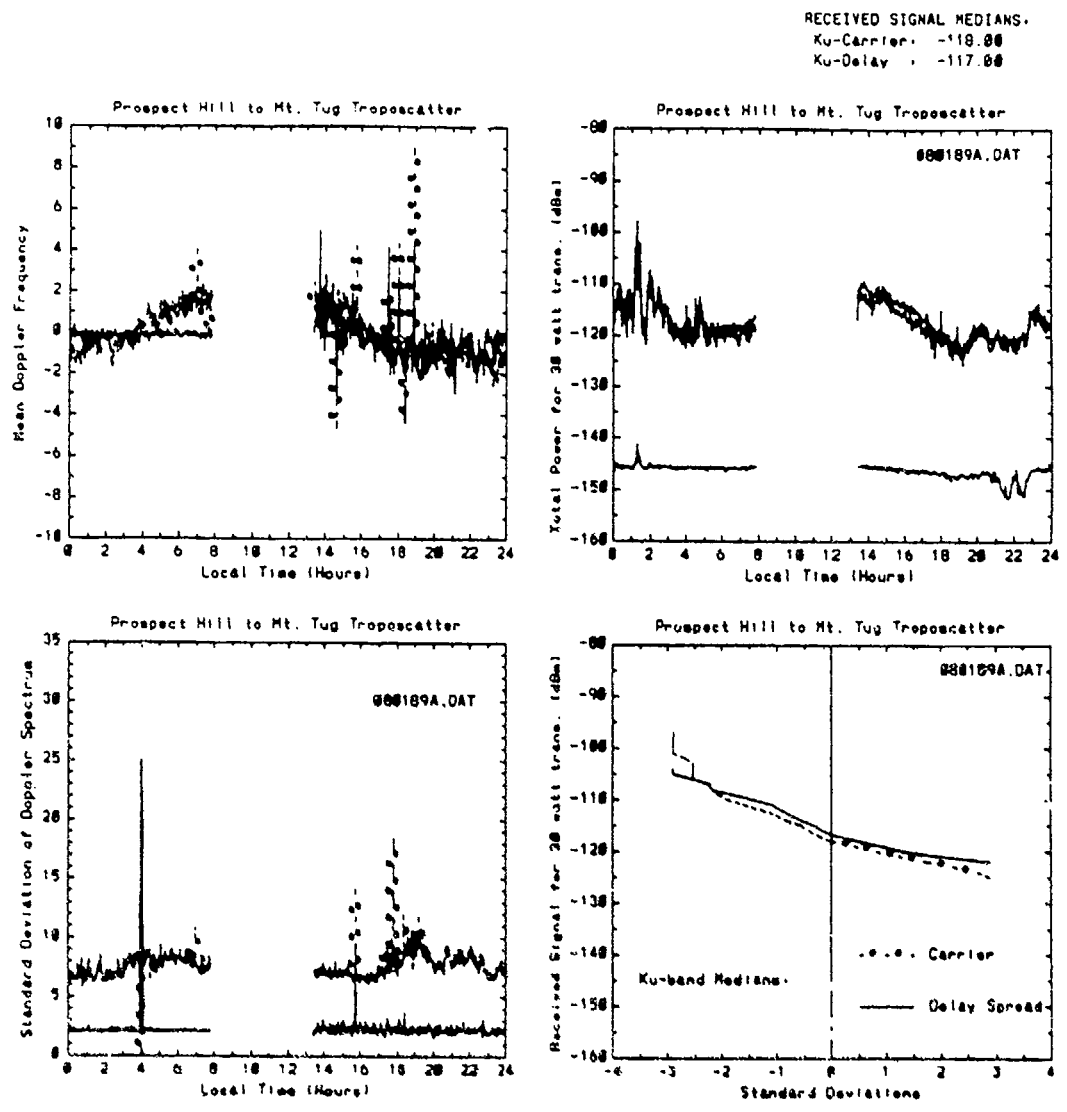


Figure 14: Day plots for the small aperture Ku band transmit antenna under elevated ducting conditions on August 1, 1989: time series of mean Doppler frequency shift and Doppler frequency spread, time series and sample cumulative distribution function for carrier channel and delay channel measurements of Ku band received power levels.

Prospect Hill to Mt Tug  
June 1989

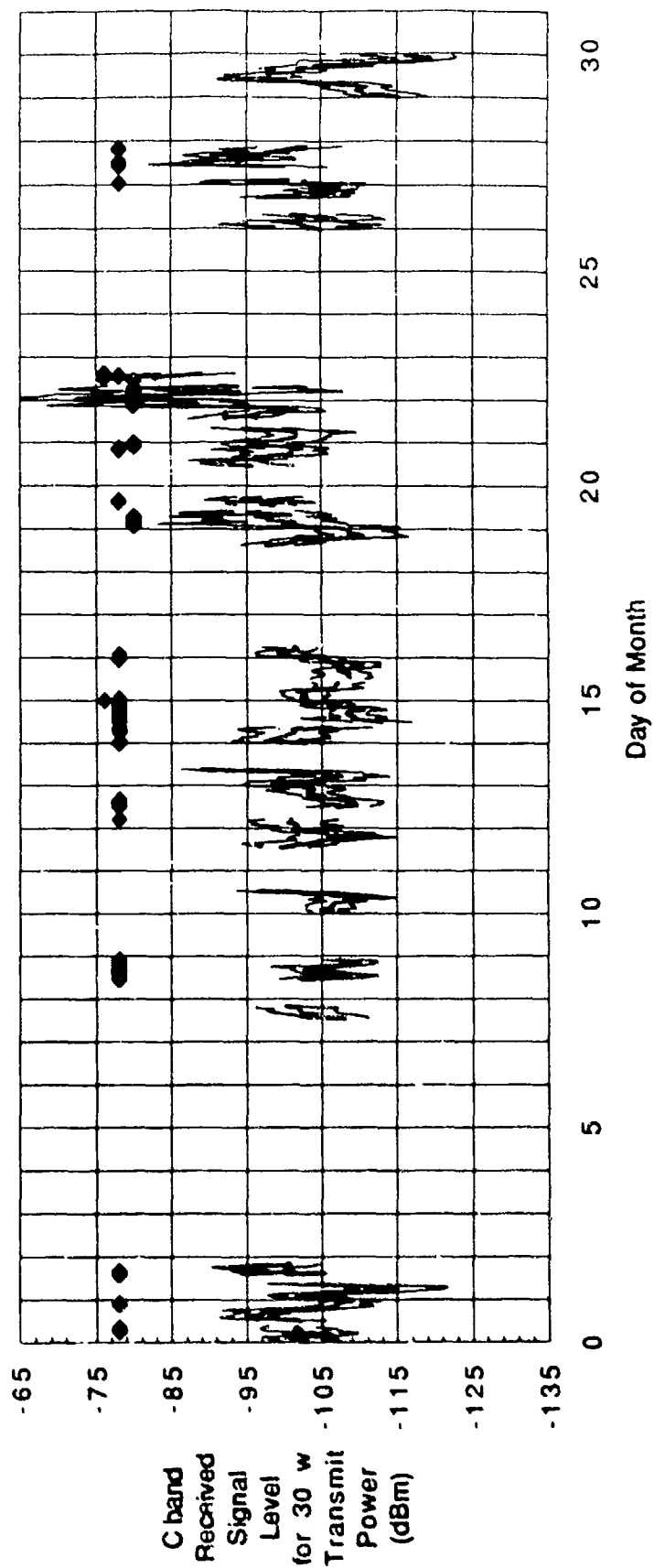


Figure 15: C band carrier received power levels for the month of June, 1989.

Prospect Hill to Mt Tug  
June 1989

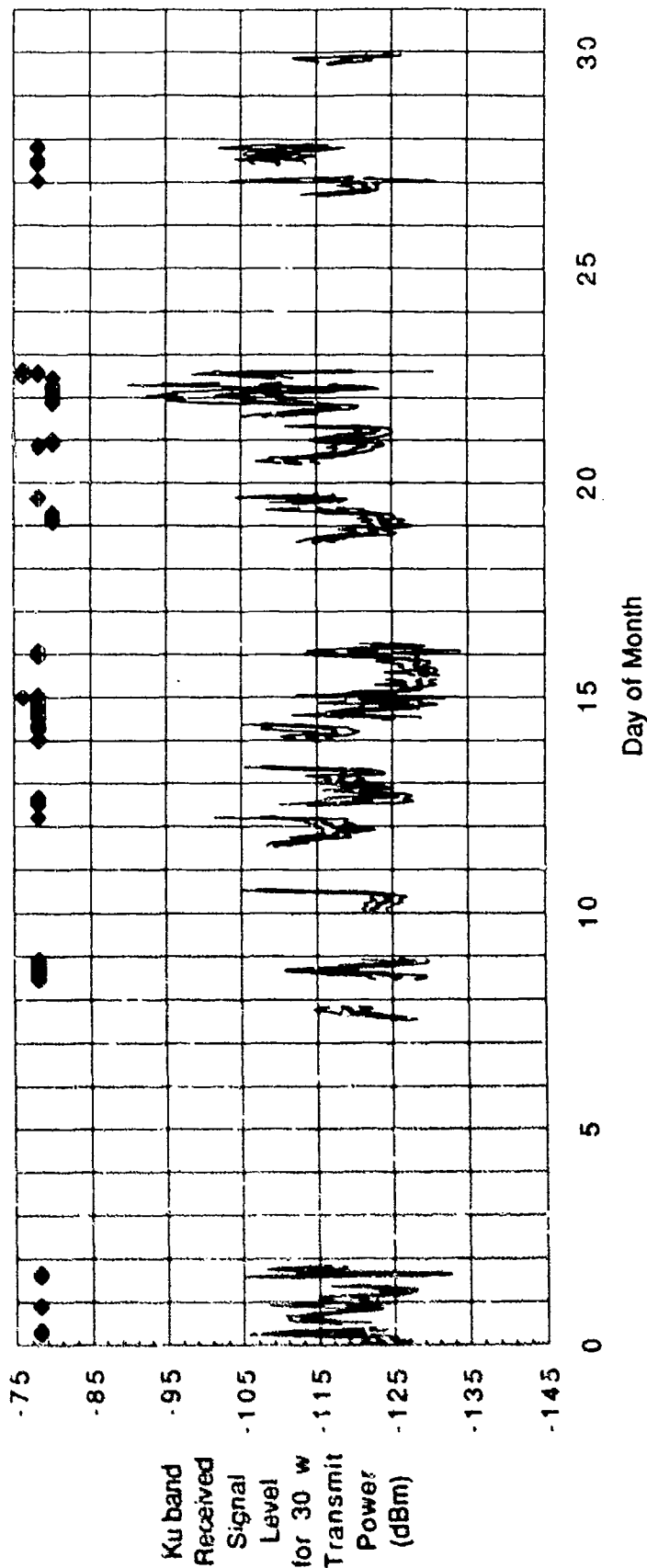


Figure 16: Ku band carrier received power levels for the month of June, 1989.

Prospect Hill to Mt Tug  
June 1989

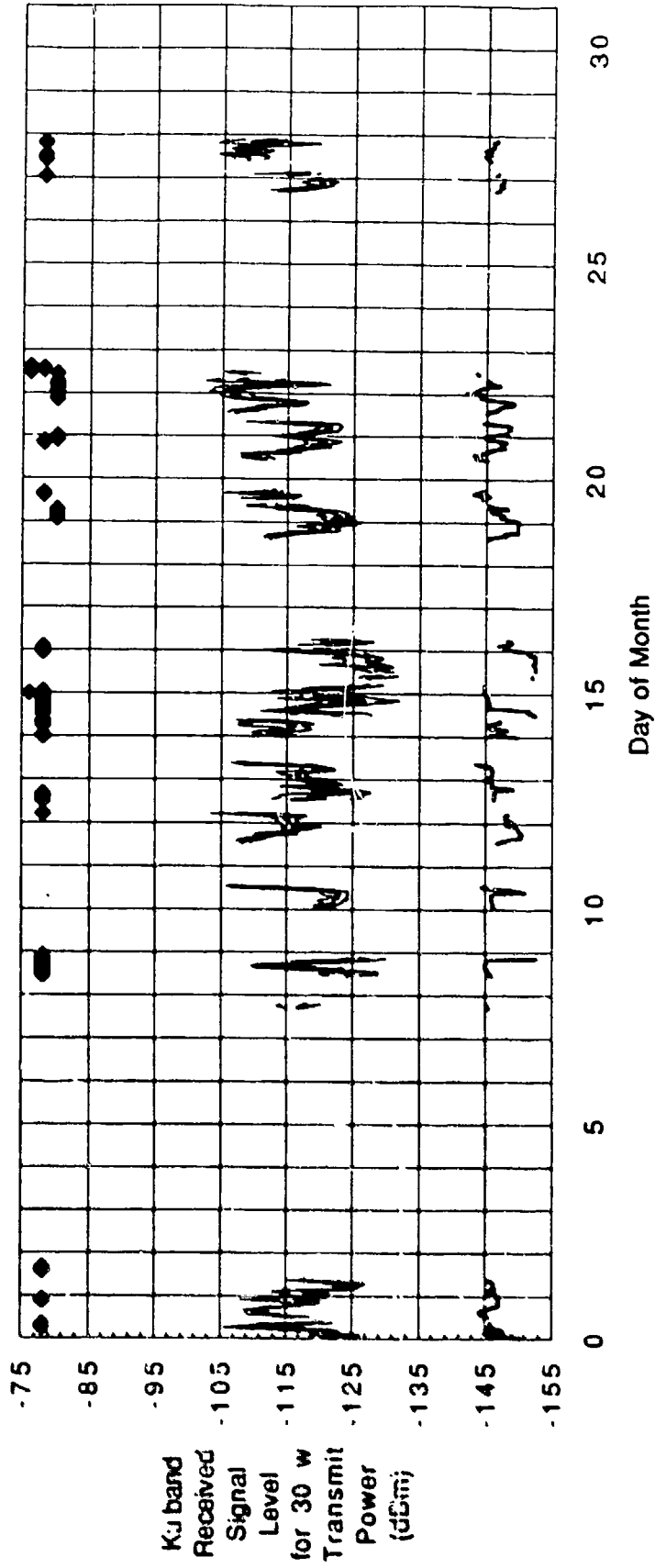


Figure 17: Ku band delay channel received power levels for the month of June, 1989.

Prospect Hill to Mt Tug  
June 1989

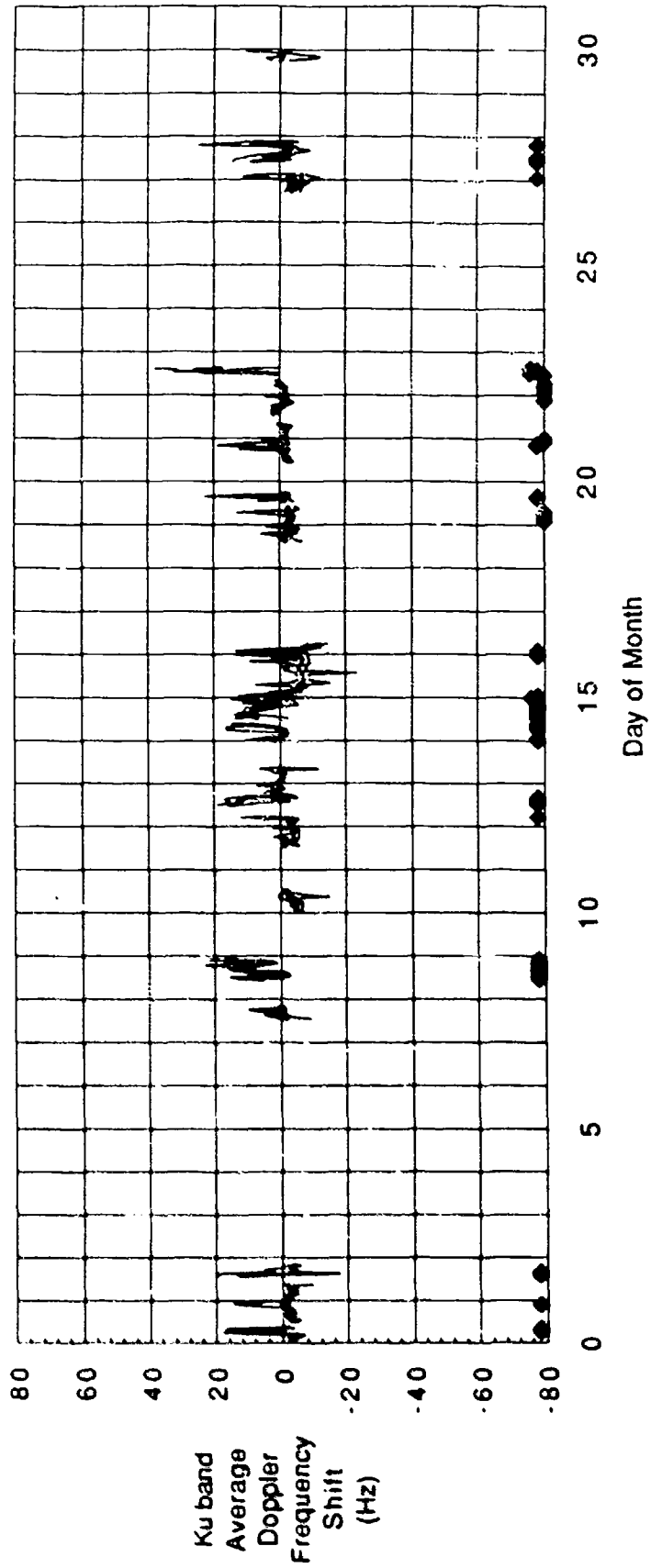


Figure 18: Ku band average Doppler frequency shifts for the month of June, 1989.

Prospect Hill to Mt Tug  
June 1989

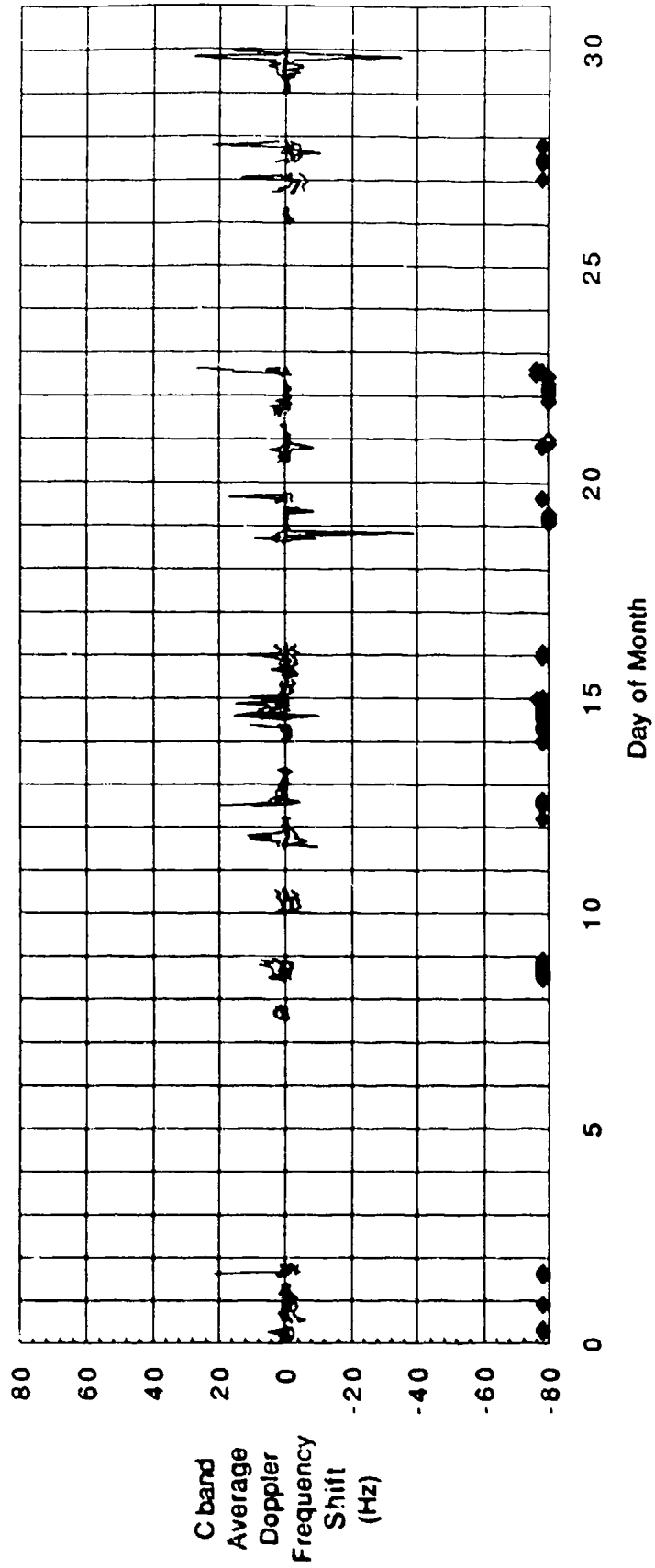


Figure 19: C band average Doppler frequency shifts for the month of June, 1989.

Prospect Hill to Mt Tug  
June 1989

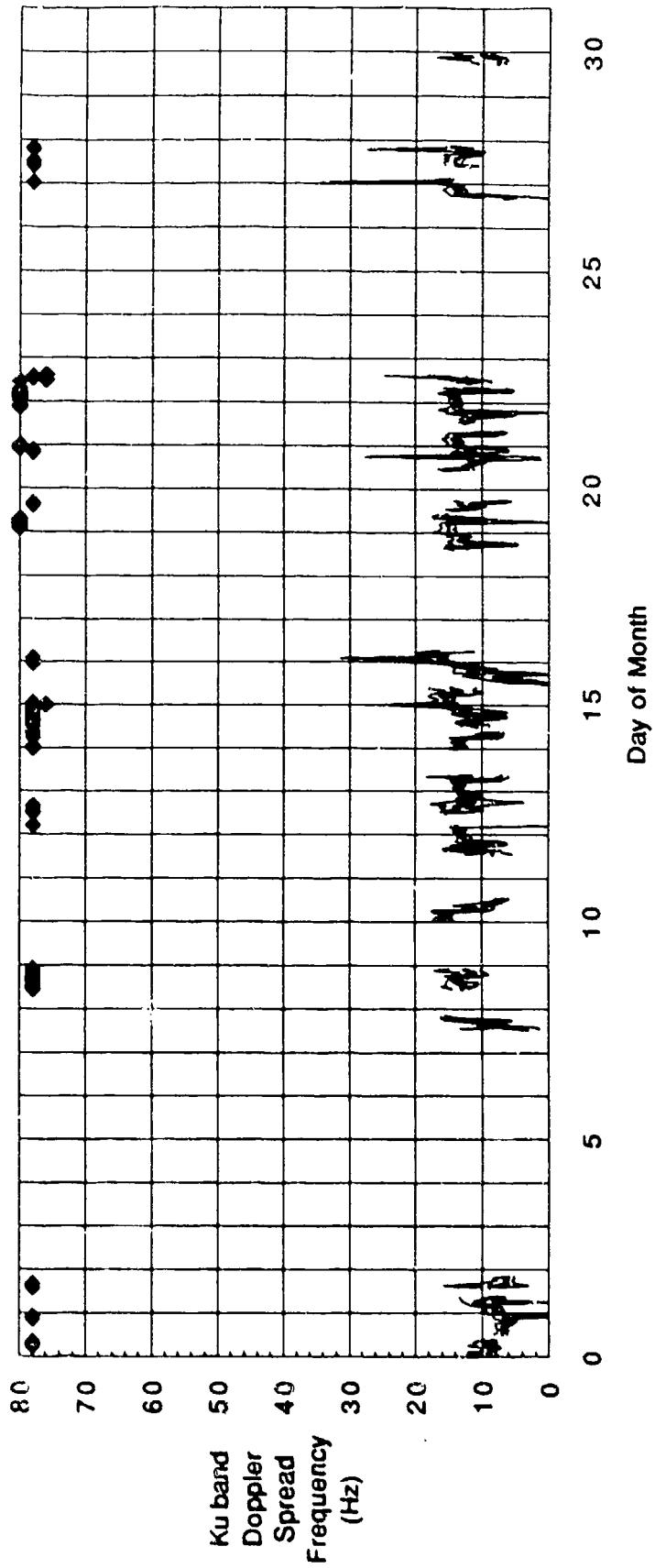


Figure 20: Ku band Doppler frequency spreads for the month of June, 1989.

Prospect Hill to Mt Tug  
June 1989

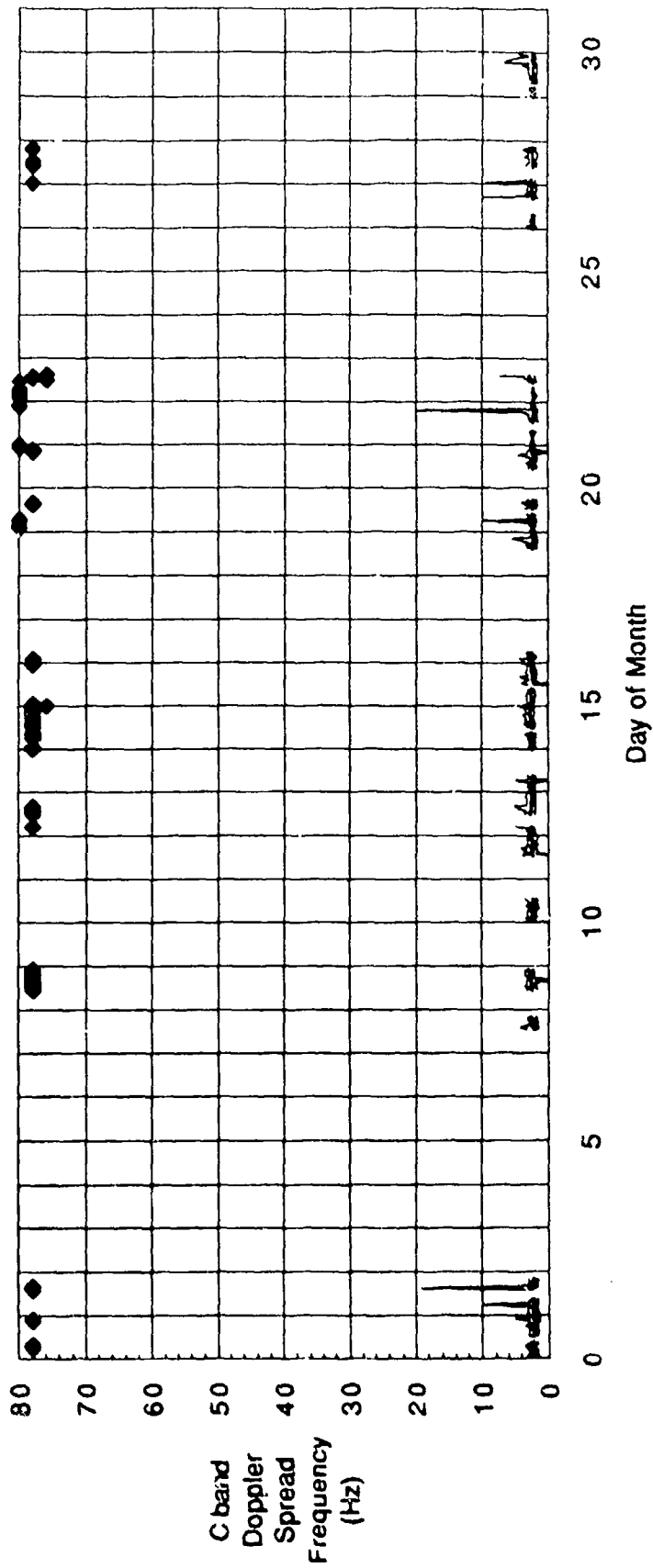


Figure 21: C band Doppler frequency spreads for the month of June, 1989.

Prospect Hill to Mt Tug  
June 1989

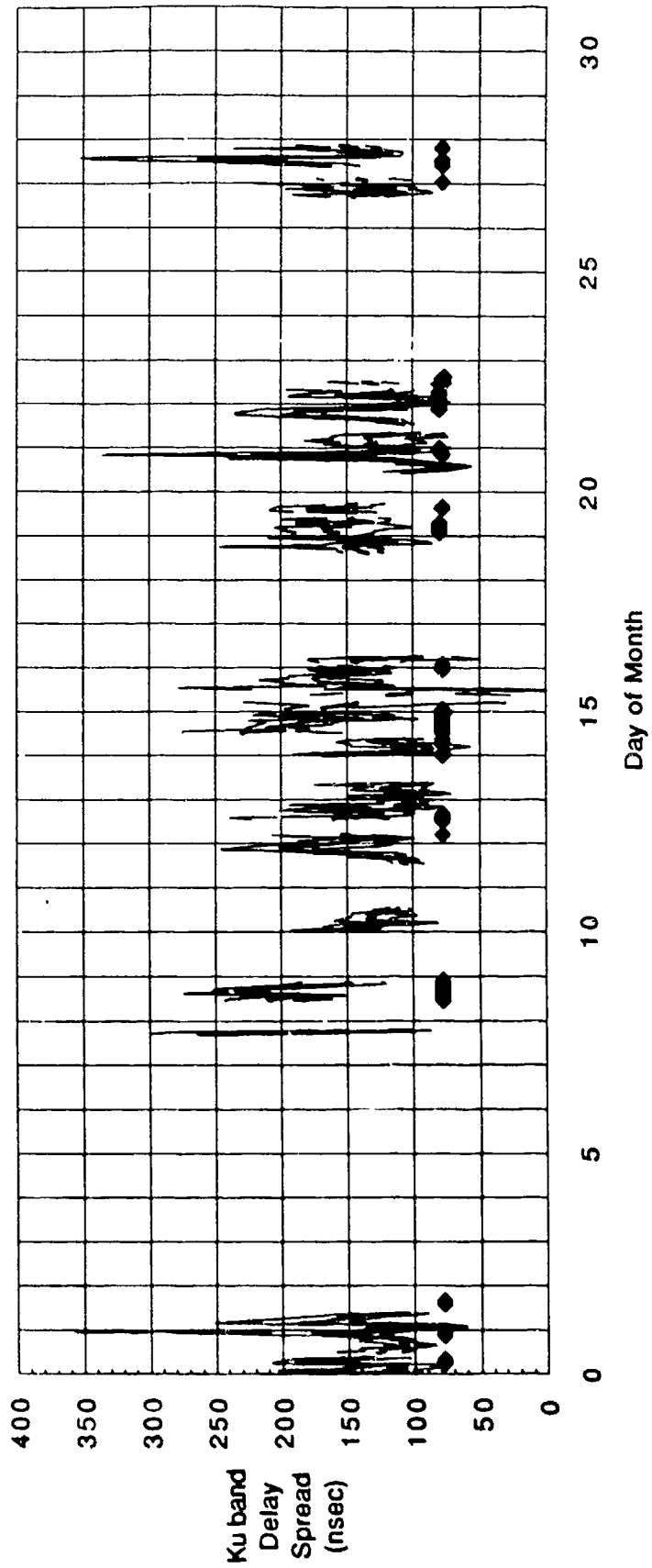


Figure 22: Ku band two sigma multipath delay spreads for the month of June, 1989.

Diurnal Variation  
Prospect Hill to Mt Tug Troposcatter Path  
Summer 1989

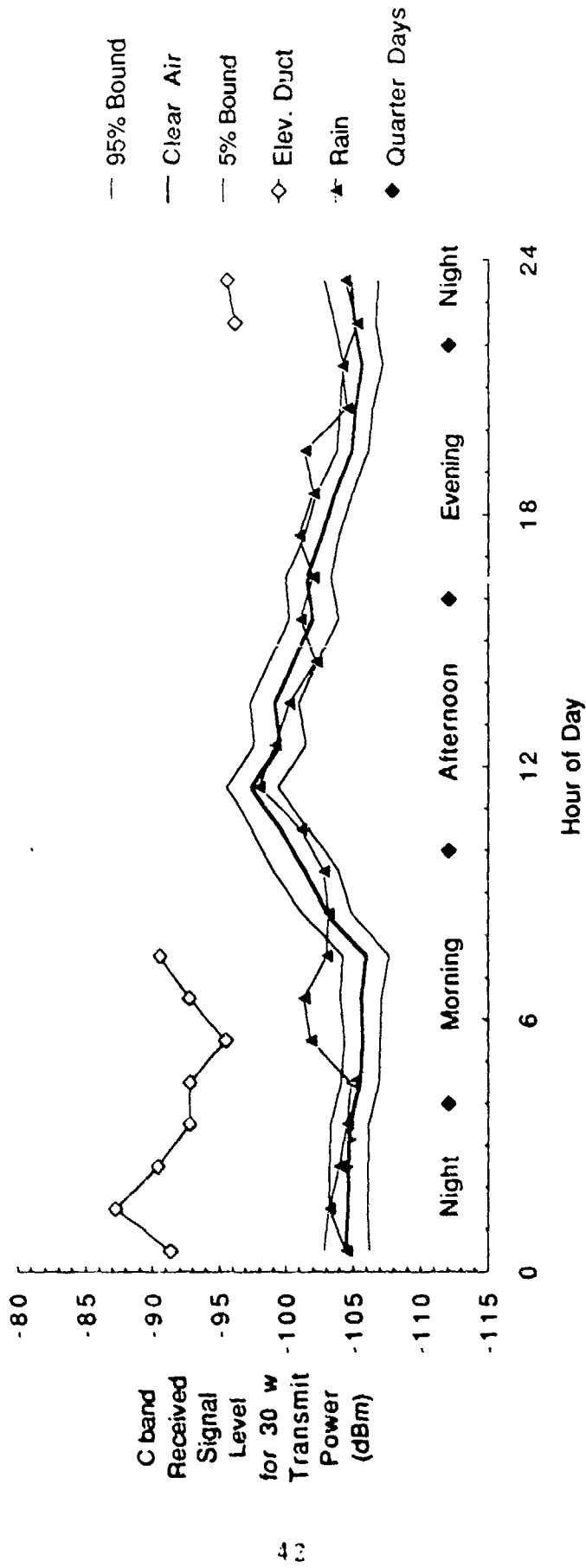


Figure 23: Average diurnal variation in C band received carrier power, summer, 1989

Diurnal Variation  
Prospect Hill to Mt Tug Troposcatter Path  
Summer 1989

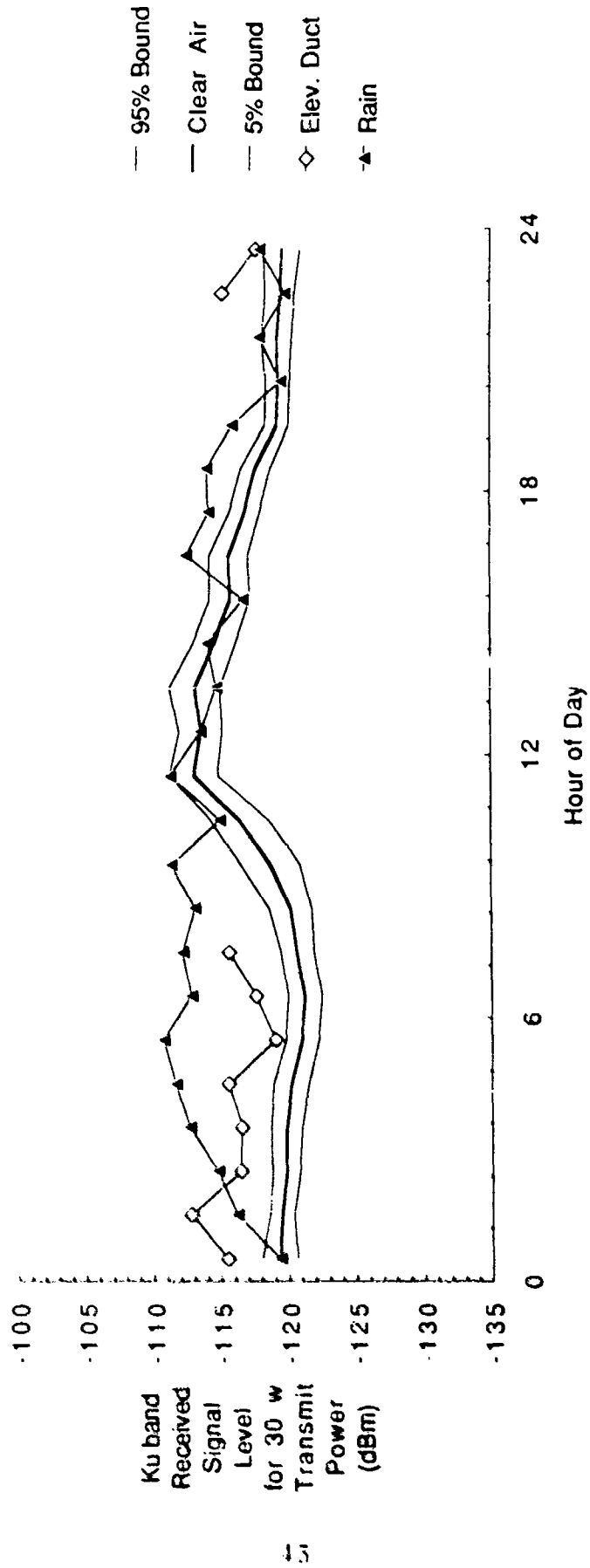


Figure 24: Average diurnal variation in Ku band received carrier power, summer, 1989

Diurnal Variation  
Prospect Hill to Mt Tug Troposcatter Path  
Summer 1989

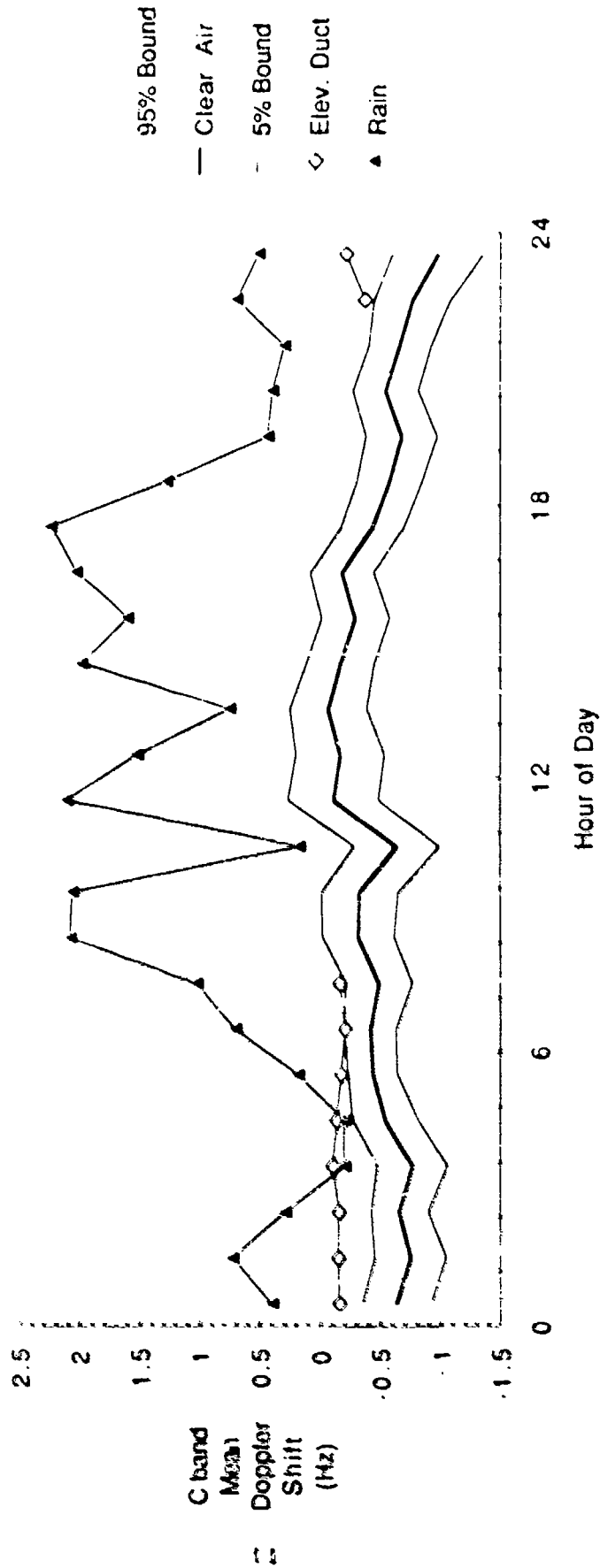


Figure 25: Average diurnal variation in C band Doppler frequency shift, summer, 1989

Diurnal Variation  
Prospect Hill to Mt Tug Troposcatter Path  
Summer 1989

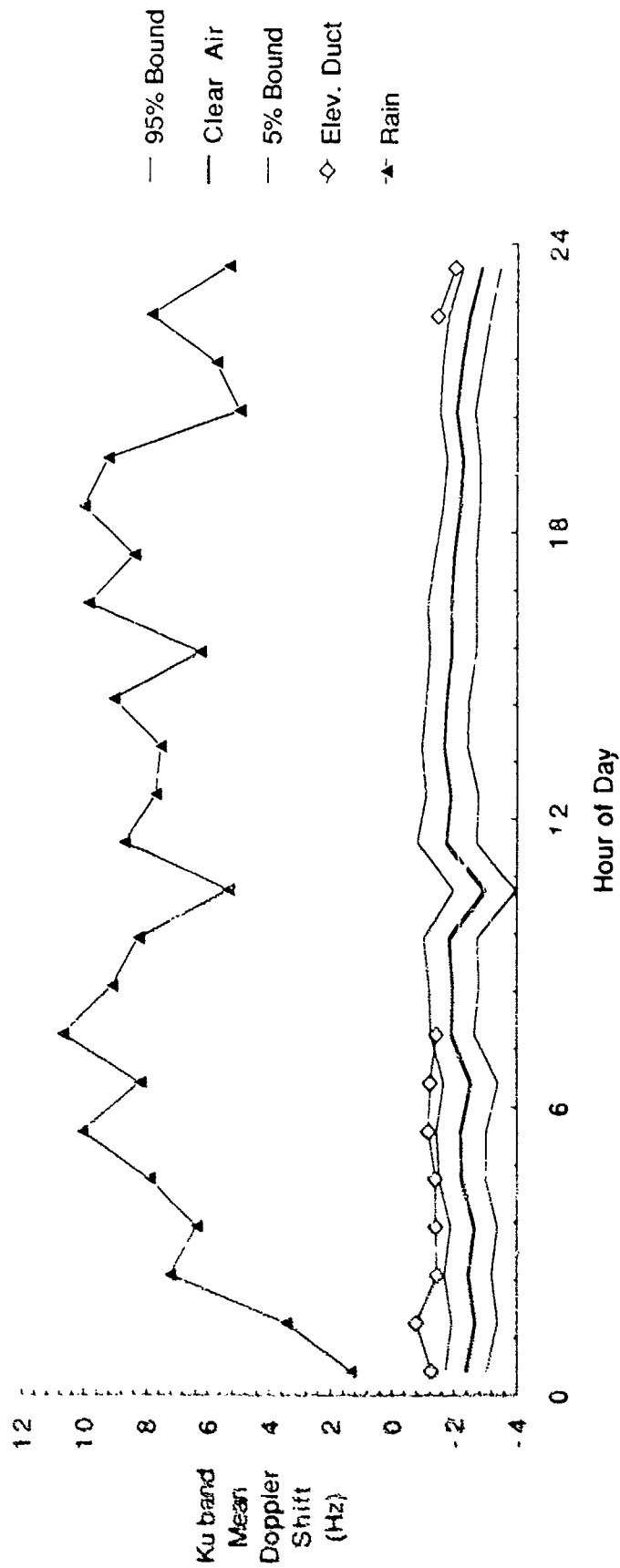


Figure 26: Average diurnal variation in Ku band Doppler frequency shift, summer, 1989

Diurnal Variation  
Prospect Hill to Mt Tug Troposcatter Path  
Summer 1989

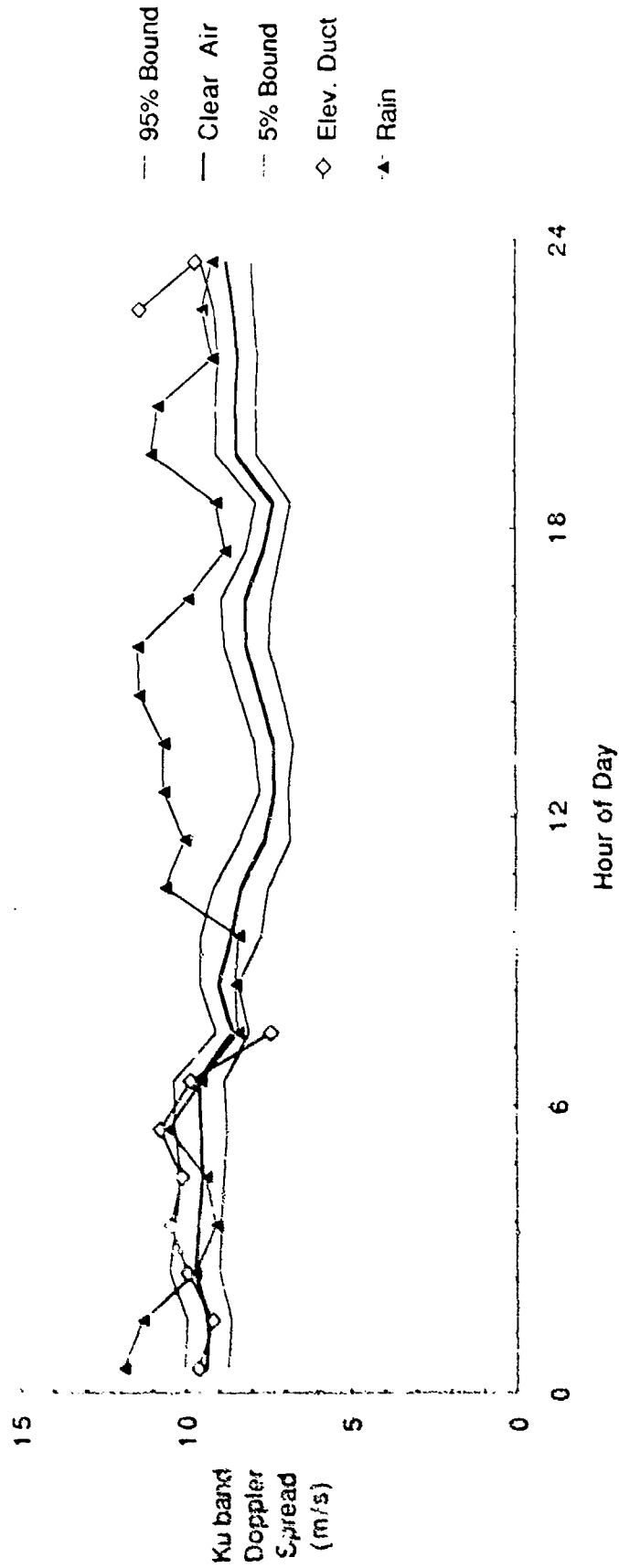


Figure 27: Average diurnal variation in Ku band Doppler spread, summer, 1989

Diurnal Variation  
Prospect Hill to Mt Tug Troposcatter Path  
Summer 1989

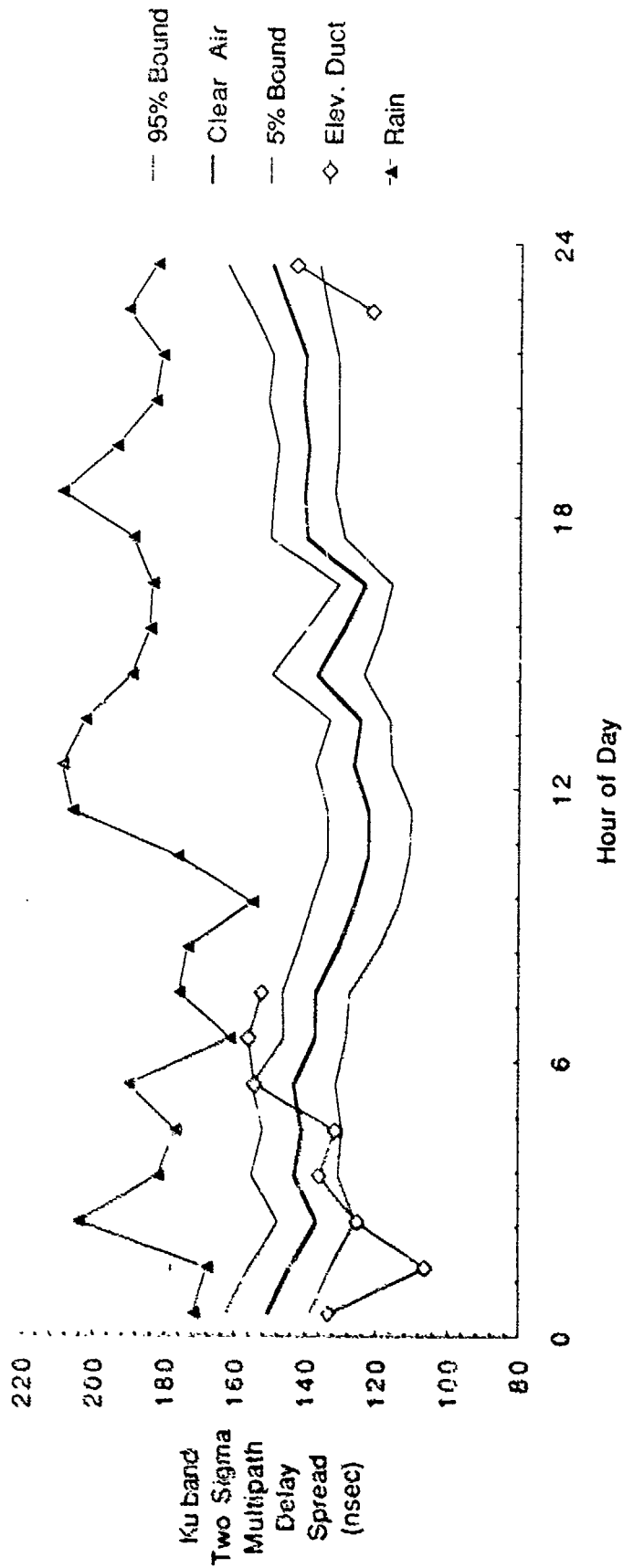


Figure 28: Average diurnal variation in Ku band two sigma multipath delay spread, summer, 1989

Sample Cumulative Distribution Functions  
 Prospect Hill to Mt Tug Troposcatter Path  
 Summer Nighttime - 1989 - Clear Weather Conditions

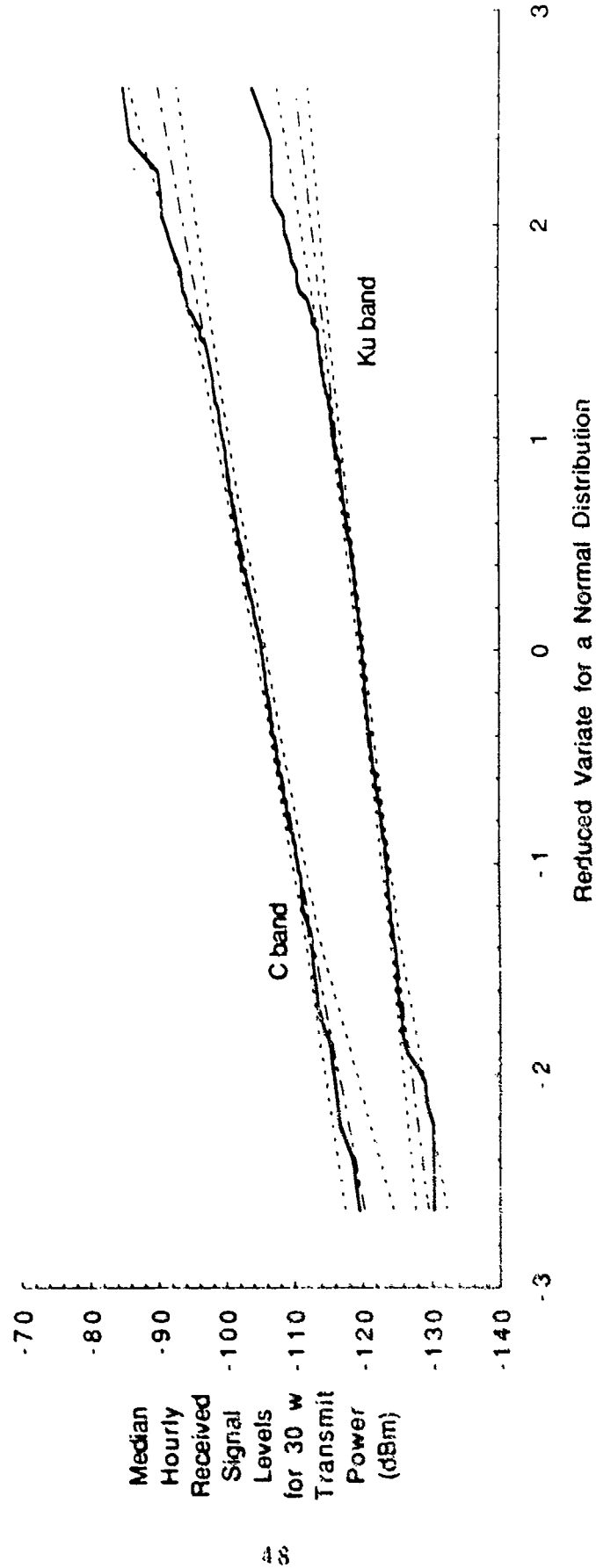


Figure 29: Sample cumulative distributions for carrier received power levels, nighttime, summer, 1989, clear weather conditions.

Sample Cumulative Distribution Functions  
 Prospect Hill to Mt Tug Troposcatter Path  
 Summer Morning - 1989 - Clear Weather Conditions

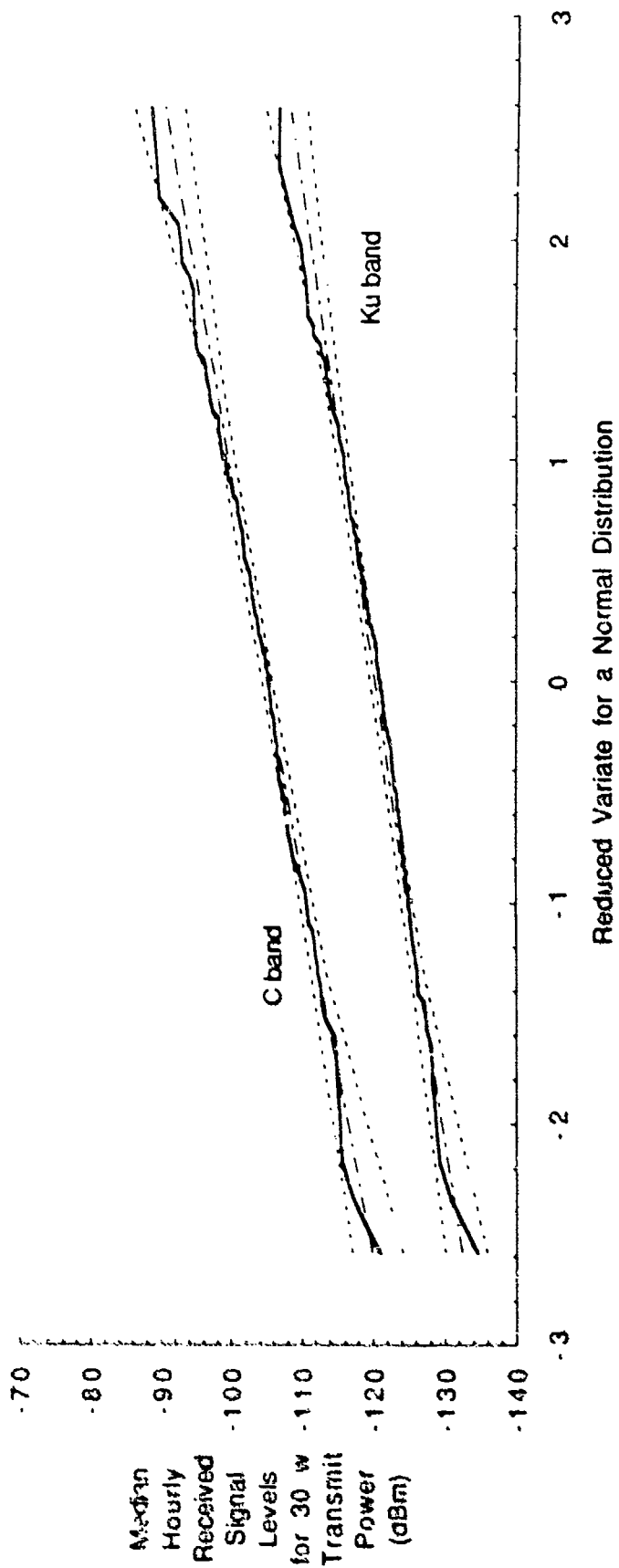


Figure 30: Sample cumulative distributions for carrier received power levels, morning, summer, 1989, clear weather conditions.

Sample Cumulative Distribution Functions  
 Prospect Hill to Mt Tug Troposcatter Path  
 Summer Afternoon - 1989 - Clear Weather Conditions

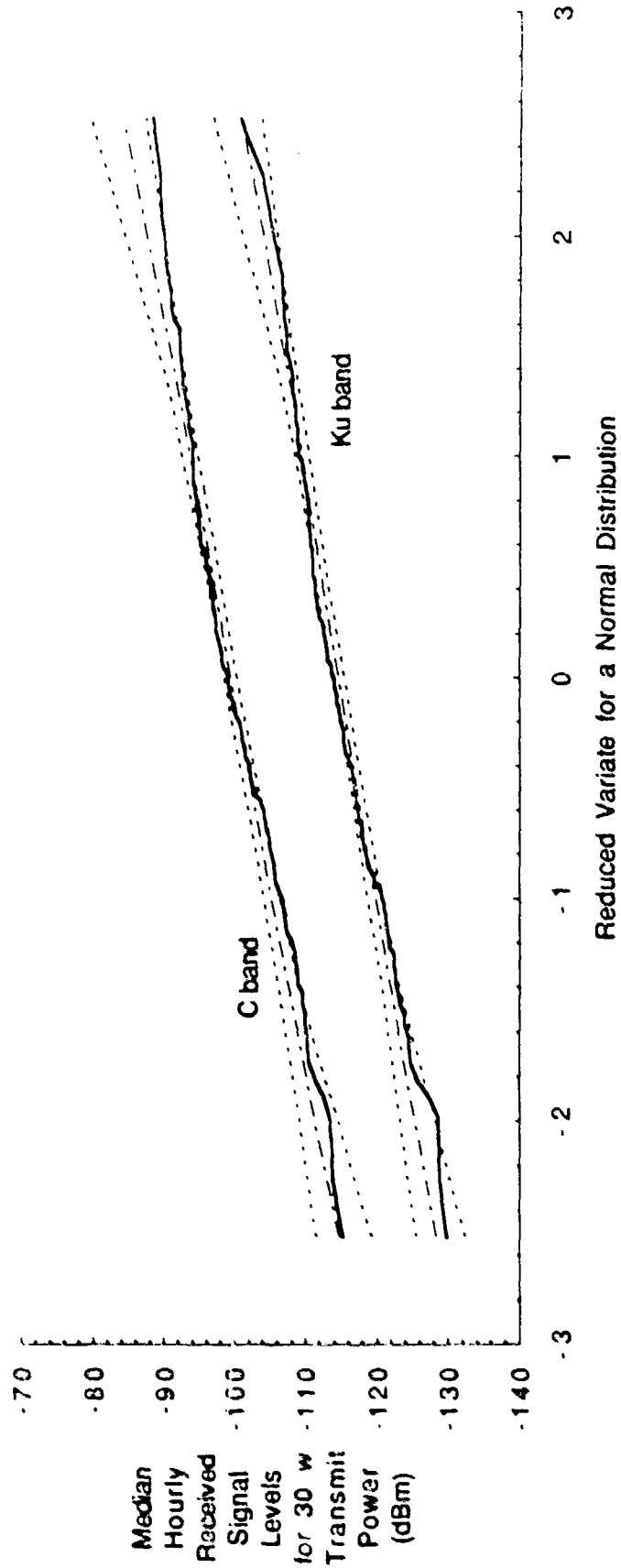


Figure 31: Sample cumulative distributions for carrier received power levels, afternoon, summer, 1989, clear weather conditions.

Sample Cumulative Distribution Functions  
 Prospect Hill to Mt Tug Troposcatter Path  
 Summer Evening - 1989 - Clear Weather Conditions

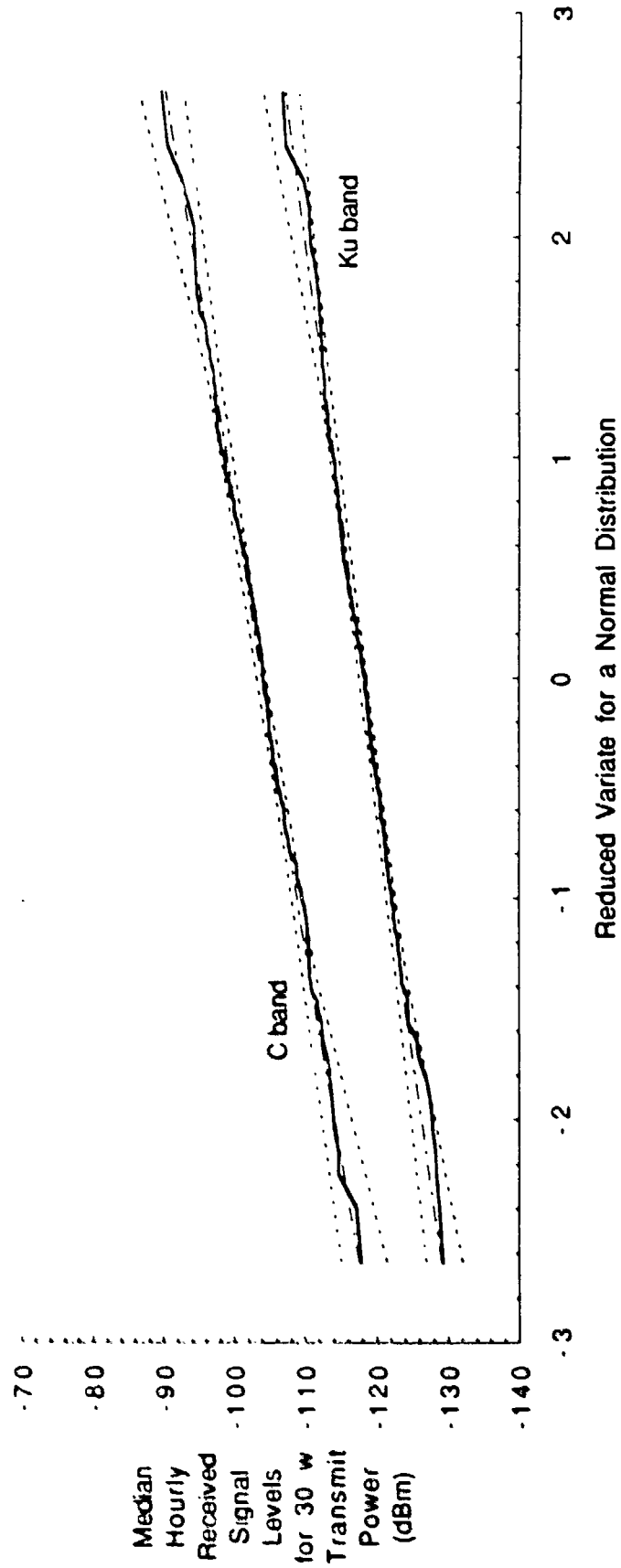


Figure 32: Sample cumulative distributions for carrier received power levels, evening, summer, 1989, clear weather conditions.

Sample Cumulative Distribution Functions  
 Prospect Hill to Mt Tug Troposcatter Path  
 Summer Afternoon - 1989 - Clear Weather Conditions

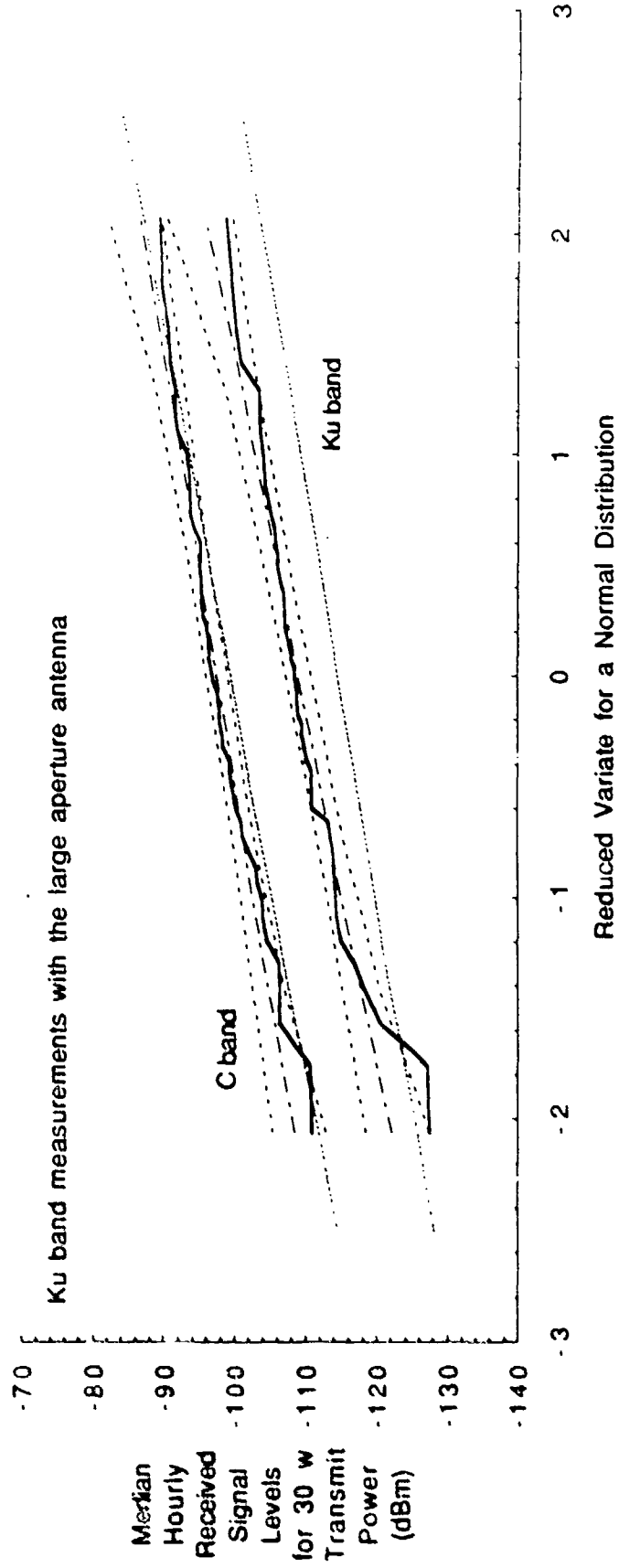


Figure 33: Sample cumulative distributions for carrier received power levels, large aperture antenna at Ku band, afternoon, summer, 1989, clear weather conditions.

Sample Cumulative Distribution Functions  
 Prospect Hill to Mt Tug Troscatter Path  
 Summer - 1989 - Clear Weather Conditions

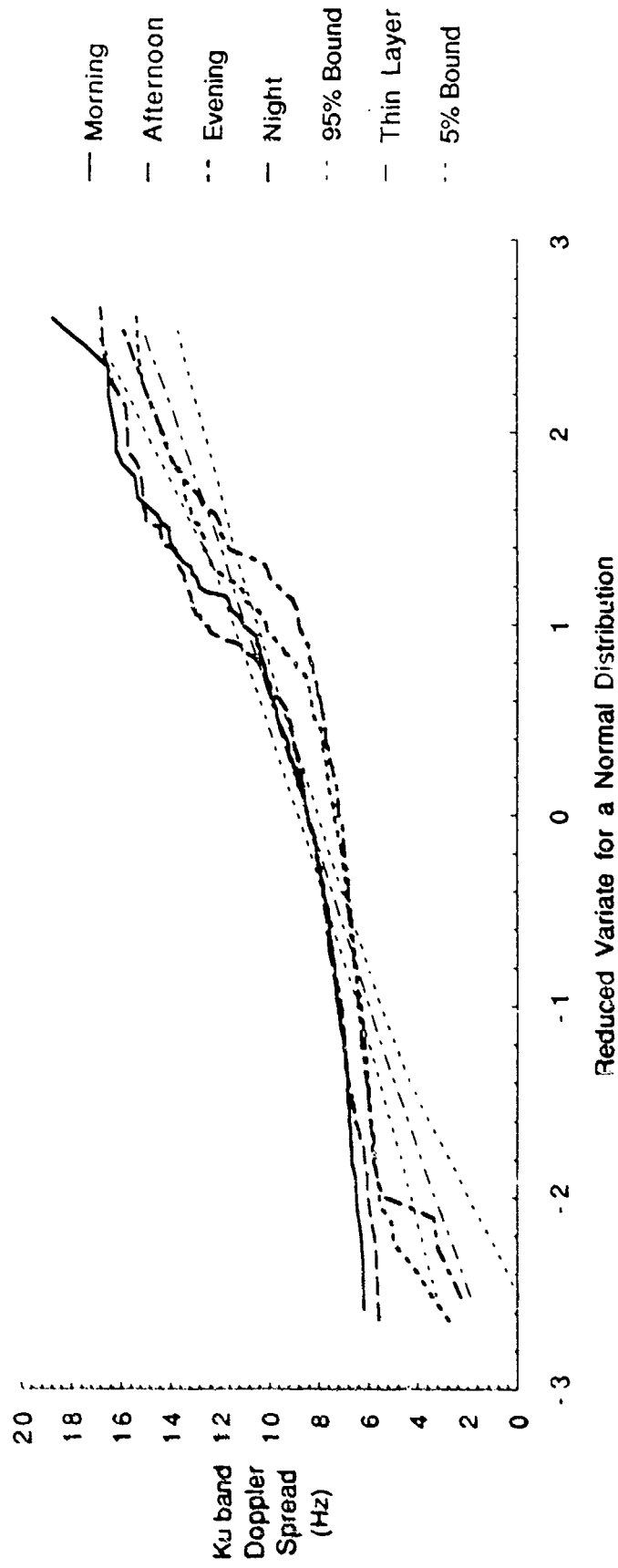


Figure 34: Sample cumulative distributions for Ku band Doppler spread values, summer, 1989, clear weather conditions.

Sample Cumulative Distribution Functions  
 Prospect Hill to Mt Tug Troposcatter Path  
 Summer - 1989 - Clear Weather Conditions

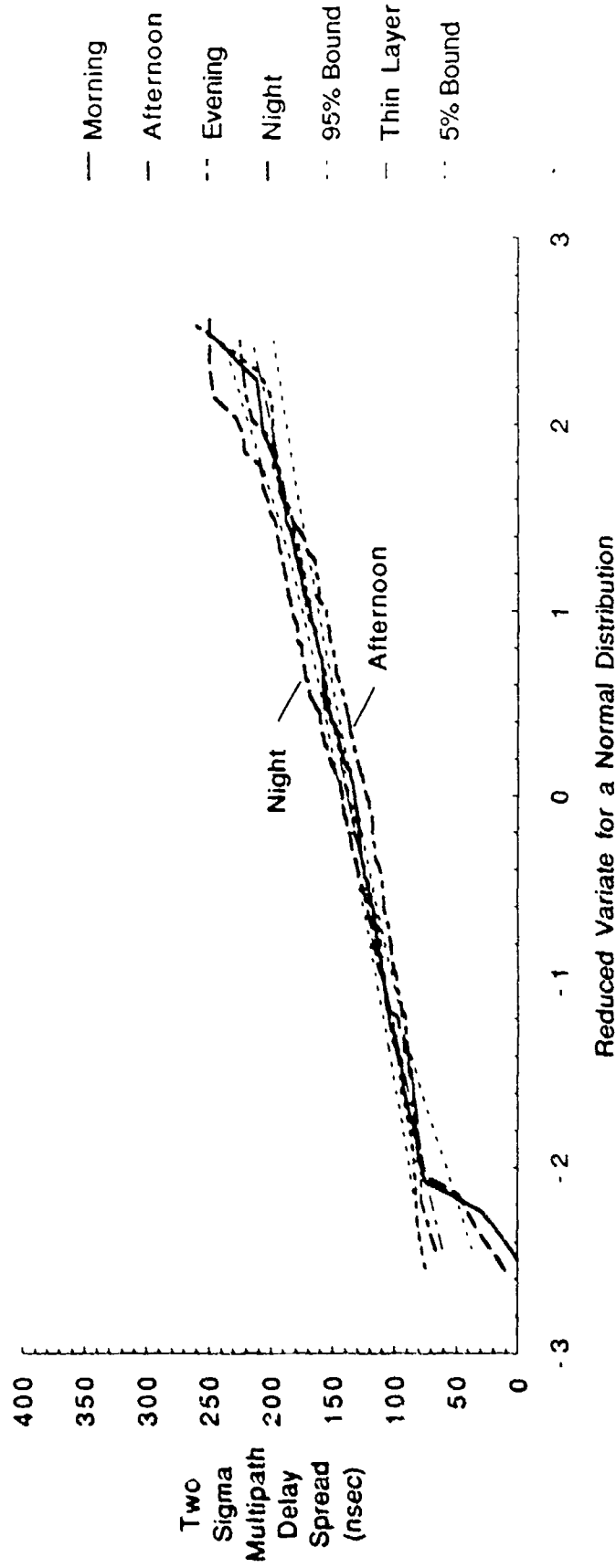


Figure 35: Sample cumulative distributions for Ku band two sigma multipath delay spread values, summer, 1989, clear weather conditions.

Sample Cumulative Distribution Functions  
 Prospect Hill to Mt Tug Troposcatter Path  
 Summer Nighttime - 1989 - Rainy Conditions

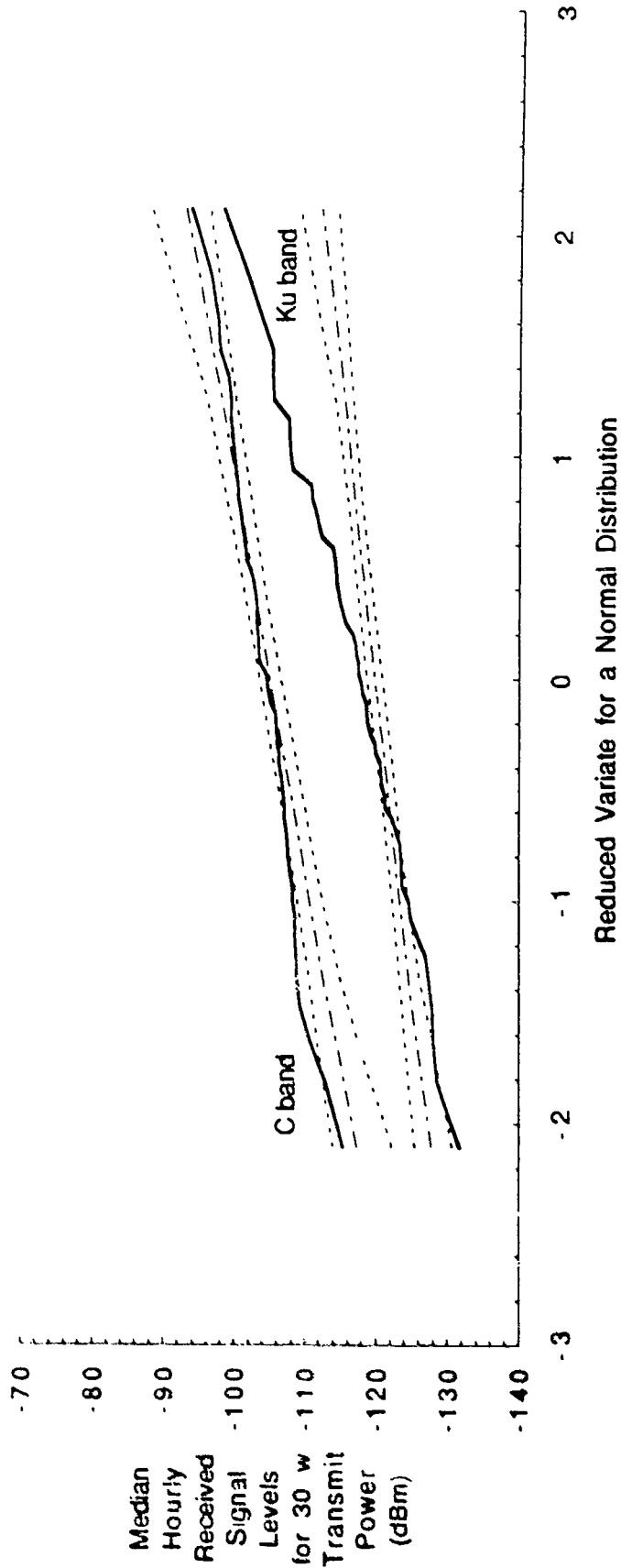


Figure 36: Sample cumulative distributions for carrier received power levels, nighttime, summer, 1989, rainy conditions.

Sample Cumulative Distribution Functions  
 Prospect Hill to Mt Tug Troposcatter Path  
 Summer Morning - 1989 - Rainy Conditions

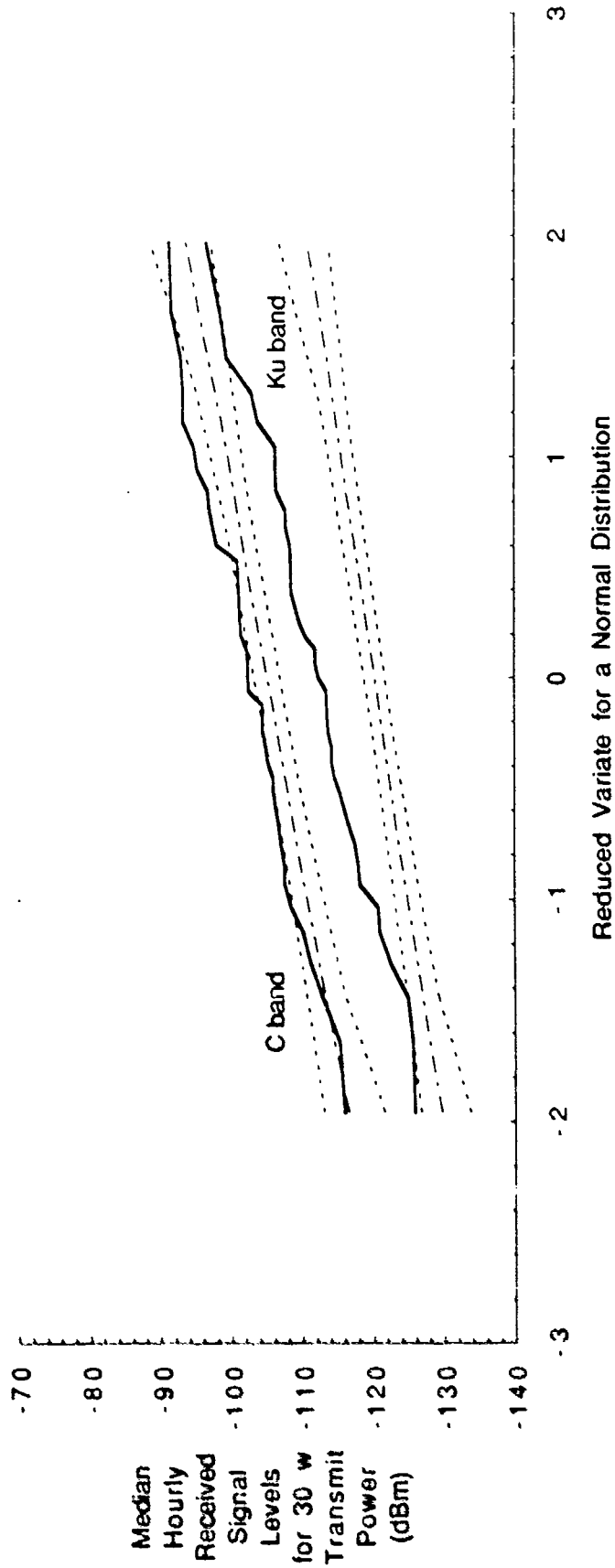


Figure 37: Sample cumulative distributions for carrier received power levels, morning, summer, 1989, rainy conditions.

Sample Cumulative Distribution Functions  
 Prospect Hill to Mt Tug Troposcatter Path  
 Summer Afternoon - 1989 - Rainy Conditions

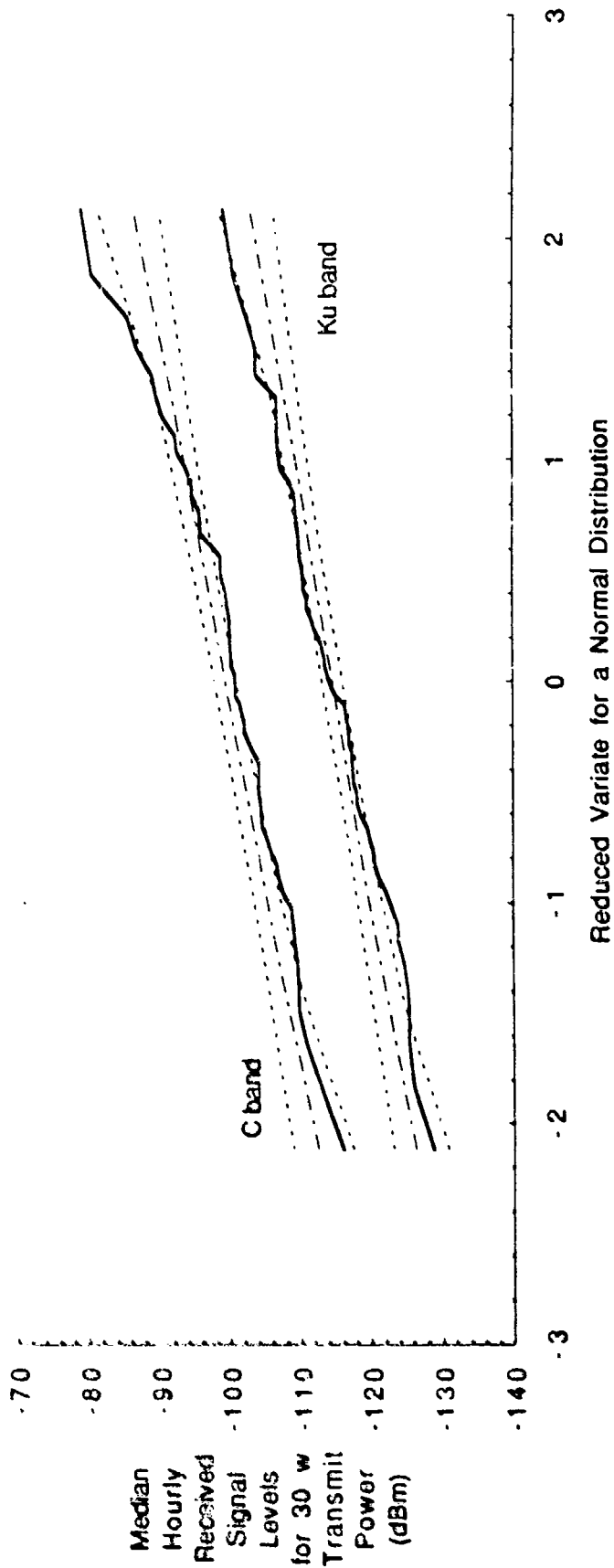


Figure 38: Sample cumulative distributions for carrier received power levels, afternoon, summer, 1989, rainy conditions.

Sample Cumulative Distribution Functions  
 Prospect Hill to Mt Tug Troposcatter Path  
 Summer Evening - 1989 - Rainy Conditions

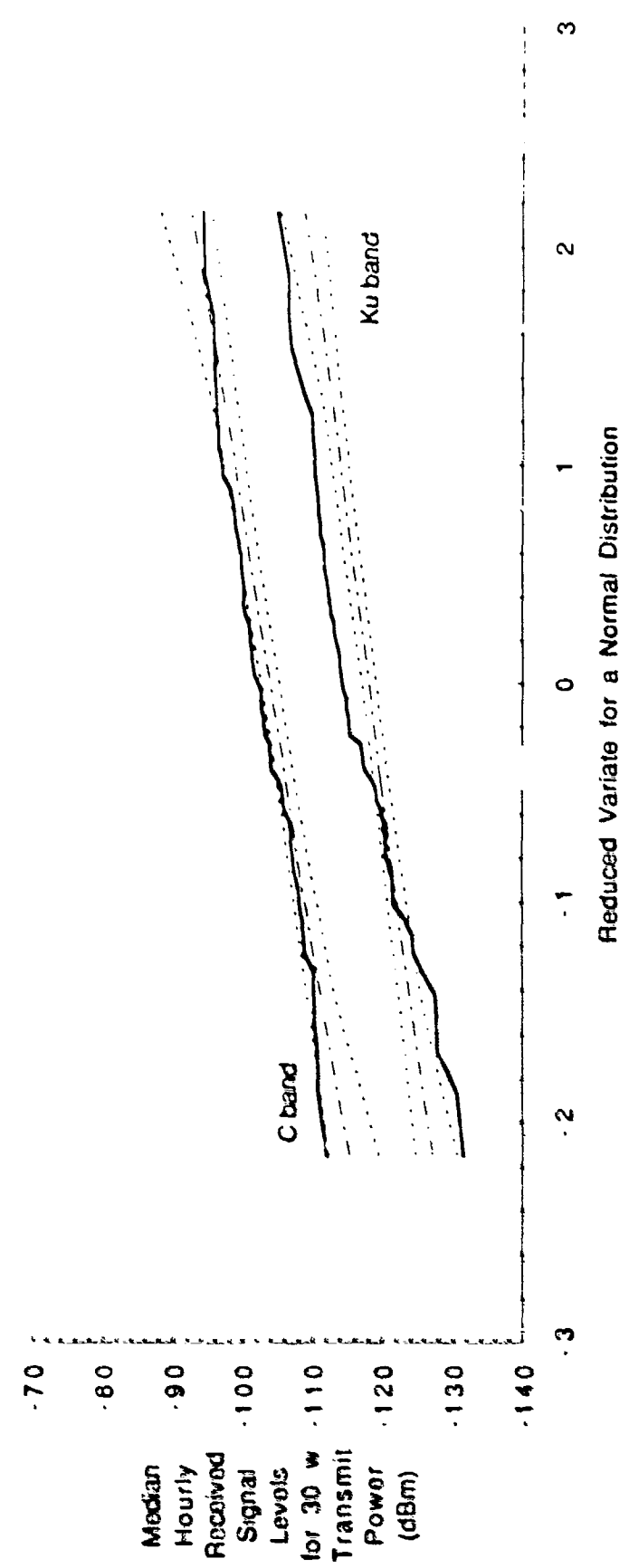


Figure 39: Sample cumulative distributions for carrier received power levels, evening, summer, 1989, rainy conditions.

Sample Cumulative Distribution Functions  
 Prospect Hill to Mt Tug Troposcatter Path  
 Summer - 1989 - Rainy Conditions

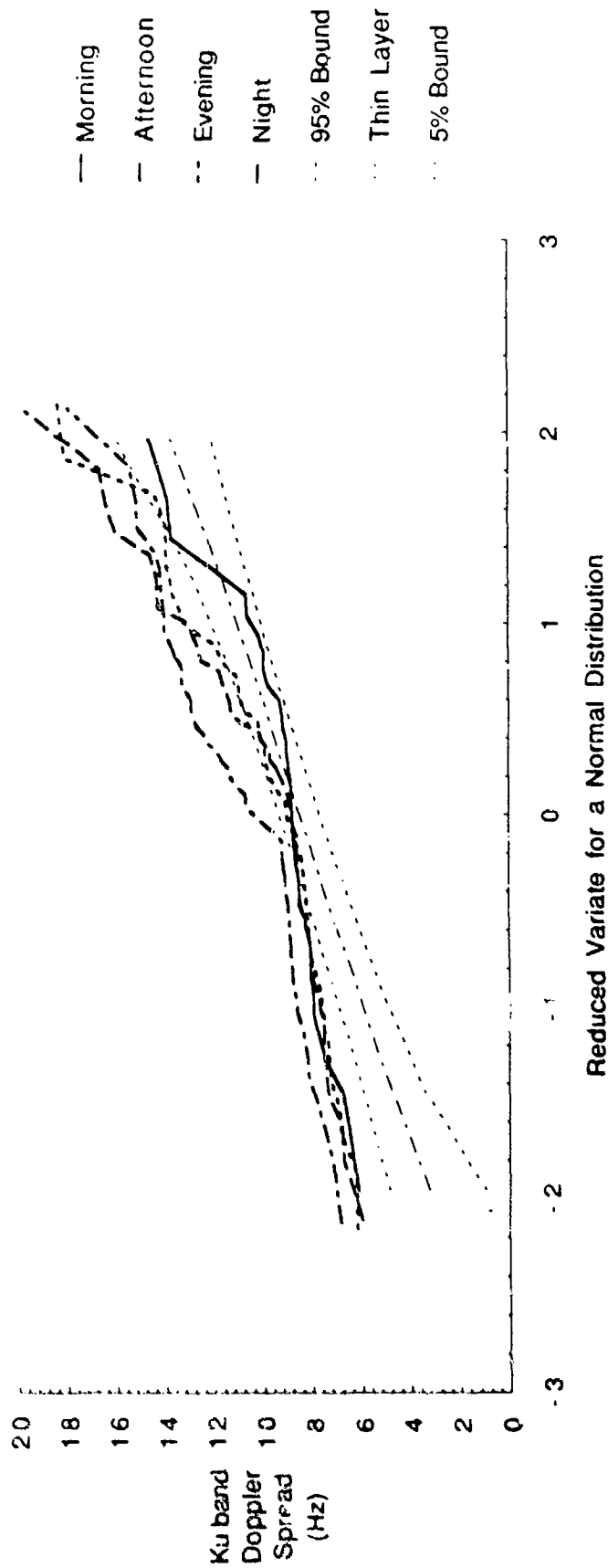


Figure 40: Sample cumulative distributions for Ku band Doppler spread values, summer, 1989, rainy conditions.

Sample Cumulative Distribution Functions  
 Prospect Hill to Mt Tug Troposcatter Path  
 Summer - 1989 - Rainy Conditions

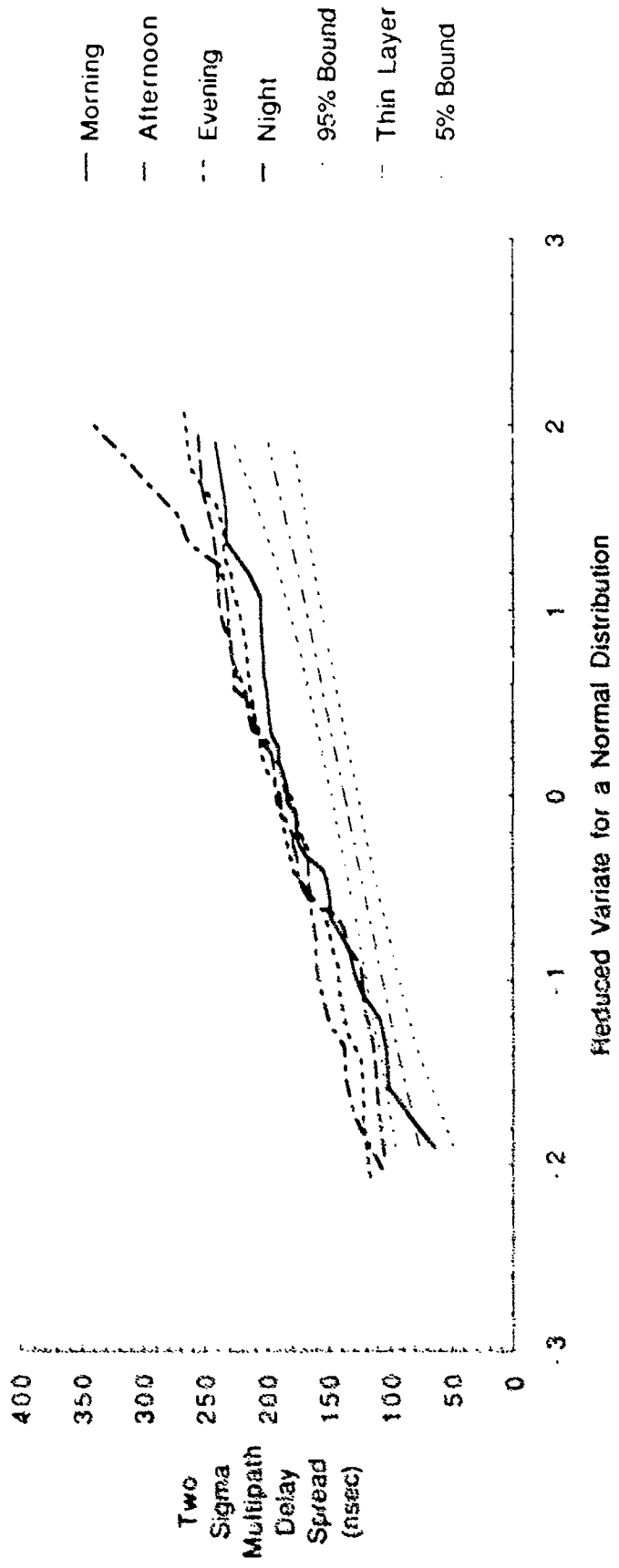


Figure 41: Sample cumulative distributions for Ku band two sigma multipath delay spread values, summer, 1989, rainy conditions.

Sample Cumulative Distribution Functions  
 Prospect Hill to Mt Tug Troposcatter Path  
 Summer Nighttime - 1989 - Elevated Ducting Conditions

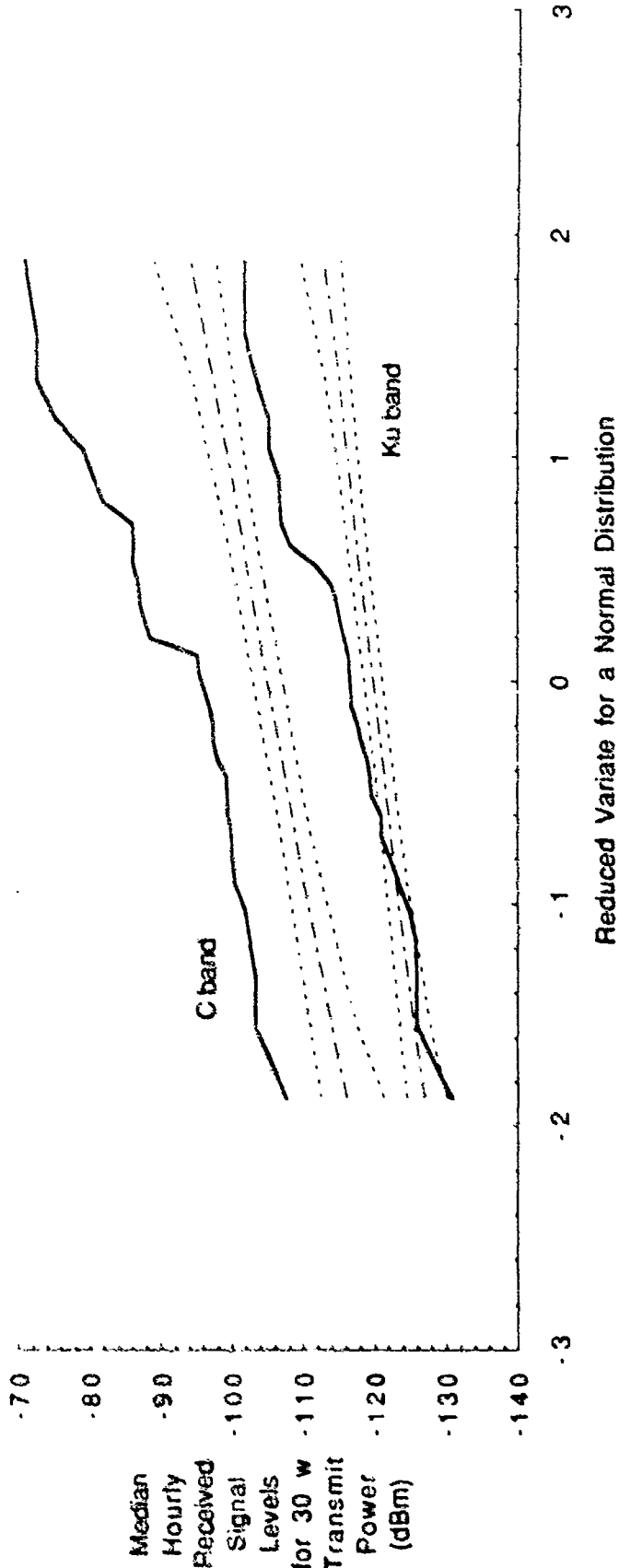


Figure 42: Sample cumulative distributions for carrier received power levels, nighttime, summer, 1989, elevated ducting conditions.

Sample Cumulative Distribution Functions  
 Prospect Hill to Mt Tug Troposcatter Path  
 Summer Morning - 1989 - Elevated Ducting Conditions

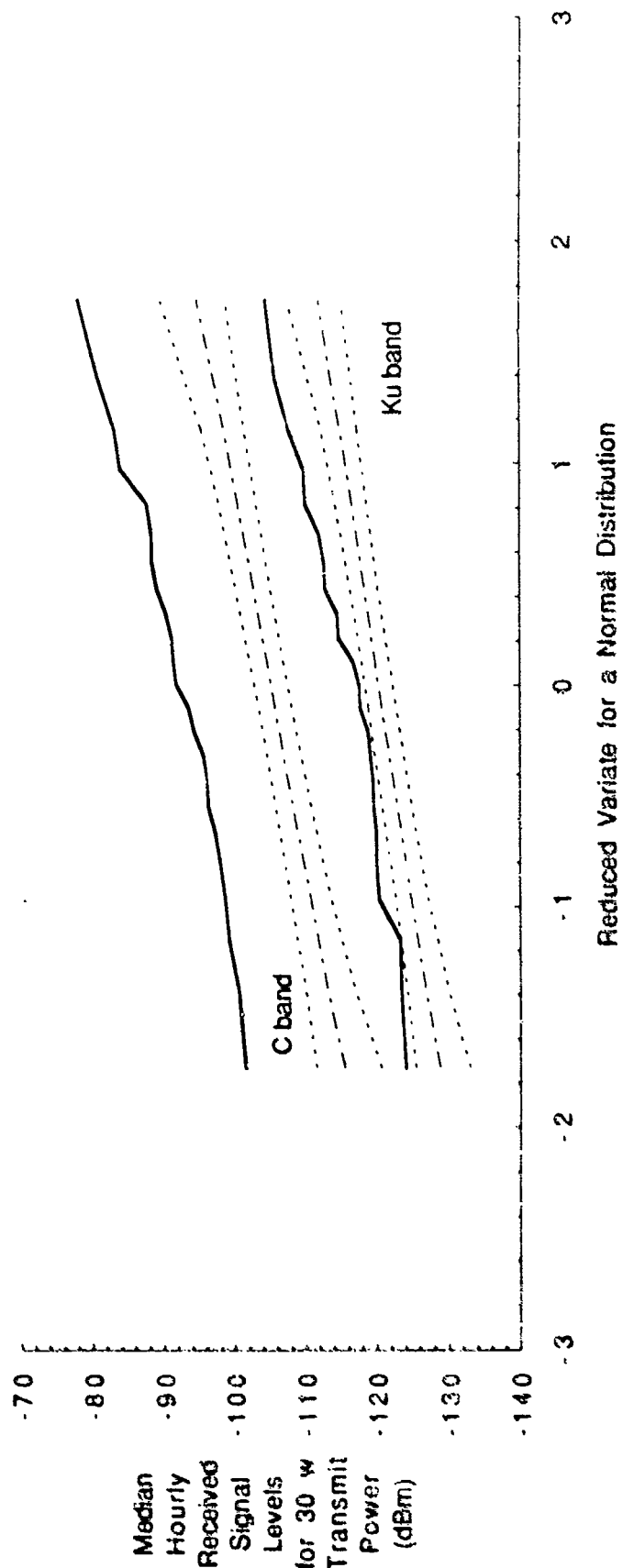


Figure 43: Sample cumulative distributions for carrier received power levels, morning, summer, 1989, elevated ducting conditions.

Sample Cumulative Distribution Functions  
 Prospect Hill to Mt Tug Troposcatter Path  
 Summer - 1989 - Elevated Ducting Conditions

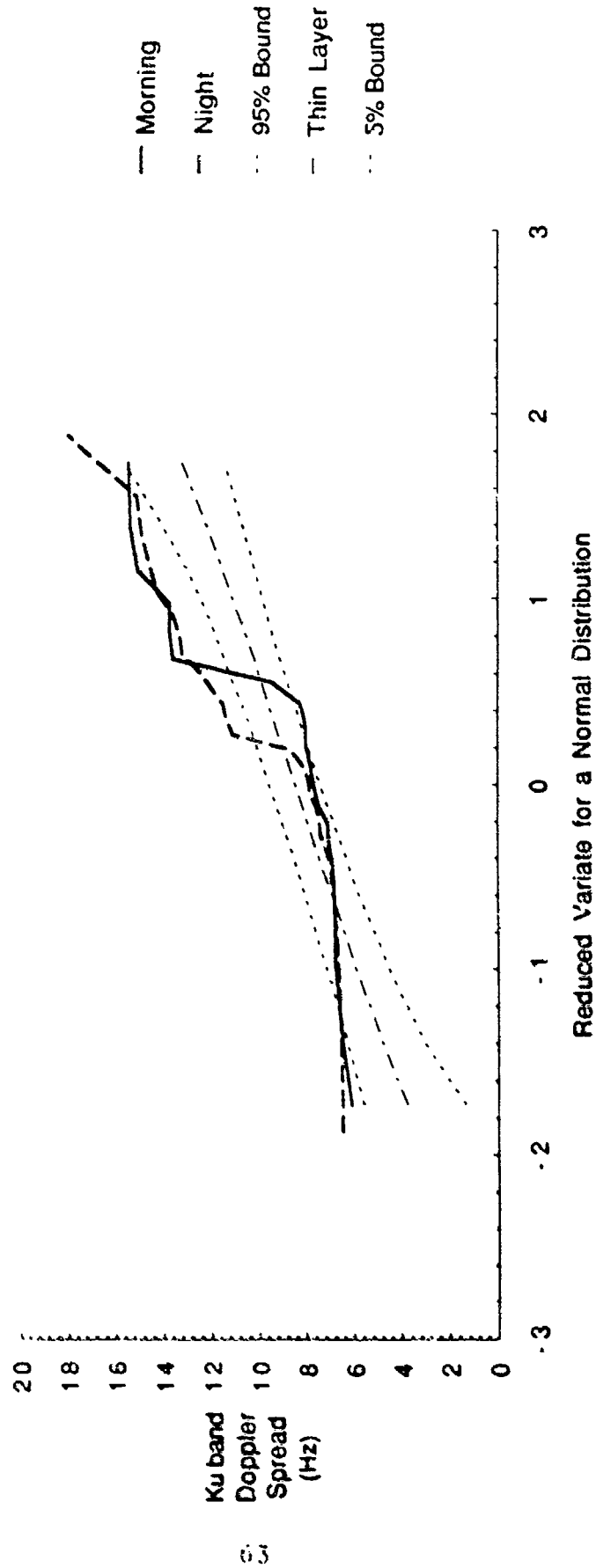


Figure 44: Sample cumulative distributions for Ku band Doppler spread values, summer, 1989, elevated ducting conditions.

Sample Cumulative Distribution Functions  
 Prospect Hill to Mt Tug Troscasser Path  
 Summer - 1989 - Elevated Ducting Conditions

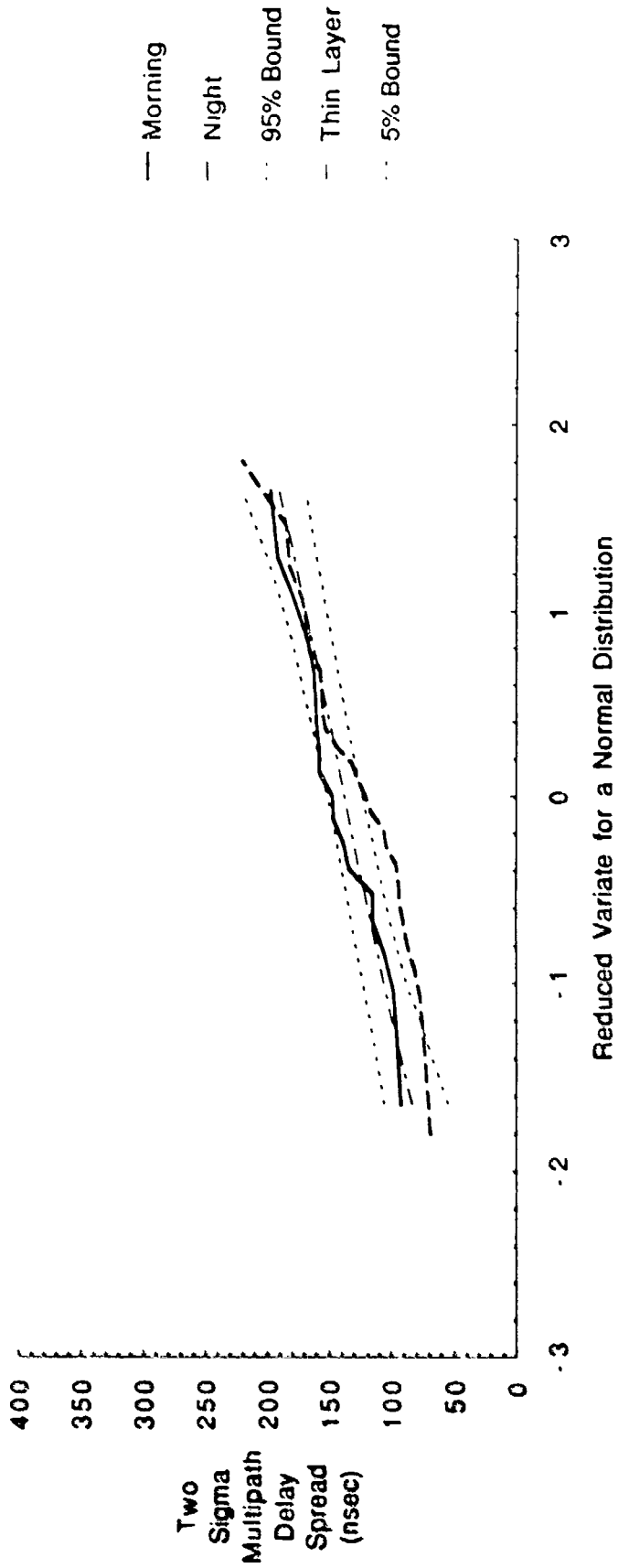


Figure 45: Sample cumulative distributions for Ku band two sigma multipath delay spread values, summer, 1989, elevated ducting conditions.

Sample Cumulative Distribution Functions  
Prospect Hill to Mt Tug Troposcatter Path  
Summer 1989

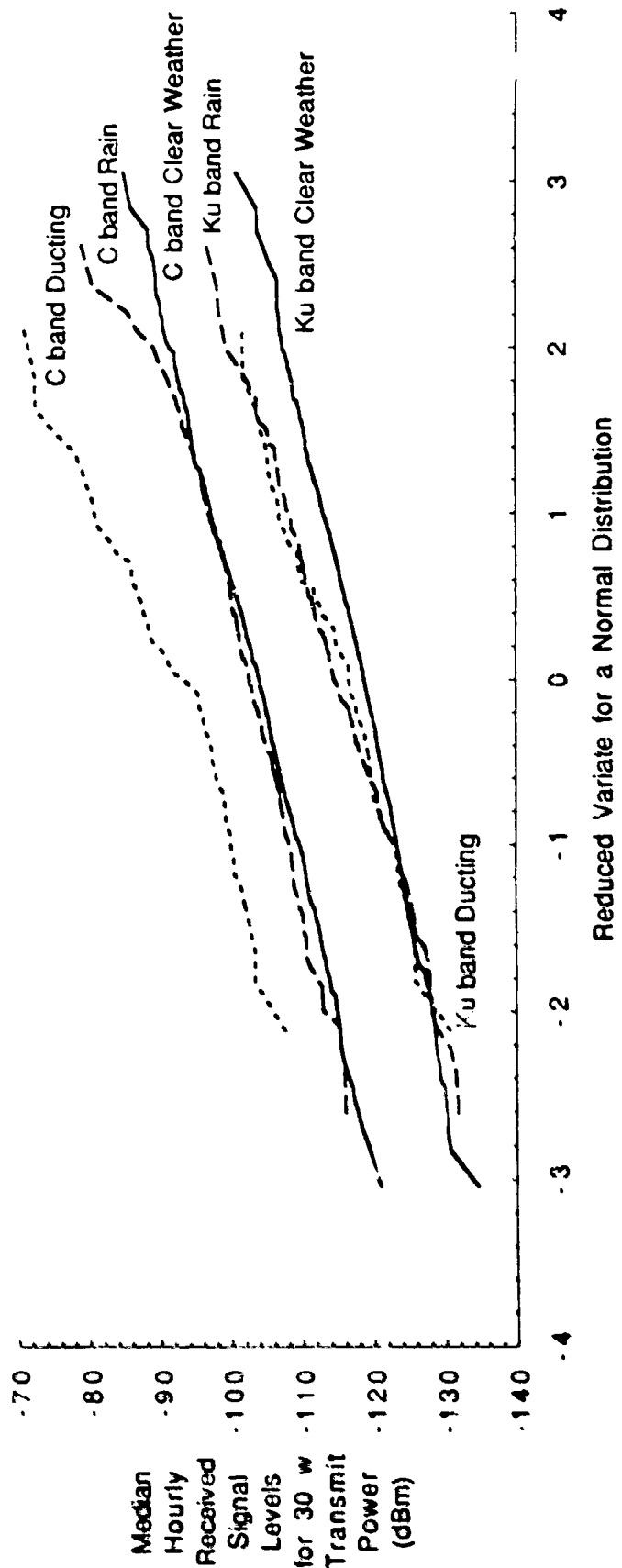


Figure 46: Sample cumulative distributions for carrier received power levels for different propagation mechanisms, summer, 1989.

**MISSION  
OF  
ROME LABORATORY**

Rome Laboratory plans and executes an interdisciplinary program in research, development, test, and technology transition in support of Air Force Command, Control, Communications and Intelligence (C<sup>3</sup>I) activities for all Air Force platforms. It also executes selected acquisition programs in several areas of expertise. Technical and engineering support within areas of competence is provided to ESD Program Offices (POs) and other ESD elements to perform effective acquisition of C<sup>3</sup>I systems. In addition, Rome Laboratory's technology supports other AFSC Product Divisions, the Air Force user community, and other DOD and non-DOD agencies. Rome Laboratory maintains technical competence and research programs in areas including, but not limited to, communications, command and control, battle management, intelligence information processing, computational sciences and software producibility, wide area surveillance/sensors, signal processing, solid state sciences, photonics, electromagnetic technology, superconductivity, and electronic reliability/maintainability and testability.